2008-07-16

Ability of ADV Measurements to Detect Turbulence Differences Between Angular and Rounded Gravel Beds of Intermediate - Roughness Scale

Benjamin B. Haws
Brigham Young University - Provo

ABILITY OF ADV MEASUREMENTS TO DETECT TURBULENCE DIFFERENCES BETWEEN ANGULAR AND ROUNDED GRAVEL BEDS OF INTERMEDIATE - ROUGHNESS SCALE

by

Benjamin B. Haws

A thesis submitted to the faculty of

Brigham Young University

in partial fulfillment of the requirements for the degree of

Master of Science

Department of Civil and Environmental Engineering

Brigham Young University

August 2008

BRIGHAM YOUNG UNIVERSITY

GRADUATE COMMITTEE APPROVAL

of a thesis submitted by

Benjamin B. Haws

This thesis has been read by each member of the following graduate committee and by majority vote has been found to be satisfactory.

Date	Rollin H. Hotchkiss, Chair
Date	E. James Nelson
Date	R. Daniel Maynes

BRIGHAM YOUNG UNIVERSITY

As chair of the candidate's graduate committee, I have read the thesis of Benjamin B. Haws in its final form and have found that (1) its format, citations, and bibliographical style are consistent and acceptable and fulfill university and department style requirements; (2) its illustrative materials including figures, tables, and charts are in place; and (3) the final manuscript is satisfactory to the graduate committee and is ready for submission to the university library.

Date

Rollin H. Hotchkiss
Chair, Graduate Committee

Accepted for the Department

E. James Nelson
Graduate Coordinator

Accepted for the College

Alan R. Parkinson
Dean, Ira A. Fulton College of Engineering and Technology

ABSTRACT

ABILITY OF ADV MEASUREMENTS TO DETECT TURBULENCE DIFFERENCES BETWEEN ANGULAR AND ROUNDED GRAVEL BEDS OF INTERMEDIATE - ROUGHNESS SCALE

Benjamin B. Haws
Department of Civil and Environmental Engineering
Master of Science

A set of laboratory experiments was carried out to distinguish flow characteristics (bed origin, shear velocity, turbulence intensity, turbulent kinetic energy) between beds of differing gravel angularity. Ten vertical profiles of velocity measurements were taken from angular and rounded fixed gravel beds with a 16 MHz micro acoustic Doppler velocimeter (ADV) sampling at 50 Hz. Both gravel beds had a bottom slope of 0.2% and were in the intermediate - roughness scale. Shear velocities were calculated using three common methods: St Venant, Reynolds stress, and Clauser. The Reynolds stress method resulted in the closest visual match to turbulence distributions proposed by others. The bed origin was found to be on average $0.24D_{50}$ and $0.21D_{50}$ for the angular and rounded gravel beds respectively. These differences, however, were not statistically significant. Turbulence intensity within

20% of the bed showed considerable scatter. The difficult measuring conditions likely prevented the ADV to detect significant differences of turbulence intensity in the longitudinal and transverse directions between the two gravel beds. But the ADV measurements in the vertical direction may well resolve turbulence even in difficult flow conditions (determined by acoustic Doppler performance curve formulation). For the vertical direction, the angular gravel bed showed an increase in TI_{max} that extended throughout the profile. The increased turbulence intensity had a concomitant effect of increasing the turbulent kinetic energy for the angular bed.

ACKNOWLEDGMENTS

I am indebted to Dr. Rollin H. Hotchkiss for the past two years of guidance, friendship, and encouragement on this project. I would also like to thank the Civil Engineering department for providing the excellent experimental facilities that made this work possible. I am especially grateful for the support of my wife, Emily. Those frequent chats about this work helped me develop solutions to every bump along the way.

Table of Contents

List of Tables

List of Figures

Chapter 1

Introduction

Local bed characteristics such as shape, size, position and concentration of roughness elements have been shown to strongly influence the flow field. Various experiments have been conducted to determine flow resistance as a function of form, pattern and concentration of sand, gravel, and cobbles, as well as cubical, spherical and other shapes of roughness elements [57] [58]. These studies have shown that intermediate densities (15% to 25%) of roughness elements on the bed create the highest resistance to flow [57][85]. The roughness height, k_s, has also been shown to be a function of gravel angularity [28]. In addition to velocity profiles, turbulence distribution has been investigated for gravel beds in laboratory settings as well as field settings with fixed, loose, and mobile beds [37] [82] [12] [15] [52] [60] [69]. Although the relative roughness, H/k_s (where H is the mean flow depth), has been shown to affect the turbulence distribution [82], the effects of gravel angularity on turbulence distribution are still unknown.

Research on turbulence has been limited due to the inability to make accurate and precise measurements. Basic research on turbulent boundary layers in open-channel flow started in the 1970's, using thermal anemometry. In the 1980's the laser anemometry greatly reduced artifacts inherent in thermal anemometry, which was a great improvement, but was expensive [48]. With the advent of Doppler technology, a new way of collecting velocity data for characterizing flow emerged. This has

provided a relative simple and inexpensive means of collecting velocity and turbulence measurements that has been widely adopted.

In spite of its wide usage, or perhaps because of it, the accuracy of the ADV has come into question [27], especially with its measurement of turbulence for which it was not originally designed [45]. Instrument noise and sampling size are major problems associated with the ADV technique [27] [41] [77]. Garcia et al. [27] recommend a relationship (acoustic Doppler performace curve formulation) for determining optimal flow conditions for the ADV to resolve turbulence. They recommend $Lf_R/U_c > 20$ where L is the integral length scale, f_R is the user-set sampling frequency, and U_c is the convective velocity. Unfortunately, this excludes using the ADV for flows that are often found in laboratory and natural settings [70].

This investigation was conducted to determine the capabilities of the ADV to detect changes in turbulence between angular and rounded fixed gravel beds in difficult flow conditions. The difficulty here refers to measurements near the bed in intermediate - roughness scale (definition by Bathurst [7]) conditions resulting in Lf_R/U_c values ranging from 13 to 16. Just as angularity affects the flow resistance, it is hypothesized that increased gravel angularity produces higher turbulence production.

Chapter 2

Experimental Setup and Measurements

2.1 Flume

A 12.5 meter (m) long by 1.2 m wide recirculating laboratory flume with Plexiglas walls was used in this set of experiments. The substrate consisted of a 5 m long test section of fixed gravel with up- and downstream substrate composed of crushed loose gravel. Figure 2.1 illustrates the setup and sampling locations. A screed was used at the beginning of each experimental run to smooth the loose gravel to the same level as the fixed bed. To ensure hydrodynamic equilibrium in each test, the pumps were allowed to run for 1 hour before measurements were taken. A fully developed profile existed upstream of the sampling section as shown by velocity measurements collapsing onto one velocity profile (Figure 2.2). Flowrate (0.10 m^3/s) and slope (0.20%) were constant for all experimental runs. A gradually varied flow calculation was used to ensure that downstream effects did not influence uniform flow over the testing section. This was also verified by measuring the water surface over the fixed-bed portion of the flume.

2.2 Gravel Beds

Two different sets of gravel were used for the fixed bed portion of the flume: crushed (angular) rock, and smooth (rounded) rock. Both sets were sifted with square holed sieves to have a median diameter (geometric average of sieve opening size) of

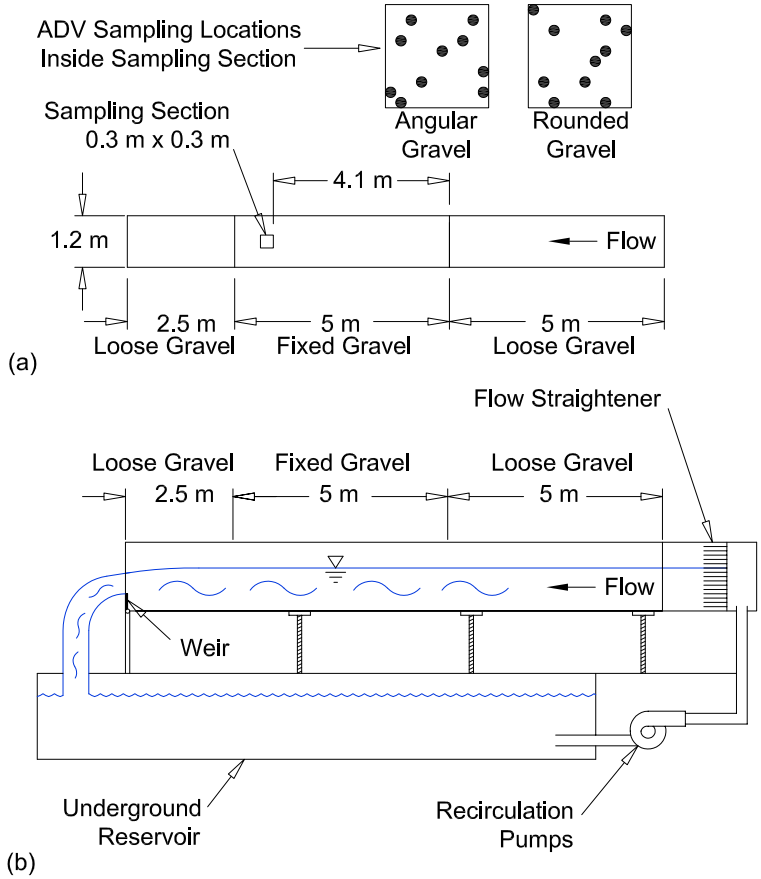

Figure 2.1: Flume schematic (a) plan view (b) elevation view

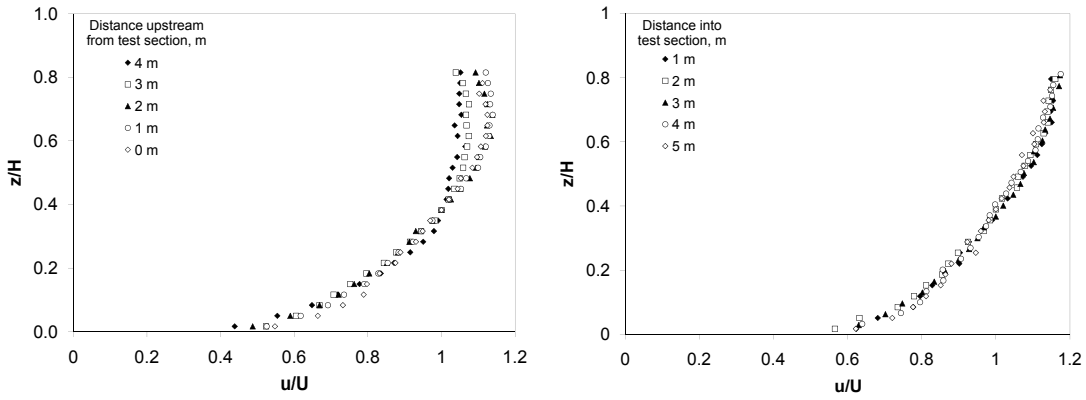

Figure 2.2: Velocity profiles showing fully-developed flow

24.6 ± 0.8 mm. Particle shape factors in each set were quantified by measuring the three principle axes of 50 random samples (Tables 2.1 and 2.2) and also by two-dimensional image analysis of 350 random samples (Table 2.3). The principle axes a, b, and c correspond to the longest, intermediate and shortest axes, respectively. The gravel was placed with the $c-$axis in the vertical, and had a random non-imbricated orientation. Further detail is provided in Appendix B. Figure 2.3 shows the fixed gravel beds.

Table 2.1: Mean axis lengths

	Axis length/standard deviation		
	a	b	c
	mm	mm	mm
Angular	39.6/6.5	27.3/4.1	15.1/4.0
Rounded	37.0/5.2	27.3/2.7	14.9/3.5

Table 2.2: Mean shape descriptors from axes lengths

	Nominal D $(abc)^{1/3}$	Flatness c/b	Elongation b/a	Form Factor $\frac{(a-b)}{(a-c)}$	Compactness c/a
Angular	25.1	0.6	0.7	0.5	0.4
Rounded	24.4	0.6	0.8	0.4	0.4

Table 2.3: Mean shape descriptions from image analysis

	Form Factor $\frac{4\pi A}{p^2}$	Roundness $\frac{4A}{\pi\sqrt{a}}$	Compactness $\frac{\sqrt{(4/\pi)A}}{a}$	Aspect Ratio a/b
Angular	0.75/0.06	0.71/0.12	0.84/0.08	1.46/0.30
Rounded	0.82/0.04	0.76/0.11	0.87/0.07	1.35/0.22

2.3 Instrumentation

A Sontek 16 megahertz (MHz) field micro acoustic Doppler velocimeter (ADV) was deployed for velocity measurements and corresponding turbulence quantities. The sampling frequency was set at 50 Hz, and the center of the sampling volume was located 5 cm from the transmitter. The sampling volume roughly resembles a cylinder

Figure 2.3: Angular and rounded gravel panels

with a diameter of 4.5 mm ± 0.3 mm [68][64]. The height of the sampling volume is defined by the "convolution of the transmitted acoustic pulse with the receive window over which the return signal is sampled" [64]. In the standard configuration it can be estimated that the sample volume height is between 4.5 mm [64] and 5.6 mm [66].

A single estimate of velocity is referred to as a *ping*. Depending on the velocity setting of the instrument, the ADV pings at a rate of 150-250 times per second [65]. Pings are averaged together for each sample specified by the user frequency (f_R) setting. These settings provided a 99% accuracy in mean velocity [68].

A sampling time of 3.5 minutes was determined so that mean velocity measurements in the streamwise direction were time independent.

The coordinate system for data collection and analysis was set with the the x-direction (u) positive in the streamwise direction, the z-direction (w) positive in the vertical, and the y-direction (v) followed the right-hand rule and was positive to the left when facing downstream.

A traversing system with two step-type motors was set up to control the ADV location in the y and z directions (Figure 2.4). Each step in either the y or z direction had a spatial resolution of 0.00635 mm. The traversing system was connected to a trolley on the flume which allowed movement in the streamwise direction. A digital point gauge with 0.01 millimeter (mm) resolution was used to measure water depth.

Figure 2.4: Trolley containing the ADV

2.4 Data Filtering

The instrument noise and measurement strength were quantified using two parameters. The "signal-to-noise ratio" (SNR) is a reflection of the amount of scattering matterial in the sampling volume. The "correlation" (COR) is a function of how dissimilar successive pulse echoes are from each other [42]. Filtering the raw ADV data usually involves choosing a cut-off value (CR) for the signal-to-noise ratio (SNR_{CR}) and correlation (COR_{CR}). Data outside the cutoff values are filtered from the data set.

Sontek recommends using $\text{SNR}_{CR} = 15$ and $\text{COR}_{CR} = 70$, but these values, especially COR_{CR}, have come under scrutiny recently since they filter out much of the data in turbulent flows near the bed [80][42][70][13]. The average SNR values recorded in this set of experiments were higher than the recommended value (see Figure 2.5) (meaning there was a high amount of scatter material in the water), so SNR_{CR} was set at 15. Leaving the COR_{CR} at 70, however, filtered out many of the

individual points in the data files. Low correlation scores can be caused by turbulent flows, air bubbles, low SNR values, large velocity gradients in the sampling volume, large individual particles near the sampling volume, and/or interference from the boundary [42]. The following procedure was developed to find a value for COR_{CR} that would allow the most data to be filtered out but still leave sufficient data to gain insight into the flow characteristics. The velocity distribution at each measuring point

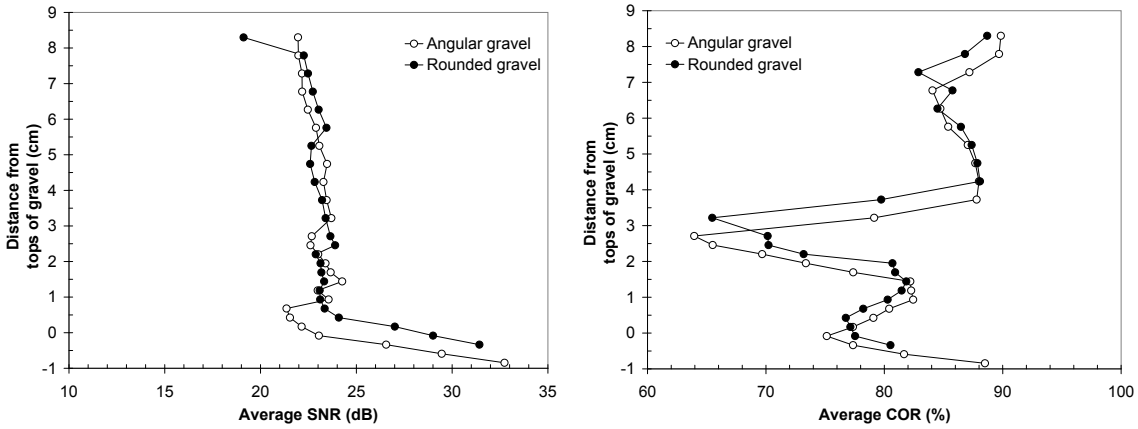

Figure 2.5: Average SNR and COR values

tends to follow a Gaussian distribution. As points were filtered from the data set, the distribution increasingly strayed from Gaussian [70]. The coefficient of determination (R^2) between the standardized data z-score and a normal distribution was used to measure the change in normality due to an increase in COR_{CR}. This was similar to the method proposed by Strom and Papanicolau [70]. A cut-off value of 50 was visually selected based on Figure 2.6, which illustrates how COR_{CR} affected the R^2-value at periodically spaced locations from the bed. Each data trace in Figure 2.6 represents a different sampling elevation from the bed. This COR_{CR} value is in agreement with Strom and Papanicolaou's value of 50 [70] and Martin et al.'s value of 40 [42].

Along with the SNR_{CR} and COR_{CR} parameters, the phase space threshold despiking algorithm developed by Goring and Nikora [29] and modified by Wahl [81] was used to filter out data points with high levels of instrument noise. A two-step

filtering process was applied in order to retain as much meaningful data as possible. The data were first filtered using the despiking algorithm, along with a SNR_{CR} of 15 and COR_{CR} of 70. If more than 70% of the data was retained, then no more filtering was done. If the data set had more than 30% of the data removed, then the original data were re-filtered with the COR_{CR} set at 50 instead of 70. The entire data set was thrown out if more than 30% of the data was removed after the second filter. The second filter was needed for 15% of the data (13% of the angular and 16% of the

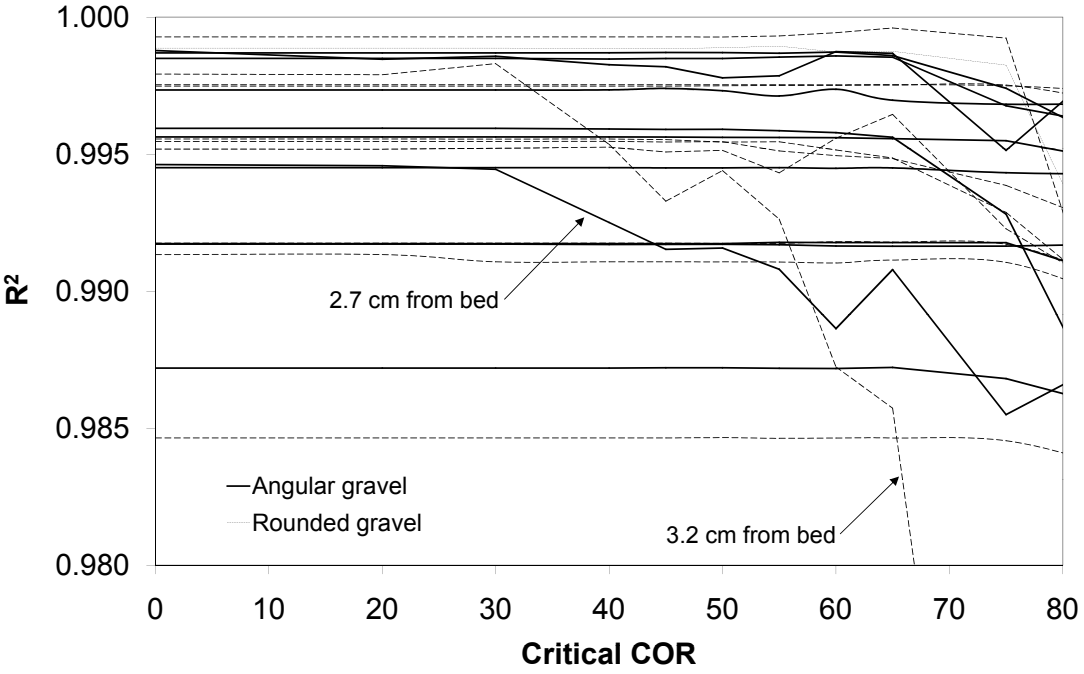

Figure 2.6: Determining COR_{CR} at various depths

rounded. Of those 15% needing the second filter, 21% (27% of the angular and 15% of the rounded) of the point data were thrown out.

The mean velocity and turbulence intensity profiles were examined after the filtering process to remove any visually non-conforming points. There was a "velocity hole" located at about 3 cm from the bed. This is shown by the large spike in low COR values in Figure 2.5. The spike is believed to be due to boundary interference [67], that occurs when the return signal from the boundary reaches the ADV receivers

at the same time as the return signal from the sample volume. Although the ADV is set up to detect and correct these boundary interferences, the multiple boundary reflections off of the gravel confused the instrument [39]. Consequently, the signal from the sample volume was hidden by the noise from these multiple boundary reflections [42] [39] [29]. Further details on the filtering process are provided in Appendix C.

Chapter 3

Results and Discussion

3.1 Test Conditions

Profiles of velocity measurements were taken at ten random sampling locations inside the testing section (see Figure 2.1). The flow for each experimental run contained the same input energy and slope (0.2%). Uniform flow was achieved by adjusting the weir on the downstream end of the flume. The ratio of depth to mean short-axis length fell within the intermediate - roughness scale ($H/S_{50} \approx 9 - 10$ [7]; where S_{50} refers to the short axis length for which 50% of the particles are smaller). Table 3.1 gives the flow conditions associated with the experimental setup.

3.2 Bed Origin Level

The vertical origin of a streambed has been defined in several ways. Many have difined the vertical origin at a point located below the tops of roughness elements; e.g. $0.25k_s$ [23] [74] (where k_s is Nikuradse's equivalent sand roughness height); $0.5D_{50}$ [73];$0.2k_s$ [37]; or $0.033k_s$ [22]. Others use a more complex method of defining the bed origin. For example, some locate the origin at the equivalent point where a smooth bed origin would be having the same volume as the rough bed and constant thickness [25] [12]. Clauser [18] argued that the origin could be located anywhere between the highest peak to the lowest point between roughness elements and could be found

Table 3.1: Hydraulic Characteristics

	Angular	Rounded
Slope, S (%)	0.20	0.20
Flow rate, Q (m^3/s)	0.10	0.10
Depth, H (m)	0.15	0.14
Relative Roughness, H/S_{50}	10	9
Average velocity, U (m/s)	0.55	0.58
Hydraulic radius*, R (m)	0.14	0.13
Global shear velocity, u_τ (m/s)	0.053	0.050
Reynolds number, $\mathbb{R}$	7.75E+04	7.52E+04
Roughness Reynolds number, $\mathbb{R}_\tau$	533	382

*Side-wall corrected with Vanoni and Brooks [75]

experimentally by extrapolating the logarithmic portion of the velocity profile to where the velocity goes to zero.

The vertical origin was found for each experimental run by extending a curve fit of the inner layer data to where the velocity equals zero as suggested by Clauser [18]. Angular run 9 produced an unrealistic origin (above the tops of the gravel) most likely due to a lack of good data close to the bed. For further calculations the origin for run 9 was assumed equal to the average of the origin found for the other nine rounded gravel runs. All origin distances are reported in Figure 3.1 as a function of D_{50} (geometric average of sieve opening size).

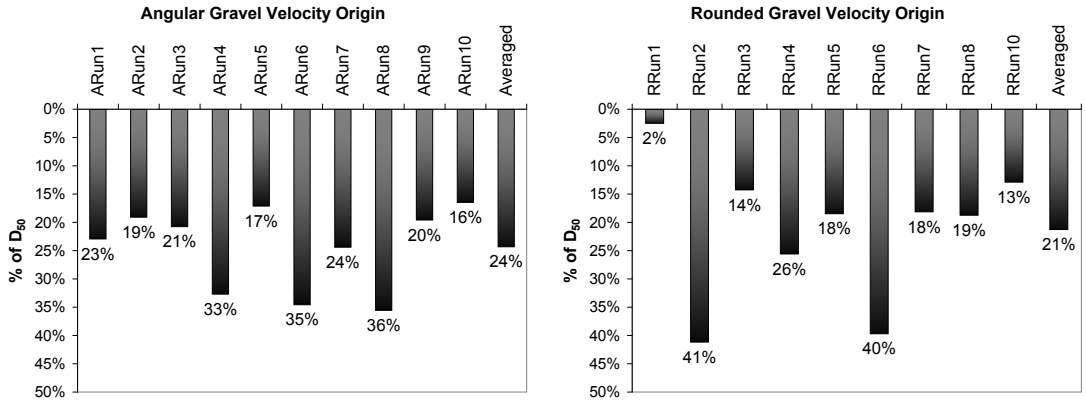

Figure 3.1: Vertical origin for angular and rounded gravel bed

A t-test indicated the difference between the angular and gravel bed origin is not statistically significant (using a 5% confidence interval). The variability in the origins for both sets of gravel is most likely a reflection of the random selection of sampling locations, and corresponds to whether the sample was taken above the peak or trough of the gravel elements. Further details on finding the bed origin are provided in Appendix C.

3.3 Shear Velocity

The shear velocity (u_τ) is a scaling factor used in describing flow parameters.

$$u_\tau \equiv \left(\frac{\tau_w}{\rho}\right)^{1/2} \tag{3.1}$$

where τ_w is shear stress on the bed, and ρ is the fluid density. Some of the most common ways to calculate u_τ include the St Venant method, the Reynolds stress method, and the Clauser method. u_τ was calculated using each of these methods to evaluate how the calculation method affected subsequent analyses.

3.3.1 St Venant Method

The shear stress on the bed, τ_w, in uniform flow can be estimated from a global perspective using:

$$\tau_w = \gamma R S \tag{3.2}$$

where R is the hydraulic radius (found for each individual bed elevation found in Section 3.2), and S is the friction slope (equal to the bed slope in uniform flow). Combining Equations 3.1 and 3.2 gives the following equation for global shear velocity

[2] [17]:

$$u_\tau = \sqrt{gRS} \tag{3.3}$$

3.3.2 Reynolds Stress Method

Shear stress for two-dimensional turbulent flow can be divided into viscous and Reynolds stresses:

$$\tau = \mu \frac{d\overline{u}}{dz} - \rho \overline{u'w'} \tag{3.4}$$

where μ is the fluid dynamic viscosity, $d\overline{u}/dz$ is the velocity gradient in the vertical direction, and $\overline{u'w'}$ (often called Reynolds stress tensor) is the time averaged cross correlation coefficient between the streamwise (u) and vertical (w) velocities. For turbulent flows away from the wall, the Reynolds stress term dominates. For two dimensional flow, the shear velocity can be found by integrating the Navier-Stokes equations for the water depth. This new equation for shear velocity based on Reynolds stress distribution can be expressed as [49]:

$$u_\tau = \sqrt{\frac{-\overline{u'w'}}{1 - \frac{z}{H}}} \quad \text{evaluated at } z = 0 \tag{3.5}$$

where z is the distance above the origin (as found for each individual experimental run in Section 3.2). Extrapolating the Reynolds stress term to the wall ($z = 0$), allows the determination of u_τ. Figure 3.2 is an example of how the shear velocity was found for all experimental runs.

The Reynolds stress distribution ($-\overline{u'w'}/u_\tau$) for the angular and rounded gravel beds are shown in Figure 3.3.

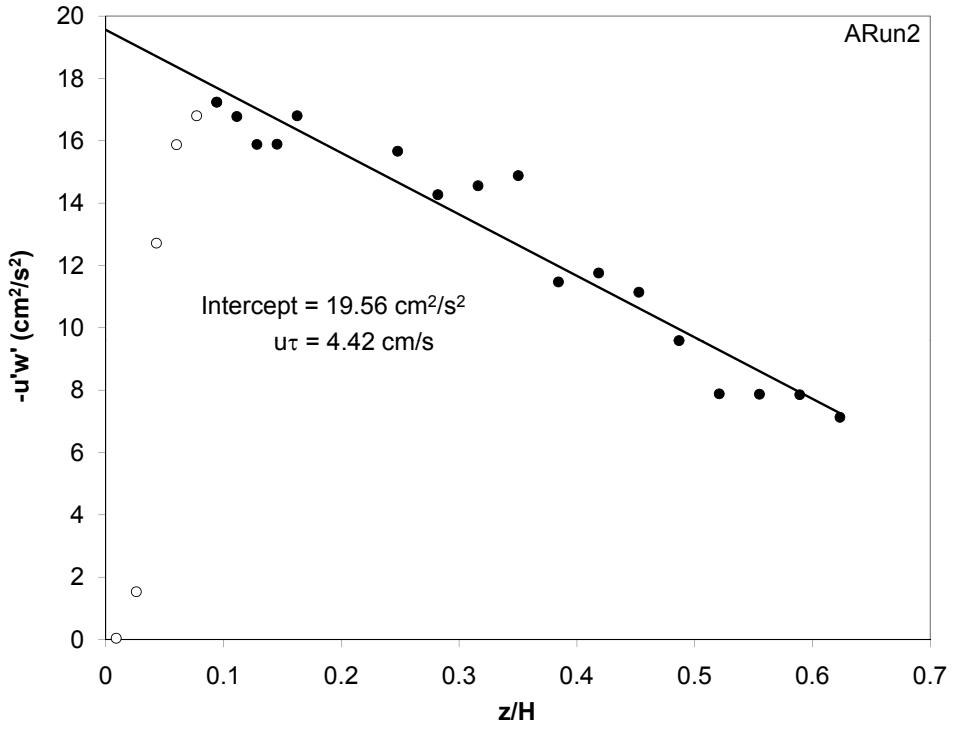

Figure 3.2: Example of Reynolds stress method for finding shear velocity

3.3.3 Clauser Method

The Clauser method of finding shear velocity is documented by Kironoto and Graf [37]. This method uses the presumption that the log-law can be fit to the inner (viscous) region. The log-law can be written as:

$$\frac{\overline{u}}{u_\tau} = \frac{1}{\kappa} \ln\left(\frac{z}{k_s}\right) + B \tag{3.6}$$

where $\overline{u}$ is the time-averaged streamwise velocity, κ is the Von Karman constant, z is the distance above the origin (as found for each experimental run in Section 3.2), and B is an integration constant.

The Von Karman value (κ) was presumed equal to 0.41. k_s was assumed equal to the median diameter (sieve size) of gravel (2.46 cm). By plotting $\ln(z/k_s)$ versus velocity, u, the shear velocity, u_τ, and integration constant, B, were found by

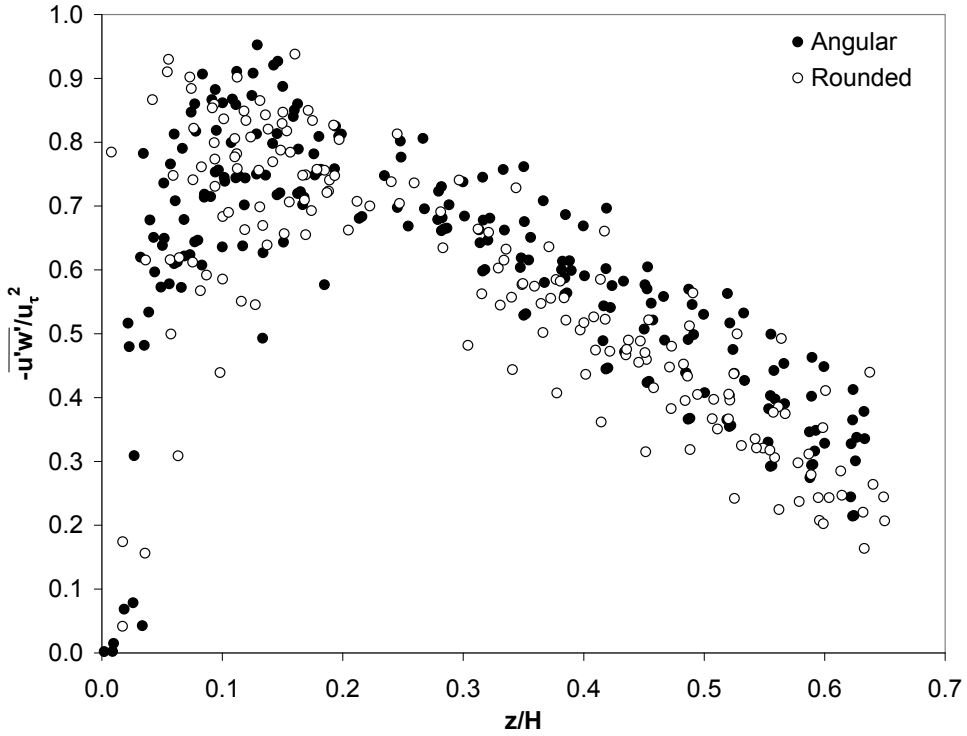

Figure 3.3: Reynolds stress distribution

evaluating the curve fit at $z = 0$. Figure 3.4 is an example of how shear velocity was found for all experimental runs.

Figure 3.5 displays a box plot of the shear velocity calculated for each method. The Clauser method showed the most variance and appears to give higher values in most of the runs. There was no significant difference between angular and rounded gravel beds for any of the methods. Appendix C contains a more detailed description on shear velocities.

3.4 Nikuradse Sand Roughness and Coles Wake Parameter

The Reynolds stress method and Clauser method were used to find the Nikuradse sand roughness (k_s) and Coles wake parameter (Π).

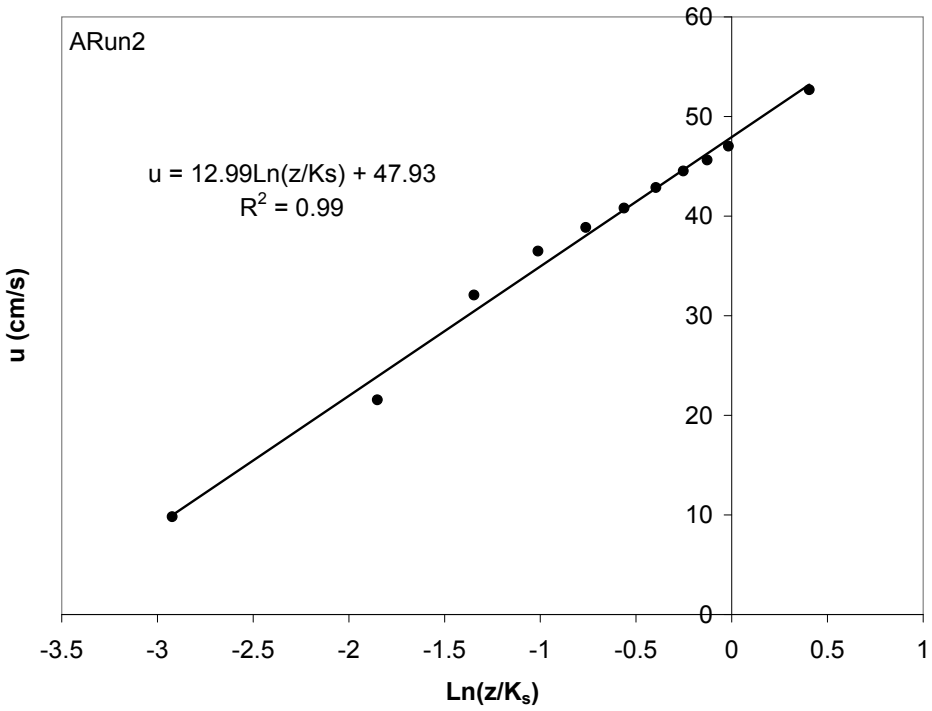

Figure 3.4: Example of Clauser method for finding shear velocity

3.4.1 Reynolds Stress Method

The law of the wake was used to calculate mean velocity based on shear velocities. found using the Reynolds stress method. The law of the wake can be written as:

$$\frac{\overline{u}}{u_\tau} = \frac{1}{\kappa}\ln\left(\frac{z}{k_s}\right) + B + \frac{2\Pi}{\kappa}\sin^2\left(\frac{\pi z}{2H}\right) \tag{3.7}$$

Changing the value of Nikuradse's equivalent sand roughnes, k_s, changes the location of the curve, while modifying the Coles wake parameter, Π, affects the shape of the curve. A best fit curve was visually applied for each experimental data set profile; an example of this is shown in Figure 3.6. The k_s was comparable to the gravel c-axis as suggested by others [34] [36] [14].

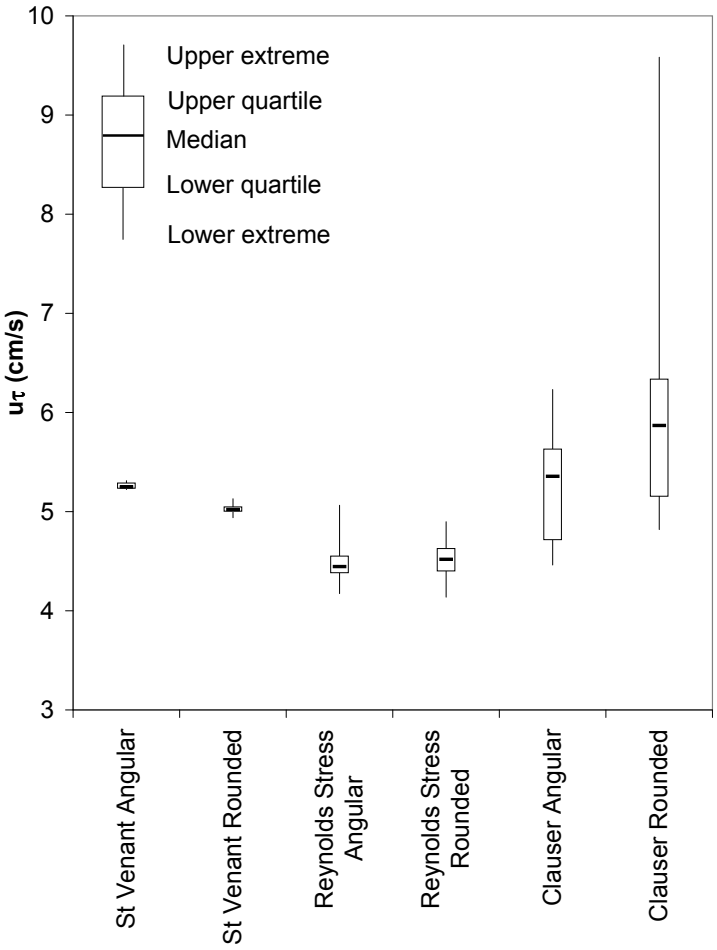

Figure 3.5: Box plot of shear velocity for all experimental runs and methods

3.4.2 Clauser Method

In the Clauser method, k_s was found from Equation 3.6 using a least-squares fit line to produce a value of $B = 8.5$. A value of 8.5 has often been sited in literature as the appropriate integration constant for rough gravel beds [63] [56] [37].

Π was found using Coles law of the wake expressed in terms of velocity defect, written as:

$$\frac{\overline{u_m} - u}{u_\tau} = -\frac{1}{\kappa} \ln\left(\frac{z}{\delta}\right) + \frac{2\Pi}{\kappa} \cos^2\left(\frac{\pi z}{2\delta}\right) \tag{3.8}$$

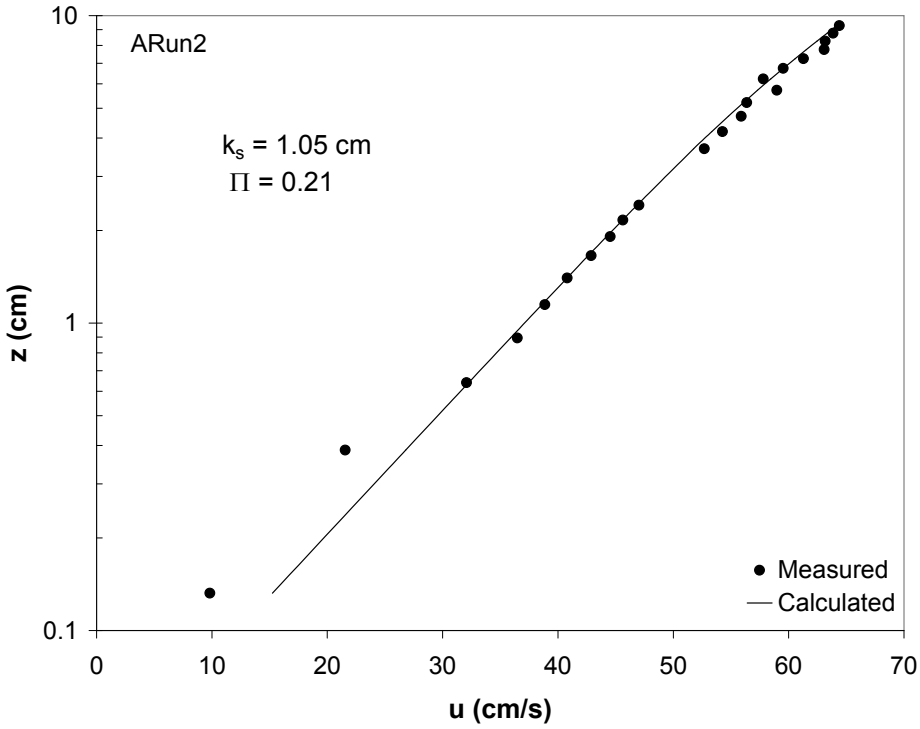

Figure 3.6: k_s **and** Π **found by Reynolds stress method**

where κ was assumed equal to 0.41, and $\overline{u_m}$ is the maximum time-averaged streamwize velocity.

Since the ADV did not allow measurements close to the water surface, the velocity profile was extrapolated to the surface and assumed to equal $\overline{u_m}$. A least squares line was fit to the inner region ($z/\delta \leq 0.2$), and extrapolated to where $z/\delta = 1$ (see Figure 3.7). When $z/\delta = 1$, Equation 3.8 reduces to:

$$\frac{\overline{u_m} - u}{u_\tau} = \frac{2\Pi}{\kappa} \tag{3.9}$$

Statistical box and whisker diagrams are shown in Figure 3.8 for the k_s and Π estimated using the Reynolds stress and Clauser methods. A statistical t-test supports the visual evaluation of Figure 3.8, namely, that no significant difference between angular and rounded beds exist except for Π when calculated with the Clauser method. More detail on k_s and Π values can be found in Appendix C.

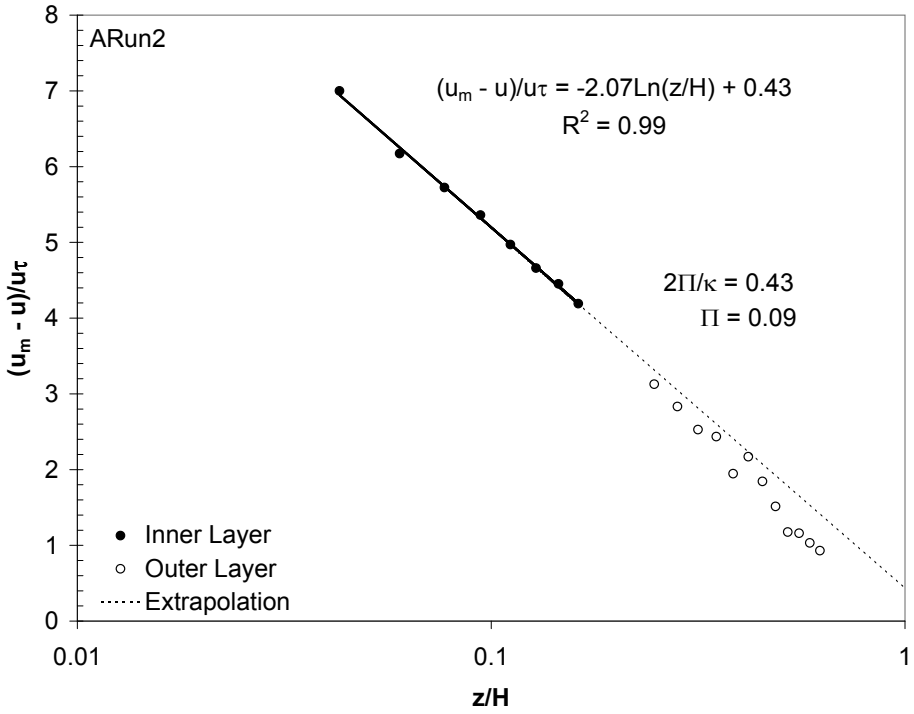

Figure 3.7: Coles wake parameter found by Clauser method

3.5 Flow Resistance

The roughness Reynolds numbers ($\mathbb{R}_\tau = k_s u_\tau/\nu$) in these experiments were much higher than 67 (Table 3.1), meaning the bed acted as a rough as opposed to a smooth wall. The roughness has been shown by others to be a function of relative roughness (k_s/H) [85] and spacing [57] [28] of roughness elements. Although on average k_s increased with angularity (38%), the increase was not statistically significant. The lack of a significant difference in k_s between angular and rounded gravel beds in this set of experiments may be a result of the spacing between the elements. It is known that roughness height (k_s) increases as the spacing between gravels increases to a maximum value. As the arrangement of roughness elements approaches maximum surface density, the roughness between different element shapes approaches the same value [57].

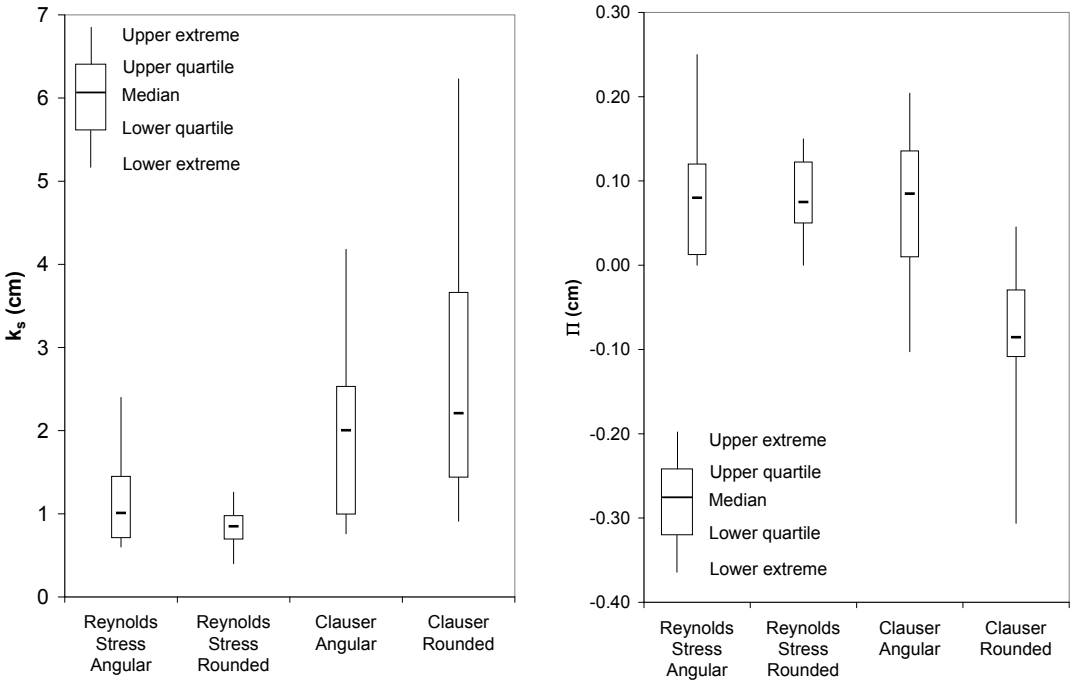

Figure 3.8: Box plot of k_s and Π values

Some of the more common resistance parameters used in engineering situations are the Chezy coefficient, Darcy-Weisbach factor, and the Manning coefficient. The hydraulic radius of the bed was found using the side-wall correction procedure of Vanoni and Brooks [75], and resulting resistance parameter values for the angular and rounded beds are shown in Table 3.2.

Table 3.2: Roughness values

Gravel Bed	Manning n	Darcy f	Chezy C $m^{1/2}/sec$
Rounded	0.020	0.059	36.4
Angular	0.022	0.073	32.8

3.6 Turbulence Characteristics

3.6.1 Turbulence Intensity Distribution

Turbulence intensity distribution is generally divided into two regions: near the bed ($z/H < 0.2 - 0.3$), and far from the bed ($z/H \geq 0.2 - 0.3$). Near the bed, the roughness elements have a direct impact on the turbulence, and the turbulence intensity increases with z up to a peak value (TI_{max}) [12]. The turbulence intensity then steadily decreases in the region far from the bed and becomes independent from the bed roughness [37] [12]. Excluding the near wall region ($z/H < 0.2$), the following exponential relationship for turbulence intensity has been proposed [46].

$$\frac{TI_i}{u_\tau} = D_i e^{-\lambda_i (z/H)} \tag{3.10}$$

where D_i and λ_i are constants for relative roughness (H/k_s) greater than 4 [82]. The subscript i corresponds to the u, v, and w directions. By fitting Equation 3.10 to the data collected away from TI_{max}, the constants D_i and λ_i were found and tested for statistical differences. If the probability of the means being equal was less than 0.05, the difference was considered significant.

The streamwise component (u) of turbulence intensity showed no statistical significance between angular and rounded gravel beds, but the vertical component showed a statistical difference in D_w using both the Reynolds stress method (P = 0.02) and the Clauser method (P = 0.02). They also showed a high probability (P = 0.99) that λ_w does not change with angularity. The maximum turbulence intensity value in the vertical direction TI_{max} was also significantly different between the alternate bed angularity using the Reynolds stress method. On average, TI_{max} in the vertical (w) direction increased by 4.9% (0.85 to 0.89 cm/s) from the rounded to angular bed.

A least-squares line was also applied to all experimental runs for each gravel set and compared with distributions recommended by others (Figures 3.9 - 3.11). The curve fit found by Nezu (1977) [47] and Nezu and Rodi (1986) [50] were for hydraulically smooth flow regimes. The distribution of Kironoto and Graf (1994) [37] were for a hydraulically rough gravel bed. The Nikora and Goring (2000) [52] distributions were found for a hydraulically rough weakly mobile gravel bed. In the outer turbulence intensity region ($z/H > 0.2$), the curve fit showed a constant increase of turbulence intensity distribution in the vertical direction of 6.1% from the rounded to angular gravel bed. Although not statistically significant, there was also an increase in the streamwise ($\approx 4.9\%$) and traverse ($\approx 4.8\%$) directions. The clear distinction between the two gravel beds shown in the vertical direction (Figure 3.11) as opposed to the other two component directions may be due to noise associated with the ADV probe geometry [77]. Voulgaris and Trowbridge [77] found that turbulence intensity measurements from an ADV seemed to agree with predictive equations much better in the vertical direction, and was thought to be a result of the probe geometry.

The TI generally reached a peak value at a distance of $z/H \approx 0.1$ as observed by others [82] [12]. For $z/H < 0.1$ no distinguishing difference could be seen between the angular and rounded gravel beds. Figure 3.12 shows the inner region of turbulence intensity.

In the region close to the bed, the gravel geometry (form, size, and position) are expected to influence the turbulence intensity [12]. The large spread of values in this region suggests that the ADV frequency sampling rate may not be high enough to accurately capture the turbulence, or boundary reflections are causing instrument noise which is distorting the turbulence intensity. All curve-fit turbulence intensity data is provided in Appendix C.

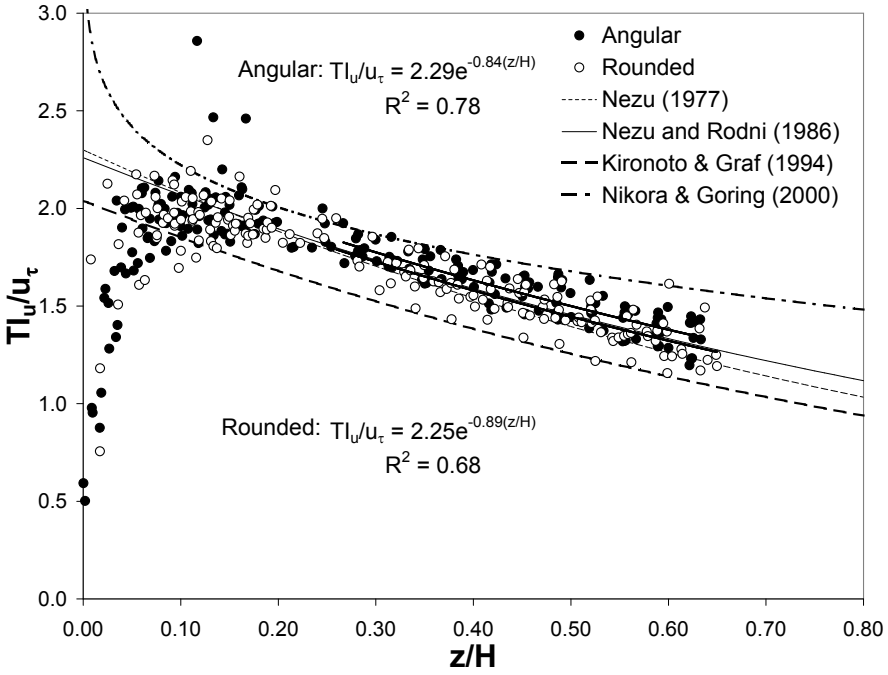

Figure 3.9: TI_u **distribution (Reynolds stress method)**

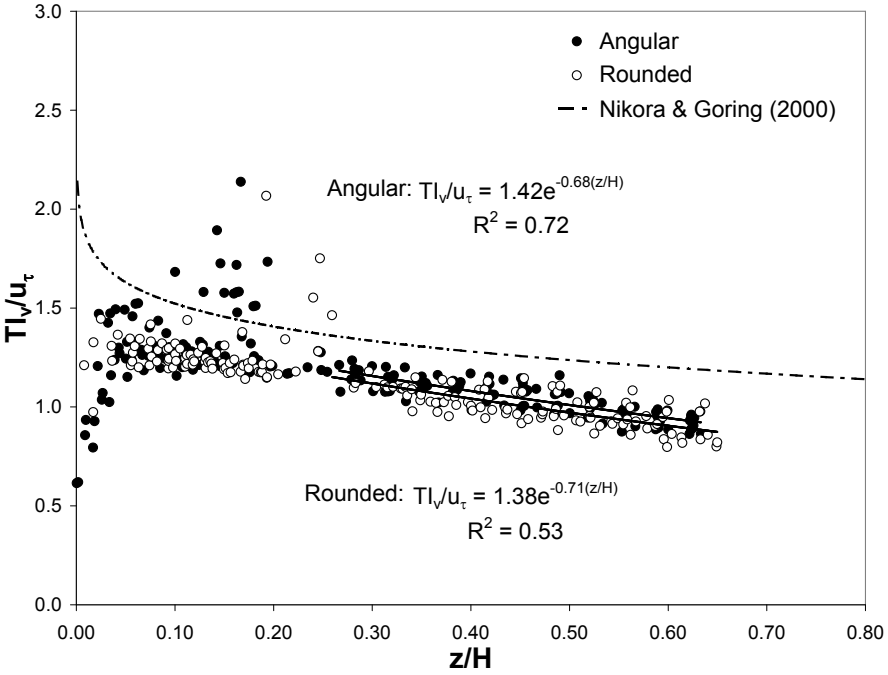

Figure 3.10: TI_v **distribution (Reynolds stress method)**

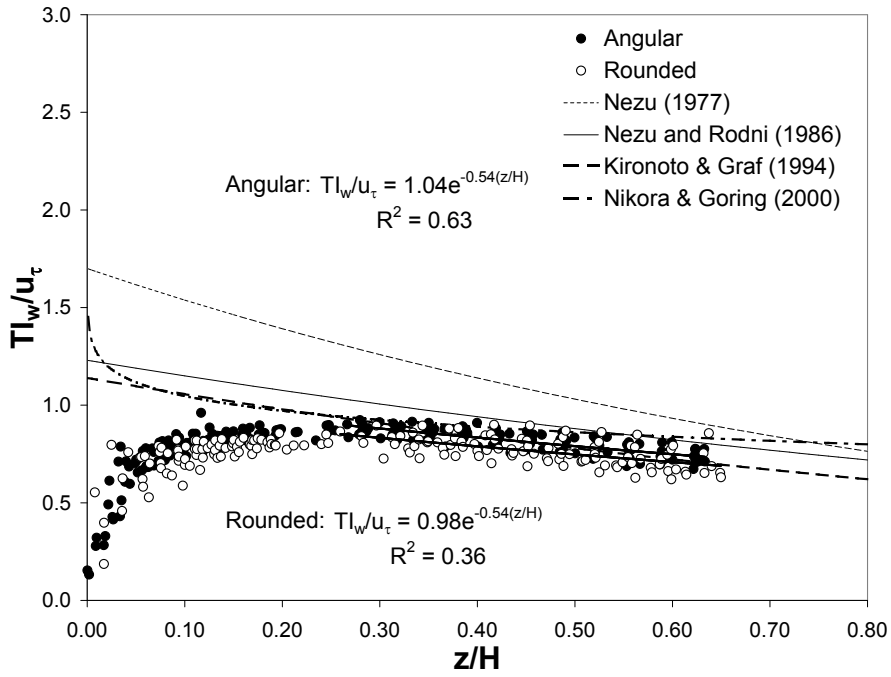

Figure 3.11: TI_w distribution (Reynolds stress method)

3.6.2 Turbulent Kinetic Energy Distribution

Turbulent kinetic energy (K) can be derived from turbulence intensity as follows:

$$K = \frac{1}{2}\left(TI_u^2 + TI_v^2 + TI_w^2\right) \tag{3.11}$$

As with TI, the Reynolds stress method of shear velocity resulted in a closer match of proposed distributions of K. The distribution between angular and rounded gravel is shown in Figure 3.13. A curve-fit of angular versus rounded gravel shows a slight increase ($\approx 2.2\%$) in the distribution ($K^{0.5}/u_\tau$) for angular gravel.

3.7 Mixing Length Scales

There are three standard scales used to give insight into the structure of turbulence. The integral scale is the largest and is representative of the energy-containing

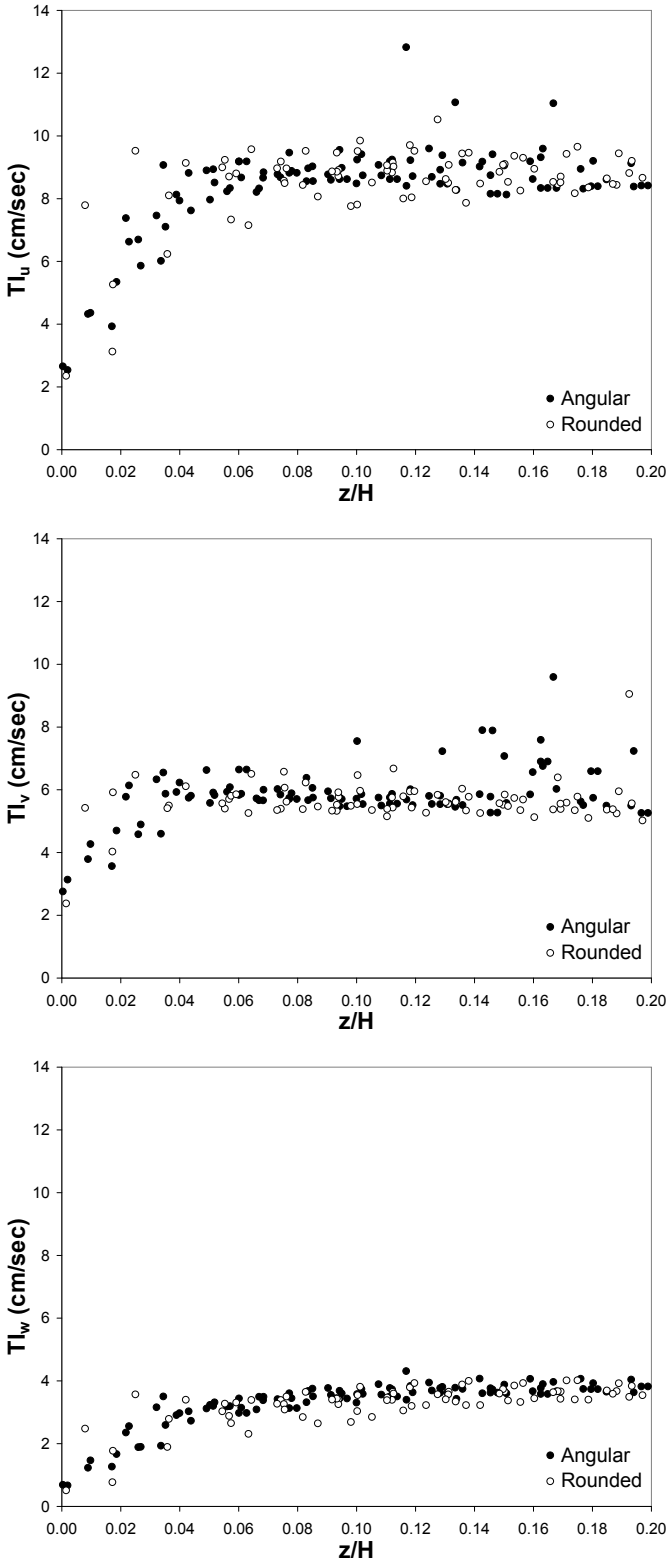

Figure 3.12: TI **distribution in inner region**

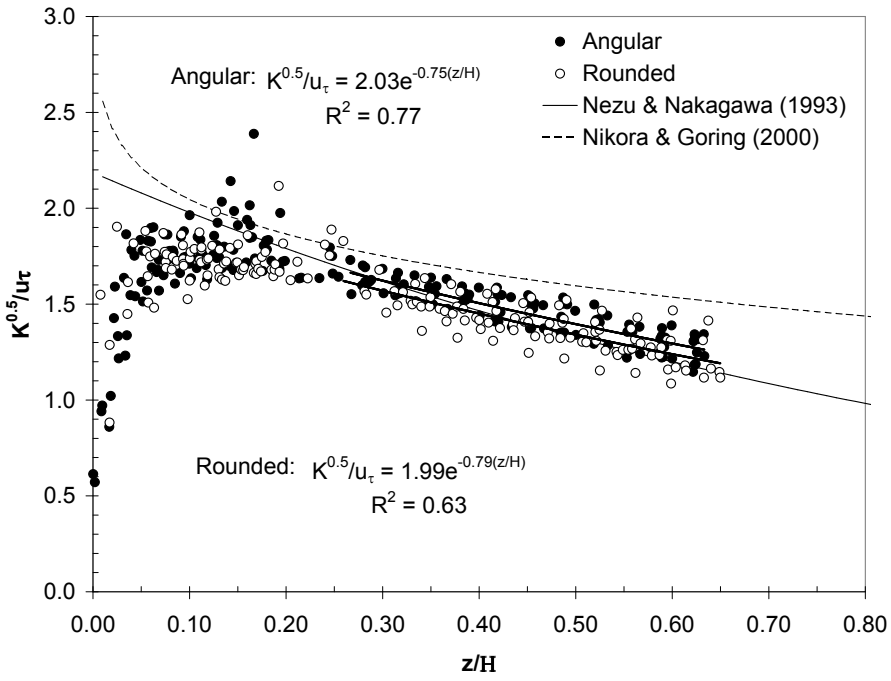

Figure 3.13: K **distribution (**u_τ **from Reynolds stress method)**

eddies. The Taylor microscale is representative of the eddy size where the turbulent kinetic energy is in equilibrium (dissipation and generation are at the same rate), and the smallest scale is the Kolmogorov miscroscale corresponding to the energy dissipation size. The integral scale (Λ) and Taylor microscale (λ) can be estimated using the autocorrelation function. The integral of the autocorrelation function to the first zero crossing was used to find the integral scale. The Taylor microscale was found by extrapolating the first three points of the autocorrelation function to zero. Appendix C provides further details of the calculation process. Figure 3.14 shows a box plot for the integral scales and Taylor microscale. Although Doppler noise may bias the autocorrelation and integral scale to higher values [27], the microscale is several orders of magnitude larger than the ADV sampling volume length. This suggests that the sampling volume size of the ADV is sufficiently small to capture turbulence measurements. Therefore, the scatter shown in TI values close to the bed

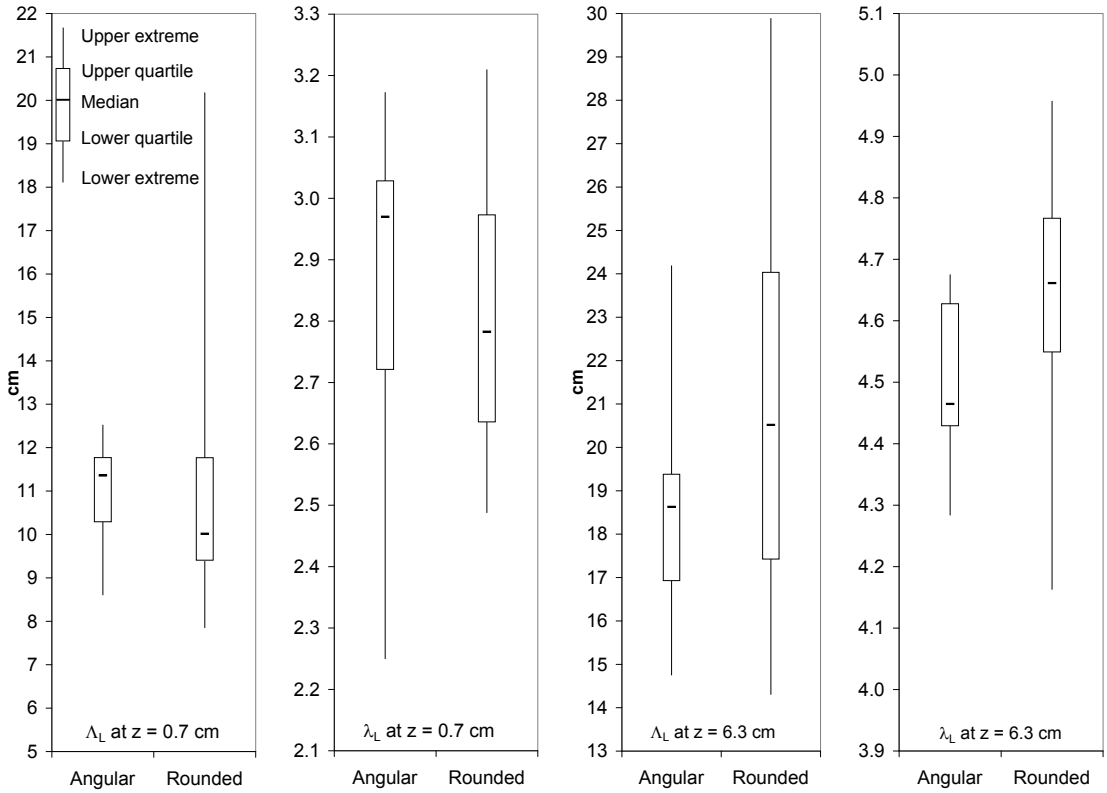

Figure 3.14: Box plot of integral scales (Λ) and Taylor microscales (λ)

are a result of Doppler noise, low sampling frequency and/or boundary reflection, and not a result of the ADV sampling size being too large.

Chapter 4

Conclusions

These experiments used an ADV to quantify the effects of gravel angularity on turbulence in open-channel uniform flow in difficult flow conditions (close to bed, intermediate-roughness scale). Nikuradse sand roughness (k_s) was found to be comparable to the gravel c-axis. Although not statistically significant for this set of experiments, k_s on average increased with angularity, as reported by others [57] [28]. Shear velocity was calculated three different ways, and the effects of each method have been outlined. Although all methods gave similar results, the Reynolds stress method resulted in the closest visual match to proposed distributions from experimental data for turbulence intensity and turbulent kinetic energy. No difference could be distinguished in shear velocity between the angular and rounded gravel beds. The average bed origin was $0.24D_{50}$ and $0.21D_{50}$ for the angular and rounded gravel respectively. Although both were similar to that found by others, no statistical significance could be distinguished between the two.

Turbulence intensity measurements showed considerable scatter near the bed ($z/H < 0.2$), which suggests that the ADV frequency sampling rate was not high enough to accurately capture the turbulence, and/or distortions occurred from boundary reflection and instrument noise. There was less scatter in the vertical (w) direction and differences were found to be statistically significant. The maximum turbulence intensity increased by about 5% for the angular bed, which occurred at a distance of $z/H \approx 0.1$. Away from the bed ($z/H \geq 0.2$) there was a 6.1% increase in tur-

bulence distribution (TI/u_τ) in the vertical (w) direction. Although not statistically significant, an increase of 4.9% and 4.8% were also seen in the u and v directions respectively. These resulted in a slight increase (2.2%) of turbulent kinetic energy distribution ($K^{0.5}/u_\tau$) for the angular gravel bed. The increased scatter in the u and v directions could be caused by instrument noise inherent in its geometry as explained by Voulgaris and Trowbridge [77].

Integral scales as well as Taylor microscales were computed at two depths ($z = 0.7$ and 6.3 cm). The Taylor length microscale was larger than the ADV sampling volume, which suggests that the sampling size of the ADV should be sufficiently small to capture the turbulence in this set of experiments. Due to the scatter of turbulence values near the bed, however, the instrument noise as well as a low sampling frequency may be hindering the resolution of turbulence as suggested by García et al. [27]. This hindrance, however, seems to have less of an effect on turbulence measurements in the vertical direction.

Based on measurements in this set of experiments it is expected that similar increases of TI_{max} and TI/u_τ for angular gravel beds should be significant in the u and v directions. Further research into the understanding of angularity on turbulence should be coupled with improving the ability of the ADV resolution capabilities.

Chapter 5

Notation

The following symbols are used in this document:

C	Chezy friction coefficient, [$L^{1/2}/T$]
D_{xx}	particle sieve size that is xx% larger than the rest of the bed material, [L]
f	Darcy-Weisbach friction factor
F	Form factor computed from particle axis
f_R	acoustic Doppler velocimeters user-set frequency, [T^{-1}]
FF	Form factor computed using image analysis
g	gravitational acceleration, [L/T^2]
H	water depth, [L]
k_s	Nikuradse's equivalent sand diameter roughness, [L]
n	Manning coefficient
P_w	wetted perimeter, [L]
Q	volumetric flow rate, [L^3/T]
R	hydraulic radius (A/P_w), [L]
$\mathbb{R}$	Reynolds number $\left(\frac{4RU}{\nu}\right)$
$\mathbb{R}_\tau$	roughness Reynolds number ($k_s u_\tau/\nu$)
S	slope of the energy grade line
S_{xx}	particle c-axis size that is xx% larger than the rest of the bed material, [L]
u	instantaneous streamwize (x) velocity, [L/T]
U	spatially-average horizontal (x) velocity, [L/T]
u_m	maximum horizontal (x) velocity, [L/T]
u_τ	shear velocity $\left(\sqrt{\frac{\tau_o}{\rho}}\right)$, [L/T]
TI_i	turbulence intensity of the i-direction, [L/T]
TI_{max}	maximum turbulence intensity, [L/T]
v	instantaneous transverse velocity, [L/T]
v'	transverse (y) velocity fluctuation, [L/T]
w	instantaneous vertical velocity, [L/T]
w'	vertical velocity fluctuation, [L/T]
z	vertical distance from bed origin, [L]
γ	specific weight of water ρg, [$ML^{-2}T^{-2}$]
κ	von Kármán's constant

ν kinematic viscosity [L^2/T]
Π Cole's wake parameter
ρ density of water, [M/L^3]
τ shear stress, [$ML^{-1}T^{-2}$]
τ_o shear stress at the boundary, [$ML^{-1}T^{-2}$]

References

[1] J. Aberle and G. M. Smart. L'influence de la structure de rugosite sur la resistance a des ecoulements en fortes pentes; the influence of roughness structure on flow resistance on steep slopes. *Journal of Hydraulic Research*, 41(3):259–269, 2003.

[2] H. Afzalimehr and F. Anctil. Accelerating shear velocity in gravel-bed channels. *Hydrological Sciences - Journal-des Sciences Hydrologiques*, 45(1):113–124, 2000.

[3] J. Aguirre-Pe and R. Fuentes. Resistance to flow in steep rough streams. *Journal of Hydraulic Engineering*, 116(11):1374–1387, 1990.

[4] T. Al-Rousan, E. Masad, E. Tutumluer, and T. Pan. Evaluation of image analysis techniques for quantifying aggregate shape characteristics. *Construction and Building Materials*, 21:978–990, 2007.

[5] P. J. Barrett. The shape of rock particles, a critical review. *Sedimentology*, 27:291–303, 1980.

[6] J. C. Bathurst. Flow resistance estimation in mountain rivers. *Journal of Hydraulic Engineering*, 111(4):625–643, 1985.

[7] J. C. Bathurst, R. M. Li, and D. B. Simons. Resistance equation for large-scale roughness. *Journal of Hydraulic Engineering*, 107(12):1593–1613, 1981.

[8] M. Bayazit. Free surface flow in a channel of large relative roughness. *Journal of Hydraulic Research*, 14(2):115–126, 1976.

[9] P. S. Bernard and J. W. Wallace. *Turbulent Flow Analysis, Measurement, and Prediction*, volume 1 of *1*. John Wiley and Sons, Hoboken, New Jersey, 1st edition, 2002.

[10] K. Bunte and S. R. Abt. Sampling surface and subsurface particle-size distributions in wadable gravel- and cobble-bed streams for analyses in sediment transport, hydraulics, and streambed monitoring. General Technical Report RMRS-GTR-74, USDA Forest Service, Rocky Mountain Research Station; 240 West Prospect Road; Fort Collins, CO 80526, May 2001.

[11] A. H. Cardoso, W. H. Graf, and G. Gust. Uniform flow in smooth open-channel. *Journal of Hydraulic Research*, 27(5):603–616, 1989.

[12] F. G. Carollo, V. Ferro, and D. Termini. Analyzing turbulence intensity in gravel bed channels. *Journal of Hydraulic Engineering*, 131(12):1050–1061, 2005.

[13] L. Cea, J. Puertas, and L. Pena. Velocity measurements on highly turbulent free surface flow using adv. *Experiments in Fluids*, (42):333–348, January 2007.

[14] F. G. Charlton, P. M. Brown, and R. W. Benson. The hydraulic geometry of some gravel rivers in britain. Report IT180, Hydraulics Research Station, Wallingford, U.K., July 1978.

[15] X. Chen and Y. Chiew. Response of velocity and turbulence to sudden change of bed roughness in open-channel flow. *Journal of Hydraulic Engineering*, 129(1):35–43, 2003.

[16] N. Chien and Z. Wan. *Mechanics of Sediment Transport*. ASCE, Reston, Virginia, 1999.

[17] V. T. Chow. *Open Channel Hydraulics*. McGraw-Hill, New York, USA, 1959.

[18] F. H. Clauser. The turbulent boundary layer. *Advances in applied mechanics*, 4:1–54, 1956.

[19] D. E. Coles. The law of the wake in the turbulent boundary layer. *Journal of Fluid Mechanics*, 1:191–226, 1956.

[20] C. C. Colosimo and M. Veltri. Friction factor evaluation in gravel-bed rivers. *Journal of hydraulic engineering*, 114(114):861–976, 1988.

[21] R. S. Crofts. A visual measure of single particle form for use in the field. *Journal of Sedimentary Petrology*, 44(3):931–934, 1974.

[22] S. Dey. Sediment threshold. *Applied Mathematical Modelling*, 23(5):399–417, 1999.

[23] S. Dey and R. V. Raikar. Characteristics of loose rough boundary streams at near-threshold. *Journal of hydraulic engineering*, 133(3):288–304, March 2007.

[24] Inc. Engineering Laboratory Design. 12.5 meter research flume operation and maintenance instructions. PO Box 278, 2021 South Highway 61, Lake City, Minnesota 55041, September 2006.

[25] V. Ferro. Friction factor for gravel-bed channel with high boulder concentration. *Journal of Hydraulic Engineering*, 125(7):771–778, 1999.

[26] E. J. Finnemore and J. B. Franzini. *Fluid Mechanics with Engineering Applications*. McGraw-Hill, 10th edition, 2002.

[27] C. M. García, M. I. Cantero, Y. Ni no, and M. H. García. Turbulence measurements with acoustic doppler velocimeters. *Journal of Hydraulic Engineering*, 131(12):1062–1073, 2005.

[28] B. Gomez. Roughness of stable, armored gravel beds. *Water Resources Research*, 29(11):3631–3642, 1993.

[29] D. Goring and V. Nikora. Despiking acoustic doppler velocimeter data. *Journal of Hydraulic Engineering*, 128(1):117–126, 2002.

[30] W. Graf, H. Cao, and L. Suszka. Hydraulics of steep, mobile bed channels. *Proc., 20th Congress of the Int. Assoc. of Hydr. Res., Moscow, USSR*, 7:301–305, 1983.

[31] A. J. Grass. Structural features of turbulent flow over smooth and rough boundaries. *Journal of Fluid Mechanics*, 50:233–255, 1971.

[32] G. A. Griffiths. Flow resistance in coarse gravel bed rivers. *Journal of Hydr. Div.*, 107(7):899–918, 1981.

[33] R. D. Hey. Flow resistance in gravel-bed rivers. *ASCE J Hydraul Div*, 105(4):365–379, 1979.

[34] C. E. Johansson. Orientation of pebbles in running water. *Geografiska Annaler*, 45(2):85–112, 1963.

[35] J. W. Johnson. The importance of considering side-wall friction in bed-load investigations. *Civil Engineering*, 12(6):329–331, June 1942.

[36] H. E. Judd and D. F. Peterson. Hydraulics of large bed element channels. Report PRWG 17-6, Utah State University, Logan, Utah, 1969.

[37] B. A. Kironoto and W. H. Graf. Turbulence characteristics in rough uniform open-channel flow. *Proc. Inst. Civ. Eng., Waters. Maritime Energ.*, 106(1):333–344, 1994.

[38] W. C. Krumbein. Measurement and geological significance of shape and roundness of sedimentary particles. *Journal of Sedimentary Petrology*, 11(2):64–72, 1941.

[39] S. N. Lane, P. M. Biron, K. F. Bradbrook, J. B. Butler, J. H. Chandler, M. D. Crowel, S. J. McLelland, K. S. Richards, and A. G. Roy. Three-dimensional measurements of river channel flow processes using acoustic doppler velocimetry. *Earth Surface Processes and Landforms*, (23):1247–1267, 1998.

[40] R. Lhermitte and R. Serafin. Pulse to pulse doppler sonar signal processing techniques. *Journal of atmospheric and oceanic technology*, 1(4):293–308, 1984.

[41] A. Lohrmann, R. Cabrera, and N. C. Kraus. Acoustic doppler velocimeter (adv) for laboratory use. In *Symposium on Fundamentals and Advancements in Hydraulic Measurements and Experimentation*, New York, 1994. ASCE.

[42] V. Martin, T. S. R. Fisher, R. G. Millar, and M. C. Quick. Adv data analysis for turbulent flows: low correlation problem. In *ASCE/EWRI and IAHR International Conference on Hydraulic Measurements and experimental methods*. ASCE/EWRI and IAHR, 2002.

[43] E. Masad and J. W. Button. Unified imaging approach for measuring aggregate angularity and texture. *Computer-Aided Civil and Infrastructure Engineering*, 15(1):273–273–280, 2000.

[44] S. McLelland and A. Nicholas. A new method for evaluating errors in high-frequency adv measurements. *Hydrological Processes*, (14):351–366, 2000.

[45] M. Muste, T. Vermeyen, R. Hotchkiss, and K. Oberg. Acoustic velocimetry for riverine environments. *Journal of Hydraulic Engineering*, 133(12):1297–1298, 2007.

[46] I. Nezu. Turbulence intensities in open-channel flows. *Proceedings of JSCE*, 261:67–76, 1977.

[47] I. Nezu. Turbulent structure in open channel flows. Doctoral dissertation, Department of Civil Engineering, Kyoto University, 1977.

[48] I. Nezu. Open-channel flow turbulence and its research prospect in the 21st century. *Journal of Hydraulic Engineering*, 131(4):229–246, 2005.

[49] I. Nezu and H. Nakagawa. *Turbulence in open-channel flows*. Balkema, Rotterdam, The Netherlands, 1993.

[50] I. Nezu and W. Rodni. Open-channel flow measurements with a laser doppler anemometer. *Journal of Hydraulic Engineering*, 112(5):335–355, 1986.

[51] V. Nikora and D. Goring. Effects of bed mobility on turbulence structure. In *NIWA Internal Report No. 48*, 1998.

[52] V. Nikora and D. Goring. Flow turbulence over fixed and weakly mobile gravel beds. *Journal of Hydraulic Engineering*, 126(9):679–690, 2000.

[53] V. Nikora, D. Goring, I. McEwan, and G. Griffith. Spatially averaged open-channel flow over rough bed. *Journal of Hydraulic Engineering*, 127(2):123–133, 2001.

[54] V. Nikora, K. Koll, I. McEwan, S. McLean, and A. Dittrich. Velocity distribution in the roughness layer of rough-bed flows. *Journal of Hydraulic Engineering*, 130(10):1036–1042, 2004.

[55] M. C. Powers. A new roundness scale for sedimentary particles. *Journal of Sedimentary Petrology*, 23:117–119, 1953.

[56] J. A. Reynolds. *Turbulent Flows in Engineering*. John Wiley, London, 1974.

[57] H. Rouse. Critical analysis of open channel resistance. *Journal of Hydraulics Division*, 91(4):1–25, 1965.

[58] H. Schlichting. *Boundar-Layer Theory*. McGraw-Hill, New York, 7 edition, 1979.

[59] E. Silberman. Friction factors in open channels progress report of the task force on friction factors in open channels of the committee on hydromechanics of the hydraulics division. *Journal of the Hydraulics Division*, 89(HY 2):97–143, March 1963. article was signed by R.W. Carter and H.A. Einstein and Julian Hinds and R.W. Powell and E. Silberman. E. Silberman was the chairman.

[60] G. M. Smart. Turbulent velocity profiles and boundary shear in gravel bed rivers. *Journal of Hydraulic Engineering*, 125(2):106–116, 1999.

[61] G. M. Smart, M. J. Duncan, and J. M. Walsh. Relatively rough flow resistance equations. *Journal of Hydraulic Engineering*, 128(6):568–578, 2002.

[62] E. D. Sneed and R. L. Folk. Pebbles in the lower colorado river, texas: a study in particle morphogenesis. *Journal of Geology*, (66):114–150, 1958.

[63] T. Song and Y. M. Chiew. Turbulence measurement in nonuniform open-channel flow using acoustic doppler velocimeter (adv). *Journal of Engineering Mechanics*, 127(3):219–232, 2001.

[64] Sontek. Acoustical doppler velocimeter (adv): sampling volume size and velocity accuracy. Technical note, Sontek/YSI, San Diego, CA, February 1998. www.sontek.com.

[65] Sontek. Acoustic doppler velocimeter principles of operation. Technical note, Sontek/YSI, San Diego, CA, September 2001. www.sontek.com.

[66] Sontek. Personal communication with sontek. e-mail, December 2007.

[67] Sontek. Personal communication with sontek. e-mail, March 2008.

[68] Sontek. Setting the record straight: Adv data acquisition rates and sampling volume size. Technical note, Sontek/YSI, San Diego, CA, 2008. www.sontek.com.

[69] M. C. Stone and R. H. Hotchkiss. Turbulence description in two cobble-bed river reaches. *Journal of Hydraulic Engineering*, 133(12):1367–1378, December 2007.

[70] K. B. Strom and A. N. Papanicolaou. Adv measurements around a cluster microform in a shallow mountain stream. *Journal of Hydraulic Engineering*, 133(12):1379–1389, December 2007.

[71] T. W. Strum. *Open Channel Hydraulics*. McGraw-Hill, 1st edition, 2001.

[72] S. M. Thompson and P. L. Campbell. Hydraulics of a large channel paved with boulders. *Journal of Hydr. Res.*, 17(4):341–354, 1979.

[73] H. M. Tritico and R. H. Hotchkiss. Unobstructed and obstructed turbulent flow in gravel bed rivers. *Journal of Hydraulic Engineering*, 131:635–645, August 2005.

[74] L. C. van Rijn. Sediment transport. part 1: Bed load transport. *Journal of Hydraulic Engineering*, 110(10):1431–1456, 1984.

[75] V. A. Vanoni. *Sedimentation Engineering*, volume 54. ASCE Manuals and Reports on Engineering Practices, New York, 1975.

[76] V. A. Vanoni, N. H. Brooks, and J. F. Kennedy. Lecture notes on "sediment transportation and channel stability". Report KH-R-1, California Institute of Technology, Pasadena, California, 1960.

[77] G. Voulgaris and J. Trowbridge. Evaluation of the acoustic doppler velocimeter (adv) for turbulence measurements. *Journal of Atmospheric and Oceanic Technology*, 15(1):272–288, 1998.

[78] H. Wadell. Volume, shape, and roundness of rock particles. *Journal of Geology*, 40:443–451, 1932.

[79] H. Wadell. Sphericity and roundness of rock particles. *Journal of Geology*, 41:310–331, 1933.

[80] T. Wahl. Analyzing adv data using winadv. Minneapolis, Minnesot, 2000. Joint Conference on Water Resources Engineering and Water Resources Planning and Management.

[81] T. Wahl. Discussion of "despiking acoustic doppler velocimeter data" by derek g. goring and vladimir i. nikora. *Journal of Hydraulic Engineering*, 129(6):484–487, 2003.

[82] J. Wang, Z. Dong, C. Chen, and Z. Xia. the effects of bed roughness on the distribution of turbulent intensities in open channel flow. *Journal of Hydraulic Research*, 31(1):89–98, 1993.

[83] L. Wang, X. Wang, L. Mohammad, and C. Abadie. Unified method to quantify aggregate shape angularity and texture using fourier analysis. *Journal of Materials in Civil Engineering*, 17(5):498–504, October 2005.

[84] F. M. White. *Viscous Fluid Flow*. McGraw-Hill, New York, NY, 3rd edition, 2006.

[85] E. Wohl and H. Ikeda. The effect of roughness configuration on velocity profiles in an artificial channel. *Earth Surface Processes and Landforms*, (23):159–169, 1998.

[86] H. J. Zippe and W. H. Graf. Turbulent boundary-layer flow over permeable and non-permeable rough surfaces. *Journal of Hydraulic Research*, 21(1):51–65, 1983.

Appendix A

Literature Review

Understanding flow interaction with rough beds has been studied for many years. The purpose of this literature review is to highlight some of the major accomplishments and understandings that are relevant to gravel angularity affecting flow characteristics. Although the affects of gravel angularity on turbulence have not been studied extensively, there are thousands of studies that have been done on other roughness objects that can be related to the roughness associated with gravel angularity. The first topic that will be covered briefly is the characterization of gravel angularity. The next topic will be flow resistance, which is closely related to and followed by the topics of velocity distribution and turbulence characteristics.

A.1 Particle Description

One of the main difficulties in predicting roughness of a non-geometric object is to quantify the physical attributes of the element. These physical attributes can be quantified by size, shape, and spacing. In many different applications particle-size can be described by using just one characteristic length such as the intermediate principle axis or the size of the sieve for which a particle was retained [10]. Since in most natural settings there is a distribution of sediment size, it has become somewhat standard to report a representative size such as D_{xx}. Where D_{xx} is the retained sieved diameter size in which $xx\%$ of the size distribution (by weight) is smaller. A particles axis refer to the three mutually perpendicular particle dimensions shown in Figure

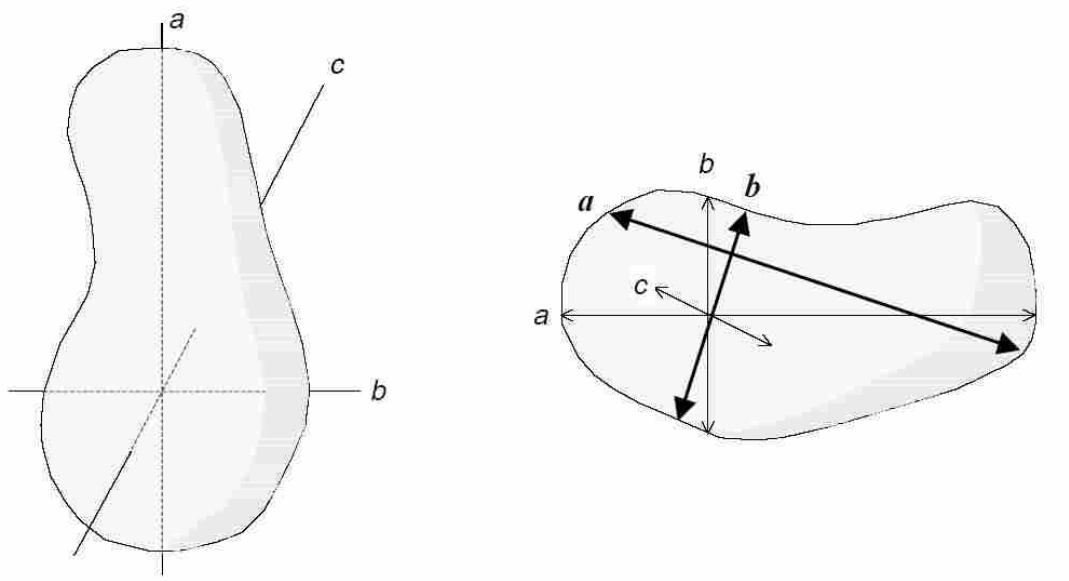

Figure A.2: Particle axes (from [10])

A.2. The longest, intermediate, and shortest axis are referred to as the a, b, and c-axis, respectively. The meaning of quantifying shape has different definitions in the literature, none of which is universally sanctioned [5]. One way is to divide the character of shape into three independent properties: form, roundness and surface texture. Figure A.3 shows the difference between the three properties. Form describes the general geometry, such as triangular, circular, etc. The roundness describes how jagged the corners are, and the surface texture describes how irregular the edges of the object are.

Form can be further described by taking ratios from the three axes lengths of the rock particle. Barrett [5] gives a summary of different formulas used to represent form from axis lengths. Bunte and Apt [10] recommend using the *nominal diameter* for studies where mass or volume of a particle may be more important than the b-axis length or the sieve diameter. The nominal diameter is the diameter a particle would have if its volume was expressed as a sphere and is computed as:

$$D_n = (a * b * c)^{(1/3)} \tag{A.12}$$

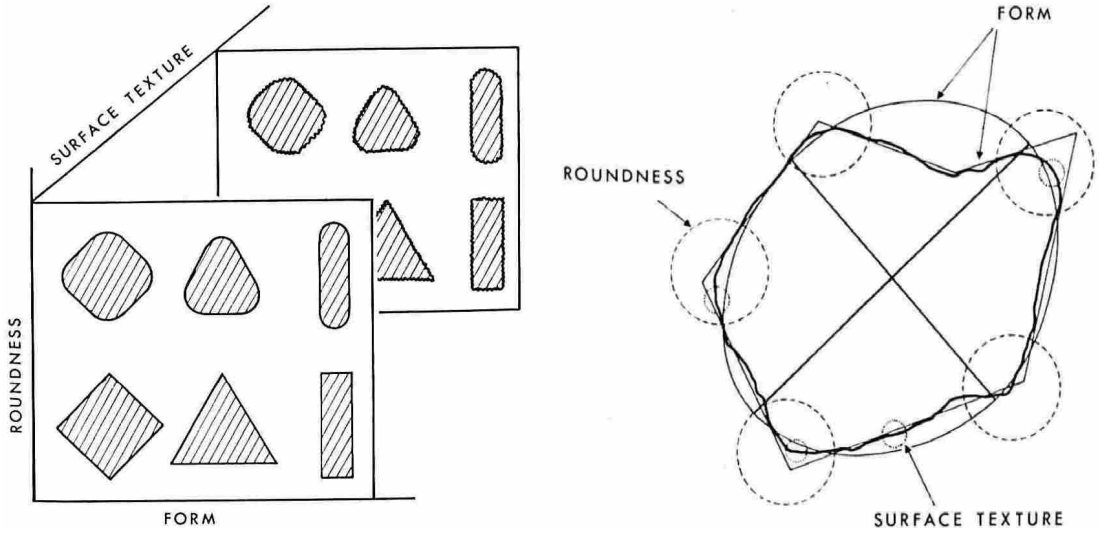

Figure A.3: Form, roundness, and surface texture (from [5])

Particles that are sieved to the same size may have different representative axis lengths. Bunt and Apt [10] have developed a way to relate a square-hole sieve opening, D_s, to b-axis size and particle flatness (c/b). This relationship is given as:

$$\frac{D_s}{b} = \sqrt{\frac{1}{\sqrt{2}} * 1 + \left(\frac{c}{b}\right)^2} \tag{A.13}$$

Roundness is a measure of smoothness or lack of angularity [79]. Measuring roundness presents difficulty since it is inherently a 3-dimensional property. Most methods have resolved the complexity of 3-dimensional measurements to one of 2-dimensions. This is largely due to the belief held by Wadell [79] that measuring the roundness in 2-dimensions does not significantly bias the 3-dimensional measurement. Wang et al. [83] recently supported this idea with a sensitivity test on 2-dimensional measurements of shape, angularity and texture. They found that orienting the rock particles on different axis did not give significantly different results.

It is also a common practice to quantify angularity in a subjective way. For gravel sized particles, one of the most common ways is to compare it with an another

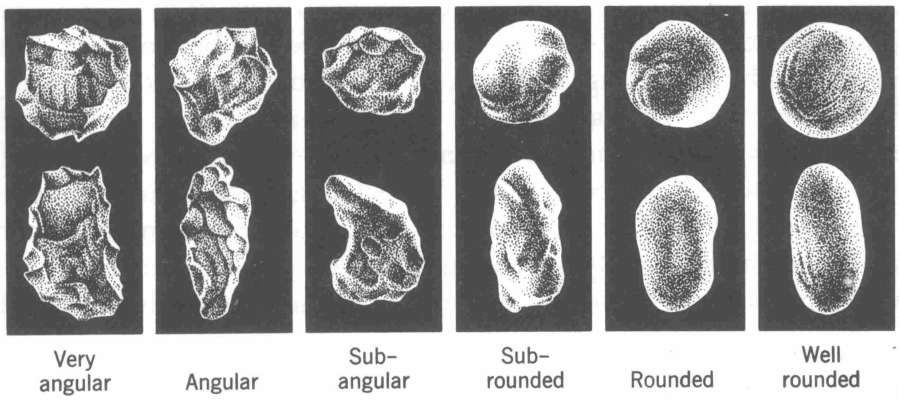

Figure A.4: Visually quantifying angularity versus roundness (from [55])

particle that has been classified. One example of these classified particles can be seen in Figure A.4 suggested by M.C. Powers in 1953. What is known as *sphericity*, is

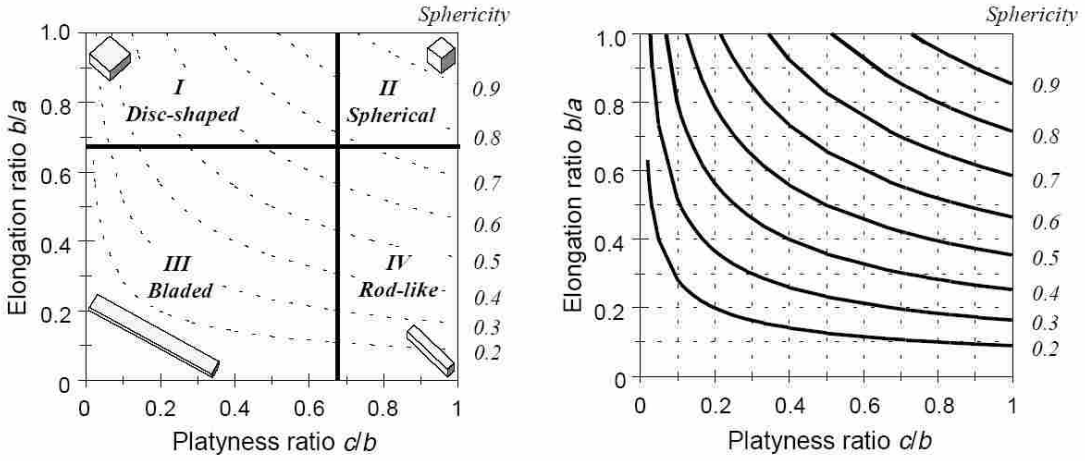

Figure A.5: Sphericity as a function of platyness and elongation (from [10])

another way to analyze angularity. Figure A.5 shows how the axis length ratios can be used to describe the sphericity. The figure also shows what is know as Zingg's classification between disc, spherical, bladed, and rod-like shapes.

What is known as *form factor*, F, can also be used to classify shape in terms of being platy (i.e., disc shaped), bladed (i.e., ellipsoid), and elongated (i.e., rod shaped)

[62]. The form factor is calculated as:

$$F = \frac{a-b}{a-c} \tag{A.14}$$

When $F < 0.33$ the particle is platy, $0.33 < F < 0.67$ defines bladed particles, and elogated particles have $F > 0.67$. The shape can further be quantifies by the *compactness* ratio S.

$$S = \frac{c}{a} \tag{A.15}$$

The form factor (F) and compactness (S) can be used with Figure A.9 to categorize particle shapes.

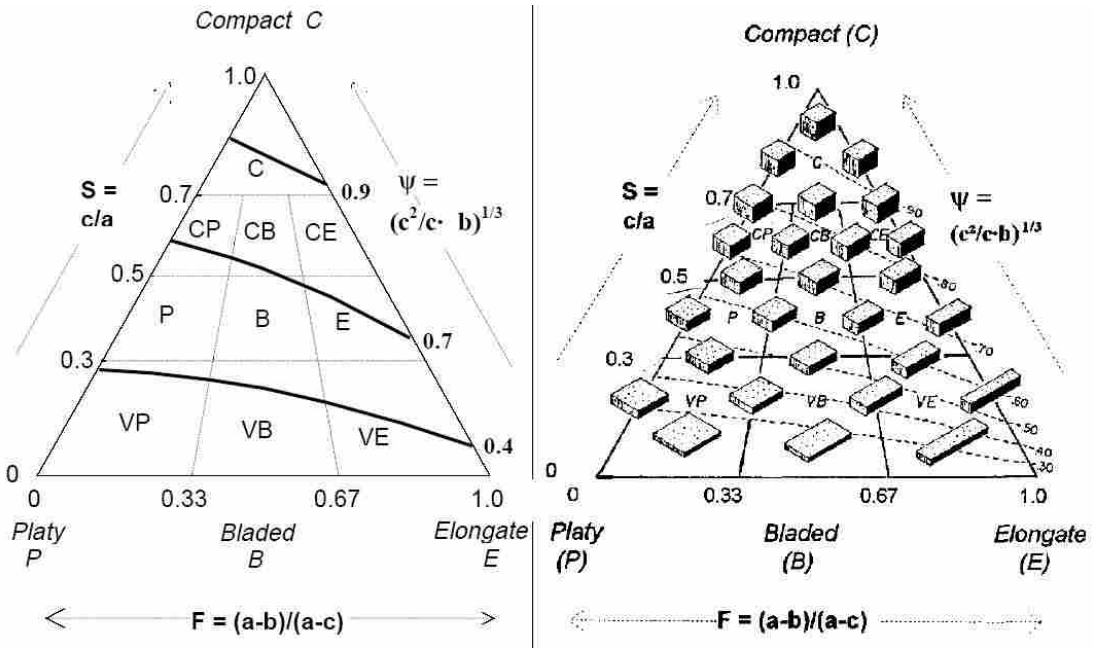

Figure A.6: Shape as a funciton of form factor and compactness (from [10])

Wadell [78] also developed a method of computing a roundness parameter, P. The computation is a bit involved and entails the mean size of the radii that can be fitted into the number of corners that a particle has which is then divided by

the radius of the maximum inscribed circle. Low values of P correspond to a more angular particle, whereas a higher value corresponds to a rounder particle. A P-value of 1, would be for a perfect sphere. Krumbein [38] developed a chart for visual estimation based on Wadell's P value. this allows visual comparison instead of doing the computation (see Figure A.7).

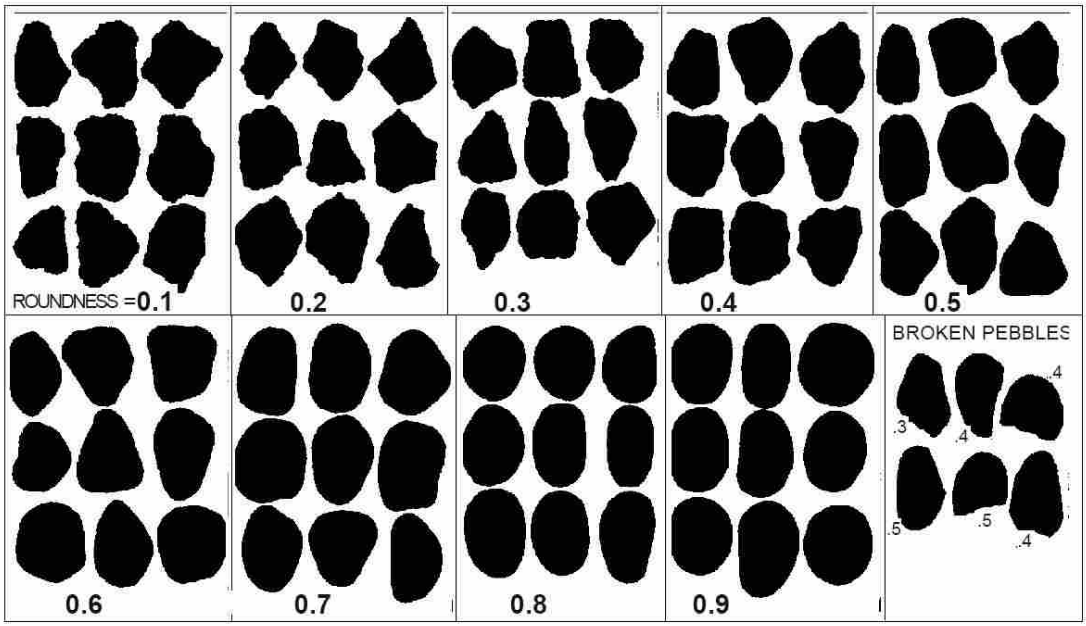

Figure A.7: Visual chart for roundness P value (from [10])

Another visual chart was developed by Crofts [21] to distinguish between sphericity and angularity. This can be seen in Figure A.8.

A.2 Flow Resistance

There have been many equations (both analytical and empirical) that have been proposed to give a relationship between average velocity and channel characteristics. These equations relate average velocity to known parameters such as slope, hydraulic radius, and roughness. For open-channel flow, there is the commonly used

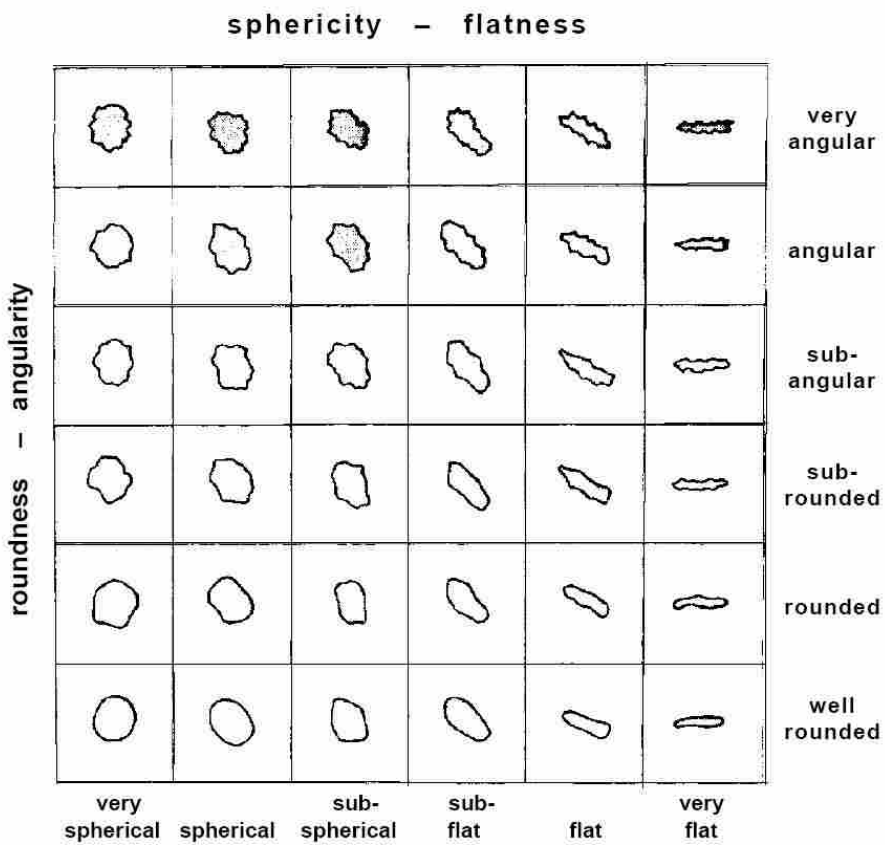

Figure A.8: Visual chart to categorize angularity and sphericity (from [10])

Manning and Chezy equations [71]. For pipe flow, there is the Darcy-Weisbach and Hazen-Williams equations [26].

A task force committee was set up by the hydraulic division of the American Society of Civil Engineers (ASCE) to summarize current thoughts on certain aspects of friction in open channels. The resulting report, written by the committee, was published in 1963 in the Journal of the Hydraulics Division [59]. The report starts by giving a brief history of the major flow resistance equations that have been used over the years for steady fully-developed flow.

In 1911, H. Blasius, proposed that f for smooth pipe flow be a function of Reynolds number only. This led several others, using boundary layer theory as a guide, to carry out experiments determining what contributed to f. L. Hopf showed that f is a function of the relative roughness (k/h), Reynolds number ($\mathbb{R} = D\overline{U}/\nu$),

and the shape of the channel cross-section. S.J. Davies and C.M. White concluded that there seemed to be two types of rough surfaces: those in which f continuously decreases as the Reynolds number increases, and those where f is constant at a sufficiently high Reynolds number. In 1934 J. Nikuradse performed his experiment of uniform sand grains glued to the inside of a pipe. He developed a formula for f in terms of the ratio of the radius of the pipe to the diameter of the sand grains. In 1937, C.F. Colebrook and White used non-uniform roughness and developed another equation to determine f based on the sand grain diameter, and Reynolds number. It can be written as:

$$\frac{1}{\sqrt{f}} = -c \log\left(\frac{k_s}{aR} + \frac{b}{\mathbb{R}\sqrt{f}}\right) \tag{A.16}$$

where k_s is the sand grain diameter, $\mathbb{R}$ is the reynolds number, and R is the hydraulic radius. In the original equation by Colebrook $c = 2$, $a = 14.83$, and $b = 2.52$.

In 1938, G.H. Keulegan developed the idea of using the roughness Reynolds number, $\mathbb{R}_\tau$ which is computed as [59]:

$$\mathbb{R}_\tau = \frac{k_s u_\tau}{\nu} \tag{A.17}$$

where k_s is the Nikuradse sand roughness, u_τ is the shear velocity and ν is the kinematic viscosity. He determined that if the Reynolds roughness number was less than 3.3 it would act as a smooth wall, and if it was greater than 67 it would be rough. Flow in-between these two limits is partly rough and f is a function of both the relative roughness and the Reynolds number. Keulegan's formula can be expressed the same as equation A.16, with c = 2.03, a = 11.09, and b = 0.

In 1944, J.W. Johnson showed that the Chezy coefficient in open-channels could be expressed as follows:

$$C = 42 \log \left(\frac{R}{\epsilon} \right) \tag{A.18}$$

where ϵ is a function of size, spacing, and shape of the roughness elements.

In 1950, Straub and Morris, did tests involving concrete and corrugated metal pipes and concluded that the Manning coefficient seemed to be the most nearly consistent measure of surface roughness for practical design use.

In 1955, Morris proposed that the energy loss over a rough surface is largely due to the formation of wakes behind each roughness element. This supported the idea of using a coefficient such as ϵ in Equation A.18 to characterize the spacing between elements.

In 1959, Chow published a book that gave tables and photographs that can be used to select a value of Manning's n for different channels.

In 1961, Koloseus and Davidian used cubical roughness elements and derived the following equation:

$$\frac{1}{\sqrt{f}} = 2 \log \frac{(0.56\lambda^{-0.9} R)}{k_s} \tag{A.19}$$

The task committee concluded that for fully rough uniform flow in a fixed bed channel the resistance is best expressed as:

$$\frac{1}{\sqrt{f}} = c \log \left(a \frac{R}{k_s} \right) \tag{A.20}$$

The value for c is taken as 2 or 2.03. The value of a depends on the value of c along with the shape of the cross section of the channel and the spacing and form of the roughness elements. It seems that each researcher has recommended a different

value of a. It was concluded that there was still room for improvement in both the definition and measurement of k_s.

Various experiments have been conducted to determine the effective roughness as a function of form, pattern and concentration. Hunter Rouse sited a few experiments that have been done in his article, "Critical analysis of open channel resistance" [57]. Koloseus and Davidian performed measurements from cubical elements arranged in different patterns and concentrations. O'Loughlin and Macdonald looked at different concentrations of sand cemented to a channel bed. Spheres have also been studied, arranged in different configuration and concentrations. Figure A.10 shows the results of some of these findings. There is a certain concentration that produces the greatest relative roughness (k_s/H). This optimum concentration, λ , ranges from 15% to 25%, depending on the shape and arrangement of the roughness. The square and round "simple" shapes used as roughness elements were used and encouraged for experimental and analytical exploration of the roughness function because of the "extreme complexity of natural roughness" [57].

Hey [33] recommended using the Darcy - Weisbach friction factor, f, to represent the flow resistance in gravel - bed channels. By comparing data from 21 different field sites, he found the Colebrook-White equation can be used to find the Darcy-Weisbach friction factor, f. For straight regular channels with fixed rough uniform gravel, the equation takes the form of:

$$\frac{1}{\sqrt{f}} = 2.03 \log\left(\frac{aR}{D}\right) \tag{A.21}$$

where R is the hydraulic radius, and D is the uniform gravel size. $a =$ is a coefficient that varies with cross-sectional geometry of the flow, and ranges from 11.1 to 13.46.

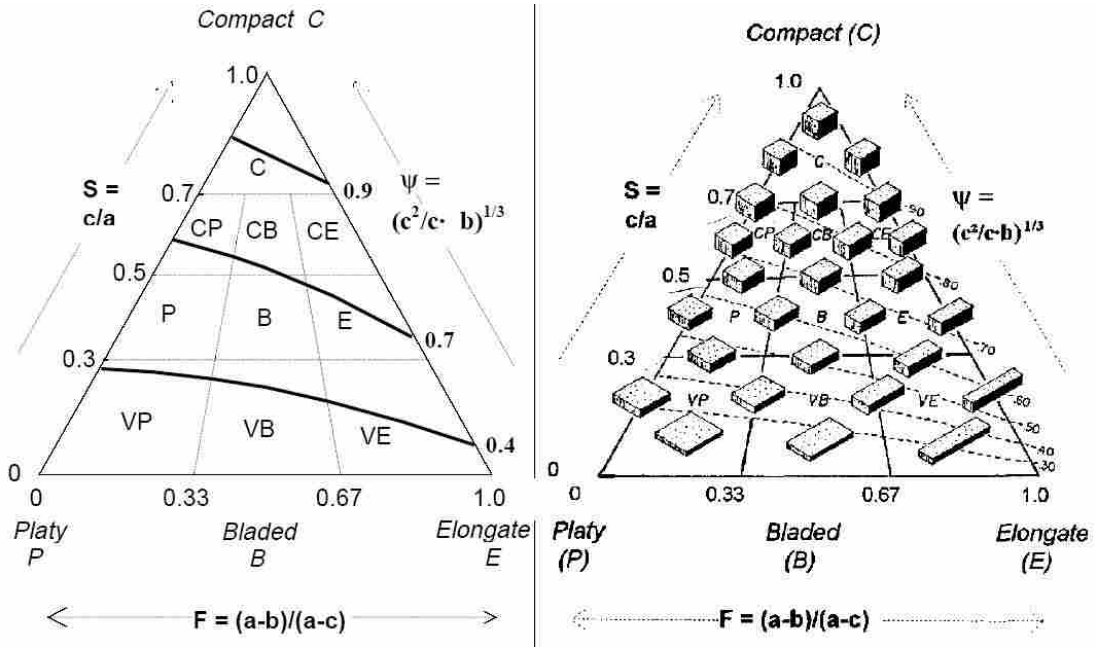

Figure A.9: Shape as a function of form factor and compactness (from [10])

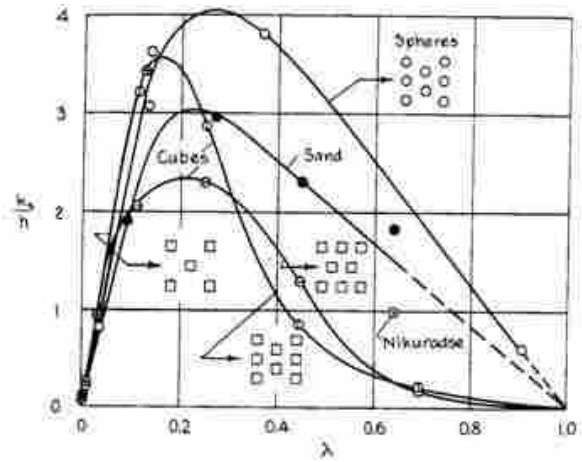

Figure A.10: k_s/H as a function of form, pattern, and concentration (λ)

Another equation (A.22) was developed by Thompson and Campbell (1979) [72] which was derived from a boulder-bed spillway. The equation is:

$$\left(\frac{8}{\sqrt{f}}\right)^{\frac{1}{2}} = 5.66\left(1 - \frac{0.1k_s}{R}\right)\log\left(\frac{12R}{k_s}\right) \tag{A.22}$$

Bathurst [6] developed equation A.23 for large scale roughness which was calibrated from field data as:

$$\left(\frac{8}{f}\right)^{2} = \left(\frac{R}{0.365D_{84}}\right)^{2.34}\left(\frac{W}{d}\right)^{(7Le-0.56)} \tag{A.23}$$

where f is the Darcy friction factor, R is the hydraulic radius, W is the channel width, and d is the channel depth. Le is the ratio of frontal cross-sectional area of roughness elements to the total area of the bed and can be approximated as Le $= 0.039 - 0.139\log\left(\frac{R}{D_{84}}\right)$.

Bathurst *et al.* [7] performed several flume experiments over large-scale roughness elements fixed to the bed. They looked at large-scale roughness for gravel ranging from 12.7 mm to 63.5 mm. (They used the following criteria to distinguish roughness scale. Large-scale roughness elements affect the free surface. This requires the ratio of d/D_{50} to be less than four. Where d is the depth, and D_{50} is the mean element height. The roughness is intermediate-scale if d/D_{50} is between 4 and 15. Anything above 15 is considered small-scale roughness.) From the data collected they were able to develop a resistance equation (A.24) that could be used to solve for a Darcy friction factor, f.

$$\begin{aligned}\left(\frac{8}{\sqrt{f}}\right)^{\frac{1}{2}} = \frac{\bar{U}}{(gdS^{\frac{1}{2}})} &= \left(\frac{0.28}{b}F\right)^{\log(\frac{0.755}{b})} \\ &\times \left(13.434\left(\frac{w}{Y_{50}}\right)^{0.492} b^{1.025(\frac{w}{Y_{50}})^{0.118}}\right) \times \left(\frac{A_w}{w'd}\right)\end{aligned} \tag{A.24}$$

where $\bar{U}$ is the average velocity, d is the depth, S is the channel slope, w is the water surface width, Y_{50} is the average between the long and median axis lengths of the grains, A_w is the roughness cross-sectional area, d' is the water depth. b is a function of the effective roughness concentration and is calculated as:

$$b = \left[1.175 \left(\frac{Y_{50}}{w} \right)^{0.557} \left(\frac{d}{S_{50}} \right) \right]^{0.648\sigma^{-0.134}} \tag{A.25}$$

where σ is the standard deviation of the roughness size distribution. It was recognized by these researchers that the equation needed further refinement for different reasons. One of those reasons was that particle roughness shape was not tested.

Another empirical resistance equation was developed by Griffiths [32] for gravel-bed rivers, and can be written as:

$$\frac{U}{u_\tau} = \left(\frac{8}{f} \right)^{\frac{1}{2}} = 5.60 \log \left(\frac{R}{D_{50}} \right) + 2.15 \tag{A.26}$$

Graf *et al.* [30] derived a similar expression for frictional resistance as:

$$\frac{U}{u_\tau} = \left(\frac{8}{f} \right)^{\frac{1}{2}} = 5.65 \log \left(\frac{R}{k_s} \right) + \zeta \tag{A.27}$$

where U is the freestream velocity, u_τ is the global shear velocity, and R is the hydraulic radius. ζ is equal to 3.25 and 4.0 when using k_s equals D_{50} and D_{85}, respectively.

In 1985, Bathurst [6] published another paper that derives an equation to find the Darcy-Weisbach friction factor for mountain rivers (slopes of 0.4% - 5% with bed material consisting of small-scale to large-scale roughness). Bathurst collected data from 16 upland rivers and from flume setups. He found that the mountain rivers show considerable differences in flow resistance behavior when compared to lowland rivers. He compared the resistance equation developed by Richard Hey to his results

and found that it seemed to underestimate the flow resistance. Bathurst proposed a new empirically derived equation that fit the data he had obtained. Admitting that there was still quite a bit of error associated with this equation, it was suggested:

$$\left(\frac{8}{f}\right)^{\frac{1}{2}} = 5.65 \log\left(\frac{d}{D_{85}}\right) + 4 \tag{A.28}$$

where d is the water depth, f is the Darcy-Weisbach friction factor, and D_{85} is the median axis particle size which is 85% larger than the cumulative bed material by size.

In 1988, Colosimo *et al.* [20] looked further at the development of a friction factor for gravel-bed rivers. They proposed the following empirical equation based on known controlling factors:

$$\frac{1}{\sqrt{f}} = 2.03 \log \frac{\alpha y_m}{M d_{85}} + (2.54\mathbb{F} - 1.65) + \left(0.75 - 0.68\frac{Y}{Y_c}\right) \tag{A.29}$$

where f is the Darcy-Weisbach friction factor, α is a cross-sectional shape factor, Y_m is the mean depth of flow, M is the grain-size curve uniformity modulus, D_{85} is the particle size for which 85% of the bed material is finer, $\mathbb{F}$ is the Froude number, Y is the sediment mobility parameter, and Y_c is the critical sediment mobility parameter. The above equation was able to fit data collected from 43 river reaches to within $\pm$ 10%.

Aguirre-Pe and Fuentes [3] in 1990 derived another formula to obtain the Darcy-Weisbach and Chezy friction factors. The equation is derived for and compared with relative roughness D/H from 0.013 to 3.3 and energy line slopes varying from 0.001% to 6.55%. The theory is derived from observing the fact that the velocity profile changes very close to the tops of the roughness elements. They divide the flow into two zones as shown in Figure A.11. The first zone is the highly turbulent wake zone created by the roughness element whose thickness is a linear factor of the particle

diameter, D. The second zone can be approximated by a logarithmic equation. The equation is calculated as follows:

$$C^{\star} = \left(\frac{8}{f}\right)^{\frac{1}{2}} = \frac{1}{\kappa}\ln\frac{d}{\alpha D} + B - \frac{1}{\kappa} + \frac{1}{\kappa}\frac{\beta D}{d} \tag{A.30}$$

where $C^{\star}$ is the dimensionless Chezy coefficient, f is the Darcy-Weisbach friction factor, κ is the Von Karman constant taken here as 0.497, B is an additive function in the semilogarithmic velocity distribution that approaches 8.5 for high-shear-velocity Reynolds numbers, α is an empirical texture factor related to Nikuradse standard by $k_s = \alpha D$, D is the bed particle diameter, and β is an empirical wake factor. The theoretically derived equation matched flume results for particle beds (cube shaped, hemispherical, gravel, and cobbles) fairly well with a mean error of $\pm 15\%$.

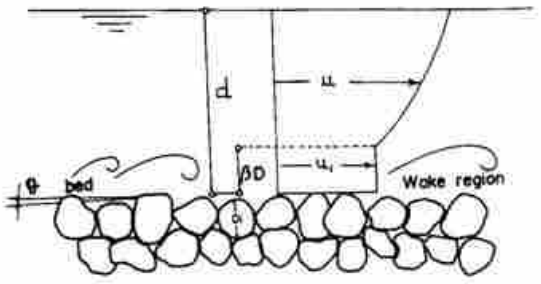

Figure A.11: Two zone flow for rough steep gradients (from [3])

In 1991, Gomez [28] argued that although well-defined relationships between roughness size and resistance to flow exist for roughness elements fixed to a flat surface, these relationships should not be used for natural water-worked gravel beds. He performed experiments on stable armored bed surfaces that were naturally developed by running steady flow over non-uniform gravel in a laboratory flume. Three particle shape mixtures were used in the experiment: rounded, flat and angular. An effective roughness height was calculated by the difference in height between the highest point on a particle and the average contact height of adjacent upstream and downstream

particles. The average height of all the effective roughness heights greater than 95% of the values was called the representative roughness height (k). The equivalent roughness height (k_s/k) was found to initially increase with increased concentration, to a maximum level, and then decrease. Overall, he found that angular gravel is the roughest and flat gravel provided the least resistance to flow. The rounded gravel roughness was somewhere between the angular and flat gravel. This can be seen graphically in Figure A.12. He also confirmed that the roughness increased with increased flow.

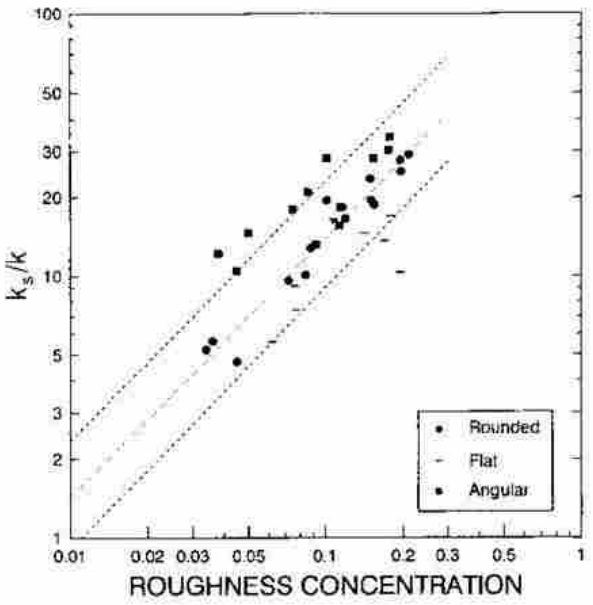

Figure A.12: (k_s/k) **versus concentration and particle shapes (from [28])**

In 1999, Vito Ferro [25] ran flume experiments that represented gravel-bed channels with high boulder concentrations. The experiments were setup by systematically increasing boulder concentrations. It was shown that the flow resistance law can be expressed by a semilogarithmic relationship as:

$$\frac{C}{\sqrt{g}} = b_o + 15.74 \log \frac{h}{D_{84}} \tag{A.31}$$

where C is the Chezy coefficient, g is acceleration due to gravity, h is the water depth, and D_{84} is the particle size greater than 84% of the bed material.

The variable b_o was found to be dependent on a particle arrangement parameter α. It was found that when the concentration of boulders was $< 50\%$, the b_o value could be estimated as:

$$b_o = -0.2590 - 0.1189\alpha - 0.01711\alpha^2 + 0.00117\alpha^3 \tag{A.32}$$

$$\alpha = \frac{\gamma_N}{\gamma_o} \tag{A.33}$$

where γ_N is the variance of the bed arrangement with N coarser elements, and γ_o is the variance of the bed layer material. When the boulder concentration became greater than 50% a "skimming" flow takes place on the surface of the boulders, and the b_o value becomes constant at -1.5.

Smart *et al.* [61] in 2002, pointed out some major difficulties associated with flow resistance equations for gravel beds. They recognized that there still is no standard equation to predict velocity in alluvial channels with large relative roughness. There is also difficulty defining the bed level which leads to uncertainty in water depth and hydraulic radius. Different resistance equations are also applicable to different ranges of relative roughness. "Flow resistance" refers to the ratio u_τ/U (U is the mean velocity). Friction factors can be related to the flow resistance by the following relationship:

$$\left(\frac{U}{u_\tau}\right)^2 = \left(\frac{8}{f}\right) = \left(\frac{C^2}{g}\right) = \frac{R^{\frac{1}{3}}}{(gn^2)} = \frac{\mathbb{F}^2}{S} = \frac{Q\rho U}{(\tau_o A_f)} \tag{A.34}$$

where u_τ is the shear velocity, U is the mean velocity, f is the Darcy friction factor, C is the Chezy friction coefficient, n is the Mannings coefficient, R is the hydraulic radius, g is the gravitational acceleration constant, $\mathbb{F}$ is the Froude number, $Q\rho U$ is

the momentum flux, τ_o is the wall shear stress, and A_f is the cross-sectional area of flow. They follow by listing six different flow resistance equations that have been developed, and argue that these equations require "robust" estimates of Z_o (hydraulic roughness parameter), k_s (equivalent sand grain diameter), or d (generic term for size of roughness elements). They conclude by stating that each of the equations can be well suited for a particular relative roughness flow. As a general equation, however, they recommended using the full log law for relatively rough flow (as long as the water level is above the tops of the roughness elements and channel slopes are moderate):

$$\begin{aligned}\frac{U}{u_\tau} =& 2.5\left[\ln\left(\frac{R_v}{Z_o}\right) - 1\right] = 5.75\log\left(\frac{0.368R_v}{Z_o}\right) \\ =& 2.5\ln\left(\frac{aR_v}{d}\right) = 2.5\ln\left(\frac{R_v}{d}\right) + B\end{aligned} \tag{A.35}$$

where R_v is the volumetric hydraulic radius, Z_o is the standard deviation in surface elevation of grain-sized elements, a is $0.368(d/Z_o)$ and B is $2.5\ln(0.368d/Z_o)$. As a practical application for finding the volumetric hydraulic radius and the value d_z, they recommend spreading a known volume of sand over a known area of the bed. In their finding they conclude that flow velocity can be predicted better by the standard deviation, d_z, of roughness rather than a representative grain size statistic.

Aberle and Smart [1], in 2003, provided a paper that focuses on high relative roughness flow of mountain streams. There is no standard equation to determine mean flow velocity for a mountain stream. To develop such an equation would require a definition of a roughness parameter. Using a single grain-size as a roughness parameter gives only a crude description of the roughness geometry. When the water depth is comparable in size to roughness elements, density can change the friction factor by an order of magnitude. Three general approaches for developing a flow resistance in mountain streams have been proposed. They are logarithmic approaches, Froude number approaches, and power-law approaches. Logarithmic approaches are

based on the law of the wall and can be written as:

$$\sqrt{\frac{8}{f}} = \frac{1}{\kappa} \ln \frac{h}{k_s} + B \tag{A.36}$$

The value of κ is usually taken as 0.4, but it has been suggested that 0.18 may be a better constant for low relative submergence. The value for B generally has different values for different cross-sections or relative submergence.

Since a component of form drag is free surface drag which varies with the Froude number and relative submergence, the slope, friction factor, and Froude number can be related as:

$$\sqrt{\frac{8}{f}} = \frac{\bar{u}}{u_\tau} = \frac{\bar{u}}{\sqrt{ghS}} = \frac{\mathbb{F}}{\sqrt{S}} \tag{A.37}$$

Equation A.37 is treated with caution since determining f from $\mathbb{F}$ may be self correlating.

Power law relationships can be written as:

$$\bar{u} = cQ^m \tag{A.38}$$

The variables c and m are constants. The exponent m indicates the rate of change of velocity and adopts certain characteristic values. It has been suggested that the exponent m increases in value as the slope and bed composition change. Sand bed channels have $m < 0.40$, gravel bed channels have $m = 0.40$ to 0.45. Cobble and boulder-bed channels have $m = 0.45$ to 0.55. Steep pool/fall streams and pool-riffle sequences have $m > 0.55$.

Aberle and Smart carried out a series of laboratory experiments using a flume with water worked (armored) bed. Two coarse sediment mixtures, 1 mm $< d <$ 64 mm and 1 mm $< d <$ 32 mm, were used. They found the hydraulic roughness

can change with different bed surfaces even though they have the same roughness parameter d_c. They proposed using the standard deviation of the bed elevations as a more appropriate roughness parameter. The following equation was found to give the best prediction of flow velocity.

$$\bar{u} = 0.96 g^{0.20} S^{0.20} q^{0.60} s^{-0.40} \tag{A.39}$$

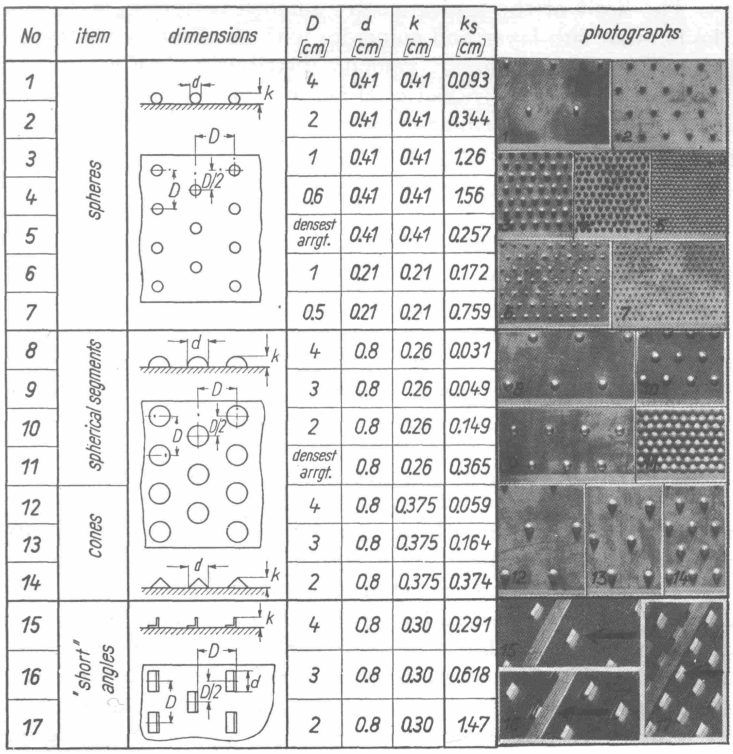

No	item	dimensions	D [cm]	d [cm]	k [cm]	k_s [cm]	photographs
1	spheres		4	0.41	0.41	0.093	
2			2	0.41	0.41	0.344	
3			1	0.41	0.41	1.26	
4			0.6	0.41	0.41	1.56	
5			densest arrgt.	0.41	0.41	0.257	
6			1	0.21	0.21	0.172	
7			0.5	0.21	0.21	0.759	
8	spherical segments		4	0.8	0.26	0.031	
9			3	0.8	0.26	0.049	
10			2	0.8	0.26	0.149	
11			densest arrgt.	0.8	0.26	0.365	
12	cones		4	0.8	0.375	0.059	
13			3	0.8	0.375	0.164	
14			2	0.8	0.375	0.374	
15	"short" angles		4	0.8	0.30	0.291	
16			3	0.8	0.30	0.618	
17			2	0.8	0.30	1.47	

Figure A.13: Roughness patterns from Schlichting experiments (from [58])

A.3 Velocity Distribution

The velocity distribution can be divided into separate layers or regions. Starting closest to the boundary they are generally termed the inner or viscous, intermediate, and outer layers. The viscous layer can further be divided into the viscous sub-layer and the buffer layer. Attempts to non-dimensionalize the mean velocity

profiles for each region have been done using some of the following variables.

$$\text{shear velocity:} \qquad u_\tau = \left(\frac{\tau_w}{\rho}\right)^{1/2} \tag{A.40}$$

$$\text{wall units:} \qquad u^+ = \overline{u}/u_\tau \qquad z^+ = zu_\tau/\nu \tag{A.41}$$

Close to the wall the velocity is thought to be a function of the wall unit z^+ only. This is referred to as the *law of the wall* [9]. It can be expressed as:

$$\frac{\overline{u}}{u_\tau} = f(z^+) \tag{A.42}$$

In the viscous sub-layer the shear stress is dominated by viscous, or molecular, forces. This results in Equation A.42 becoming a linear relationship with the distance y [9].

$$\overline{u}^+(z^+) = z^+ \tag{A.43}$$

Far from the bed boundary, what is know as the *velocity defect law* [84] is generally accepted.

$$\frac{\overline{u_m} - \overline{u}}{u_\tau} = \frac{1}{\kappa}\ln\left(\frac{z}{\delta}\right) + B \tag{A.44}$$

Coles [19] developed the idea of the *law of the wake*, from his observation that the velocity deviations from the log layer in the outer layer have a wakelike shape [84]. Coles introduced a wake parameter, Π, in order to extended the "law of the wall" to describe the outer region. The "law of the wake" can be written as:

$$\frac{\overline{u}}{u_\tau} = \frac{1}{\kappa}\ln\left(\frac{u_\tau z}{\nu}\right) + B + \frac{2\Pi}{\kappa}\sin^2\left(\frac{\pi z}{2\delta}\right) \tag{A.45}$$

For rough boundaries, the law of the wake can be re-written as [86]:

$$\frac{\overline{u}}{u_\tau} = \frac{1}{\kappa}\ln\left(\frac{z}{k_s}\right) + B + \frac{2\Pi}{\kappa}\sin^2\left(\frac{\pi z}{2\delta}\right) \tag{A.46}$$

By expressing Coles law of the wake in terms of the velocity defect function we get the following equation that is valid in both the inner and outer region for smooth and rough flows [37].

$$\frac{\overline{u_m} - u}{u_\tau} = -\frac{1}{\kappa}\ln\left(\frac{z}{\delta}\right) + \frac{2\Pi}{\kappa}\cos^2\left(\frac{\pi z}{2\delta}\right) \tag{A.47}$$

In the intermediate range there is a lack of consensus as to how best to non-dimensionalize the velocity profile [9]. Beginning with the work of von Kármán and Prandtl, the widely used profile is the *log law*. For a smooth boundary, this law can be expressed as [9]:

$$\overline{u}(z^+) = \frac{1}{\kappa} ln z^+ + B \tag{A.48}$$

For rough boundaries the log law is written as:

$$\frac{\overline{u}}{u_\tau} = \frac{1}{\kappa}\ln\left(\frac{z}{k_s}\right) + B \tag{A.49}$$

Kironoto and Graf [37] performed a series of flume experiments over rough uniform beds. Their experiments focused on flow with large relative roughness $k_s/h \approx 0.1$. Two different roughness beds were made, a rough plate and a gravel bed. The plate had crushed grains glued ($k = 4.8 \pm 0.5$ mm) to a steel plate. The gravel bed was about 0.10 mm thick and contained gravel having a D_{50} of 23 mm with a standard deviation of 1.25 mm. Velocity profiles were obtained using Prandtl tubes. Turbulence intensities and Reynolds stress profiles were measured using hot-film probes. They

found that the within the inner region ($y/\delta < 0.2$) time averaged velocities can be represented with the universal law of the wall for rough boundaries (Equation A.49).

The reference level (y_o) was taken as $0.20k_s$. (k_s was taken to equal k for the rough plate and D_{50} for the gravel bed.) They used the Clauser method to find u_τ and Br, and found that the Br values (8.47 ± 0.90) matched closely to those cited in literature.

The outer region seemed to conform to Cole's law of the wake, which is valid for both the inner and outer regions and can be written as:

$$\frac{U_c - \bar{u}}{u_\tau} = -\frac{1}{\kappa} \ln\left(\frac{y}{\delta}\right) + \frac{2\Pi}{\kappa} \cos^2\left(\frac{\pi y}{2\delta}\right) \tag{A.50}$$

where U_c isthe maximum point velocity in the profile, and δ is the distance between y_o and where $u = U_c$.

T. Song and Y.M. Chiew [63] conducted measurements for nonuniform flow over a fixed bed of sand (2.6 mm). They measured both accelerating and decelerating flow, and were able to get almost a complete velocity profile by using a down-looking and up-looking ADV probe. Although the flow in most natural open-channels is nonuniform, it can be considered to be an equilibrium flow. Equilibrium flow means that there is a"unique relationship between the parameters or profiles at different sections." They used the Clauser equilibrium parameter β. When β is constant along different reaches for the same flow then the condition can be considered equilibrium flow. For uniform flow ($dH/dx = 0$), β = -1, for decelerating flows ($dH/dx > 0$), $\beta > -1$, and for accelerating flows ($dDH/dx < 0$), $\beta < -1$. They found that the Cole's wake parameter, Π is dependent on the flow non-uniformity, the aspect ratio, and the roughness of the bed.

The Navier-Stokes equations of momentum and continuity for a Newtonian fluid with constant density and viscosity are:

$$\rho\left(\frac{\partial V_x}{\partial t}+V_x\frac{\partial V_x}{\partial x}+V_y\frac{\partial V_x}{\partial y}+V_z\frac{\partial V_x}{\partial z}\right)= \mu\left(\frac{\partial^2 V_x}{\partial x^2}+\frac{\partial^2 V_x}{\partial y^2}+\frac{\partial^2 V_x}{\partial z^2}\right)-v\frac{\partial p}{\partial x}+\rho g_x \tag{A.51}$$

$$\rho\left(\frac{\partial V_y}{\partial t}+V_x\frac{\partial V_y}{\partial x}+V_y\frac{\partial V_y}{\partial y}+V_z\frac{\partial V_y}{\partial z}\right)= \mu\left(\frac{\partial^2 V_y}{\partial x^2}+\frac{\partial^2 V_y}{\partial y^2}+\frac{\partial^2 V_y}{\partial z^2}\right)-v\frac{\partial p}{\partial y}+\rho g_y \tag{A.52}$$

$$\rho\left(\frac{\partial V_z}{\partial t}+V_x\frac{\partial V_z}{\partial x}+V_y\frac{\partial V_z}{\partial y}+V_z\frac{\partial V_z}{\partial z}\right)= \mu\left(\frac{\partial^2 V_z}{\partial x^2}+\frac{\partial^2 V_z}{\partial y^2}+\frac{\partial^2 V_z}{\partial z^2}\right)-v\frac{\partial p}{\partial z}+\rho g_z \tag{A.53}$$

$$\frac{\partial}{\partial x}\left(V_x\right)+\frac{\partial}{\partial y}\left(V_y\right)+\frac{\partial}{\partial z}\left(V_z\right) \tag{A.54}$$

Using velocity decomposition and time averaging, Reynolds developed what has come to be known as the "Reynolds averaged Navier-Stokes" equations (RANS). Equations A.52 and A.52 are re-written and re-arranged for time averaged velocities using tensor notation as follows:

$$\frac{\partial\overline{V_i}}{\partial t}+\bar{V_i}\frac{\partial\overline{V_j}}{\partial x_i}=g_i-\frac{1}{\rho}\frac{\partial\bar{p}}{\partial x_i}-\frac{\partial\overline{V_i'V_j'}}{\partial x_j}+\nu\frac{\partial^2\overline{V_i}}{\partial x_j^2} \tag{A.55}$$

$$\frac{\partial\overline{V_i}}{\partial x_i}=0 \tag{A.56}$$

Nikora *et al.* [53] argued that the RANS equations should be replaced by double-averaged Navier-Stokes equations for rough-bed open channel flows. The double-averaging refers to not only averaging temporally by also spatially. They suggested

this change is needed since the flow structure in the near bed region is highly 3-dimensional and the 2-dimensional assumption used in the RANS equations is not valid. In flow where the roughness particles are large compared to the total depth (relatively small submergence) the double-averaging is especially needed. They proposed that in a similar way that the RANS equations were developed from the Navier-Stokes equations, the spatially averaged equations can be formed from the RANS equations.

It has been shown that as the depth to roughness particle size ratio (H/D) increases, and the distance from the bed increases, the roughness has less of an effect on the velocity profile, and the double-averaged equations can reduce to the RANS equations. To help clarify the matter, Nikora *et al.* proposed dividing the flow of rough open channels into five layers. These layer can be seen in Figure A.14.

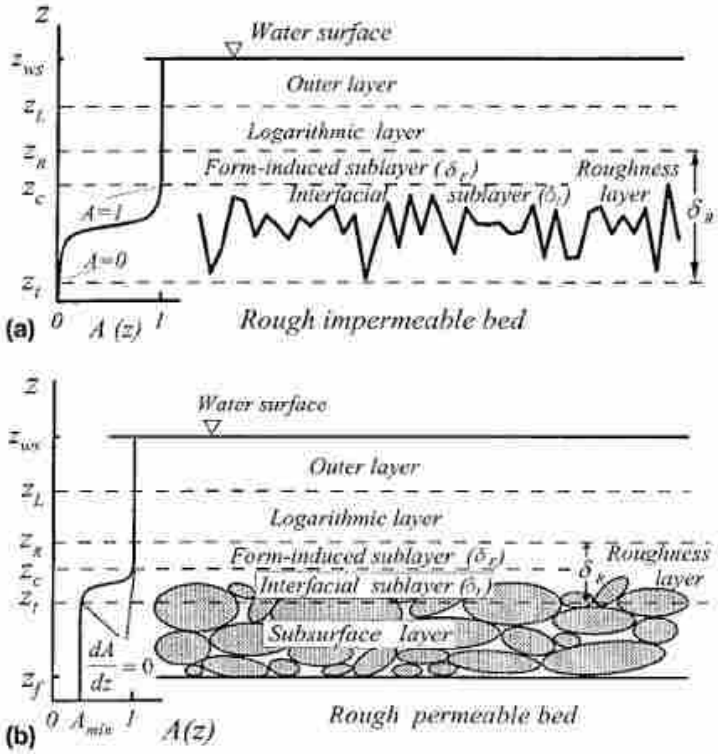

Figure A.14: Flow subdivision for a)impermeable bed and b) permeable bed (from [54])

In the outer layer and logarithmic layer the viscous and particle induced fluxes are negligible and the spatially averaged equations are identical to the time-averaged equations. The form-induced sublayer is influenced by the individual roughness elements and is located just above the roughness crests. The interfacial sublayer occupies the flow region between roughness crests and troughs. Collectively the logarithmic, form-induced, and interfacial layers make up what is usually referred to as the inner layer.

Re-writing the RANS equations A.55 and A.56, in terms of spatially averaged terms for flow regions above the crests of roughness elements $Z > Z_c$ becomes:

$$\frac{\partial\langle\overline{V_j}\rangle}{\partial t} + \langle\overline{V_i}\rangle\frac{\partial\langle\overline{V_j}\rangle}{\partial x_i} = g_i - \frac{\partial\langle\bar{p}\rangle}{\partial x_i} - \frac{\partial\langle\overline{V_i'V_j'}\rangle}{\partial x_j} - \frac{\partial\langle\widetilde{V_i'V_j'}\rangle}{\partial x_j} + \nu\frac{\partial^2\langle\overline{V_i}\rangle}{\partial x_j^2} \tag{A.57}$$

$$\frac{\partial\langle\overline{V_i}\rangle}{\partial x_i} = 0 \tag{A.58}$$

The straight $\overline{\text{overbar}}$ and $\langle$angle brackets$\rangle$ denote the time and spatial average of variables, respectively. The tilde $\widetilde{\text{overbar}}$ represents the difference between time averaged and double averaged values (similar to Reynolds decomposition), as shown below.

$$\tilde{V} = \bar{V} - \langle\bar{V}\rangle \tag{A.59}$$

For flow regions below the crests of roughness elements $Z < Z_c$ the expression is:

$$\begin{aligned}\frac{\partial\langle\overline{V_i}\rangle}{\partial t} + \langle\overline{V_i}\frac{\partial\langle\overline{V_j}\rangle}{\partial x_i} =& g_i - \frac{1}{\rho}\frac{\partial\langle\bar{p}\rangle}{\partial x_i} - \frac{1}{A}\frac{\partial A\langle\overline{V_i'V_j'}\rangle}{\partial x_j} - \frac{1}{A}\frac{\partial\langle\widetilde{V_i'V_j'}\rangle}{\partial x_j} \\ &+ \nu\frac{\partial^2\langle\overline{V_i}\rangle}{\partial x_j^2} + \nu\left\langle\frac{\partial^2\langle\widetilde{V_i}\rangle}{\partial x_j^2}\right\rangle - \frac{1}{\rho}\left\langle\frac{\partial\tilde{p}}{\partial x_i}\right\rangle\end{aligned} \tag{A.60}$$

$$\frac{\partial\langle\overline{V_i}\rangle}{\partial x_i} = 0 \tag{A.61}$$

where A is the ratio of the area A_f occupied by the fluid to the total area A_o of the averaging region. The area ratio, A, is a function of z and can be described by a cumulative probability distribution of bed elevations. The additional terms in equation A.60 represent form-induced stresses, form drag, and viscous drag on the bed. Nikora *et al.* were able to solve equations A.57 through A.60 for three different relative submergence flow conditions. They labeled these flow conditions as flow type 1 through 3. Flow type 1 is when the total depth, H is several orders of magnitude larger than the height of the roughness elements, Δ . Flow type 2 is when the depth, H, is larger than the roughness height, but less than two to five times the roughness height, Δ. Flow type 3 is when the depth, H, is less than the roughness height.

Flow Type 1 ($H \gg D$):

Outer layer:

Flow is similar to hydraulically smooth beds.

Logarithmic and interfacial layers:

$$\frac{\langle \bar{V} \rangle}{u_\tau} = \frac{1}{\kappa} \ln \left[\frac{Z}{\delta} \right] + C \qquad \text{for } (Z_L - Z_t) \geq Z \geq \delta \tag{A.62}$$

$$\frac{\langle \bar{V} \rangle}{u_\tau} = C \frac{Z}{\delta} \qquad \text{for } \delta \geq Z \geq 0 \tag{A.63}$$

The C variable is a parameter of velocity distribution where:

$$C = \frac{\langle \bar{V} \rangle (\delta)}{u_\tau} \tag{A.64}$$

u_τ is the shear velocity. δ is the boundary between logarithmic and linear flow regions.

Flow Type 2 ($(2-5)\Delta > H \geq \Delta \simeq \delta$):

The velocity distribution here can be assumed linear and equal to that shown in equation A.63. This can in turn be related to the Darcy-Weisbach friction factor,

f, to obtain:

$$\sqrt{\frac{8}{f}} = \frac{\langle \bar{V} \rangle_a}{u_\tau} = Cm\frac{H}{\delta} \quad \text{or} \quad f = \frac{8u^{\star 2}}{\langle \bar{V} \rangle_a^2} = \frac{8}{C^2 m^2}\left[\frac{\delta}{H}\right]^2 \tag{A.65}$$

Flow Type 3 ($H < \Delta \simeq \delta$):

The hydraulic resistance relationship can be assumed equal to:

$$\sqrt{\frac{8}{f}} = \frac{\langle \bar{V} \rangle_a}{u_\tau} = \frac{\alpha m}{\gamma}\frac{\delta}{H} \quad \text{or } f = \frac{8u^{\star 2}}{\langle \bar{V} \rangle_a^2} = \frac{8\gamma^2}{\alpha^2 m^2}\left[\frac{H}{\delta}\right]^2 \tag{A.66}$$

α is a coefficient which depends on bed geometry. m is a parameter that is dependent on roughness geometry.

In 2004, Nikora *et al.* [54] published a paper that took a closer look at the roughness layer (form-induced and interfacial sublayers). Using the double-averaged momentum equation for 2D, steady, uniform, spatially averaged flow over a rough bed they developed three models to characterize the velocity distribution. Model 1, shows constant velocity, and is designed for tall roughness elements (such as vegetation). It is written as follows:

$$\langle \bar{V} \rangle = \left\{ \frac{gS_b}{0.5C_D a} \right\}^{0.5} \tag{A.67}$$

where g is the gravitational acceleration constant, S_b is the bed slope, and C_D is the drag coefficient which depends on the roughness elements shape, density, and spatial arrangements. a is the local roughness density (roughness frontal area per fluid volume) and is a function of depth, z. Model 2 is written for flow conditions where inertia instead of pressure drives the flow below the roughness tops. It is written as:

$$\langle \bar{V} \rangle(z) = \langle \bar{V} \rangle(z_c) \exp \beta(z - z_c) \tag{A.68}$$

In equation A.68 $\langle\bar{V}\rangle(z_c)$ is the double-averaged velocity at the roughness tops, and β is a parameter. Model 3 is a linear distribution model, and is written as:

$$\frac{\langle\bar{V}\rangle(z) - \langle\bar{V}\rangle(z_c)}{u_\tau} = \frac{(z - z_c)}{l_c} \tag{A.69}$$

$$l_c = \frac{\rho k u^{\star 2}}{A[(f_p + f_v) - \rho g S_b]} \tag{A.70}$$

where ρ is the liquid density, and k is a constant dependent on the roughness type. u_τ is the shear velocity. A is the ratio of A_f/A_o, where A_f is the area occupied by the fluid within a fixed averaging region on the xy plane, and A_o is the total area of the region. Model 2 and 3 were compared with eight different data sets collected from experiments having roughness types varying from bead-covered to gravel-covered to two-dimensional bedform-covered roughness beds, and found to be in relative agreement. They found that the velocity distribution within the interfacial sublayer is complex and may contain a combination of the three models derived. The existence and extent of each model seemed to be a function of flow conditions, relative submergence, and roughness geometry.

In 2007, Dey and Raikar [23] performed experiments using an ADV with a laboratory flume having a loose gravel bed. They found that their velocity data followed the logarithmic law. By integrating the velocity given by the log law and law of the wake over the flow depth h and then depth averaging, gives:

$$\frac{U}{u_\tau} = \sqrt{\frac{8}{f}} = -\frac{1}{\kappa}\ln(k_s/h) + B + ((y_0/h) + 0.98\Pi - 1)/\kappa \tag{A.71}$$

By plotting relative roughness on the x-axis and $f^{-0.5}$ on the y-axis, it was shown that their experimental data followed Equation A.71.

A.4 Turbulence Characteristics

A.4.1 Turbulence Intensity

According to the Reynolds velocity decomposition, there is a fluctuating component of velocity. The "root mean square" (standard deviation) of this fluctuating component is referred to as *turbulence intensity* (TI).

$$TI_i = \sqrt{\frac{\sum_n (i - \bar{i})^2}{n}} \tag{A.72}$$

where n is the number of time-averaged velocity samplings, and i is the velocity component (u, v, or w).

Excluding the near wall region, the following exponential relationship for turbulence intensity for the streamwise direction has been proposed [46].

$$\frac{TI_u}{u_\tau} = D_1 e^{-\lambda_1 (z/H)} \tag{A.73}$$

where D_1 and λ_1 are constants. It has been proposed that $D_1 = 2.28$ and $\lambda_1 = 1.08$ [11] for a hydraulically smooth flow regime. Kironoto and Graf [37] found that smooth and rough beds both gave similar values of $D_1 = 2.04$ and $\lambda_1 = 0.97$. Similar values were also confirmed by others: $D_1 = 2.26$ and $\lambda_1 = 0.88$ [50]; $D_1 = 2.3$ and $\lambda_1 = 1.0$ [47].

A similar exponential relationship for turbulence intensity in the vertical direction has also been proposed [46].

$$\frac{TI_w}{u_\tau} = D_2 e^{-\lambda_2 (z/H)} \tag{A.74}$$

where D_2 and λ_2 are constants. Kironoto and Graf [37] found that smooth and rough beds both gave similar values of $D_2 = 1.14$ and $\lambda_2 = 0.76$. Similar values were also confirmed by others: $D_2 = 1.23$ and $\lambda_2 = 0.67$ [50]; $D_2 = 1.7$ and $\lambda_2 = 1.0$ [47].

Nikora and Goring [52][51] also developed a relationship for turbulence intensity distributions, which can be written as follows:

$$\left(\frac{TI_i}{u_\tau}\right)^2 = M_i - N_i \ln\left(\frac{z}{H}\right) \tag{A.75}$$

where the following constants were found by experimentation: $M_u = 1.90$, $M_v = 1.19$, $M_w = 0.59$, $N_u = 1.32$, $N_v = 0.49$, and $N_w = 0.22$.

Carollo, Ferro and Termini [12] did a literature review in 2005 on turbulence intensity distributions in rough bed flows. Turbulence intensity data for rough beds is still limited, and has been shown to be contradictory at times. Near the bed ($z/H < 0.2 - 0.3$) the roughness elements seem to have an effect on the turbulence intensity. Away from the bed ($z/H > 0.2 - 0.3$) the turbulence intensity profile seems to follow the same trend as a smooth wall would have, but may be dependent on the relative roughness (H/D_{50}).

Bayazit [8] found that the turbulence intensity increases with the ratio H/K_s ranging from (1.07 to 4.6) for the entire profile. Others [31] [47] [37] using higher values of H/K_s found that this was not the case. Wang et al. [82] performed a series of experiments over gravel beds using an LDV and varying values of H/K_s. They concluded that only when $H/K_s \geq 4.0$ could the coefficients D_1 and D_2 be considered constants. The maximum value of TI_u/u_τ was about 1.8 - 2.0, which was smaller than that found for a smooth bed (2.6 - 3.4). The location of the maximum turbulent intensity was found to be at about $z/H = 0.1$, wich is much greater than $y^+ = 10 - 20$ for a smooth bed.

Wang et al. [82] found that the location of maximum turbulence intensity increased with depth/roughness height ratio. They found that the constants D_1 and λ_1 in Equation A.73 could only be considered constant if $h/k_s > 4$. They also observed that for $z < 0.2H$, the profile deviated from Equation A.73, and showed a peak at about $z = 0.1H$. Carollo et al. [12] further confirmed that the relative peak value location (z_t/H) increased with relative roughness (D_{84}/H). Interestingly enough, they also found that the relative peak location (z_t) had a near one-to-one relationship with relative roughness. The maximum turbulence intensity, however, decreased as relative roughness increased. By changing the concentration of pebbles on the bed, they observed that turbulence intensity decreased for increasing values of pebble concentration. As pebble concentration was increased, this trend was less obvious.

By experimentally fitting a least squares line to turbulence intensity between the ranges of z_t and δ, Wang et al. [82] developed an exponential relationship to find the value of D_1.

$$D_1 = 2.26e^{-b_1(D_{84}/H)} \tag{A.76}$$

where $-b_1$ is a coefficient equal to 2.26.

It has also been shown that for uniform flow, turbulence intensity ratios should remain constant. TI_v/TI_u was found to be equal to 0.71 by Nezu and Nakagawa [49] and 0.75 by Song and Chiew [63]. TI_w/TI_u was also recommended to equal 0.55 [49] and 0.5 [63].

A.4.2 Turbulent Kinetic Energy

Turbulent kinetic energy, K, is found by:

$$K = \frac{1}{2}\left(\overline{u'^2} + \overline{v'^2} + \overline{w'^2}\right) \tag{A.77}$$

Nezu and Nakagawa [49] developed a universal turbulent kinetic energy distribution equation based on the $k - \epsilon$ turbulence model.

$$\frac{K}{u_\tau^2} = 4.78e^{-2(z/H)} \tag{A.78}$$

Nikora and Goring [52] have also developed a universal equation for turbulent kinetic energy distribution:

$$\frac{K}{u_\tau^2} = 1.84 - 1.02 \ln\left(\frac{z}{H}\right) \tag{A.79}$$

Appendix B

Laboratory Setup

The experiments explained in this thesis were carried out in the Brigham Young University department of civil and environmental engineering fluid mechanics laboratory located in room 171 of the Clyde Building.

B.1 Flume Description

Located in the laboratory is a 12.5 meter recirculating research flume assembled and manufactured by Engineering Laboratory Design, Inc. The flume is ideal for simulating various flow conditions since the flowrate, tailwater, and slope can all be adjusted. The channel dimensions of the flume are shown in Table B.1:

A 14 inch Venturi type meter is installed inline with the supply line leading to the flume channel to measure flow rate. The digital venturi meter reports the change in head in inches (Δh) that is calibrated to the flowrate (L/sec) by the following equation [24]:

$$Q = 15.1511\sqrt{\Delta h} \tag{B.80}$$

Tailwater depth was modified by a motorized adjustable tailgate. Uniform flow was accomplished by adjusting the tailgate until variations in depth in the streamwise direction were negligible. The flume slope was fixed by a set of three motors set at different locations along the flume that worked together in adjusting the bed slope.

Table B.1: Laboratory flume dimensions

Dimension	Value
Length	12.5 m
Width	1.20 m
Height	0.40 m
Slope	0 to 10 %

The inlet of the flume is equipped with a honeycomb entrance that encouraged laminar flow. It was found that at higher flow rates, waves would form on the water surface making the water depth difficult to measure. By placing a net on the water surface in the inlet section, the waves were drastically reduced. As expected the shear stress was largest at the entrance of the flume. In fact, the shearing stress was high enough to transport any of the $3/4 - 3/8$ inch loose gravel placed there. A concrete apron with fixed gravel on top was used to remedy the potential destruction of the shearing stress.

Figure B.2: Net placed at inlet of flume to prevent surface waves

B.2 Gravel-Bed Setup

Two different sets of gravel were used for this investigation. The first was crushed (angular) rock, and the other was smooth (rounded) rock. The crushed gravel was donated by Staker and Parsons, and came from their Gomex pit located at the mouth of Spanish Fork Canyon in Springville, Utah. The smooth rock was purchased from Woodstuff, a landscape supply company. Both sets of rock were sifted to the same size, their angularity was quantified, and they were fixed in concrete panels.

B.2.1 Sifting Gravel

The gravel was manually sifted by a handmade sifter featured in Figure B.2.1. The sifter consisted of a wooden frame that rested on top of a wheelbarrow. The

Figure B.3: Gravel sifter

frame was equipped with a set of wheels on which a sifter rested. The wheels allowed the sifter to be rocked back and forth allowing the rock to be sorted by the sifter. Two sifters were made, so that gravel would pass through one size and be retained on the other. The sifters consisted of a metal grate that was held in place by wood along its edges. The wooden edges rested on top on the frame's wheels. The grate consisted of woven wire having opening sizes of 15/16 inch (2.38 cm) and 1 inch (2.54 cm).

B.2.2 Fixing the Gravel to the Bed

10 concrete panels were constructed for each gravel set (angular and rounded) and fit side by side to create the fixed gravel bed. A wooden frame (1.2 m x 0.5 m) was constructed to set the concrete panels to the correct dimensions. Concrete was

Figure B.4: Concrete panel frame

mixed using the same amount of sand, cement, and water each time to ensure the volume of concrete was the same for each panel. Once the concrete had been poured, the gravel was hand placed into the wet mixture. Gravel was chosen at random and placed side by side for maximum concentration. The particles shortest axis (c-axis) was placed vertical. The other two axes had no specific orientation. Once the gravel

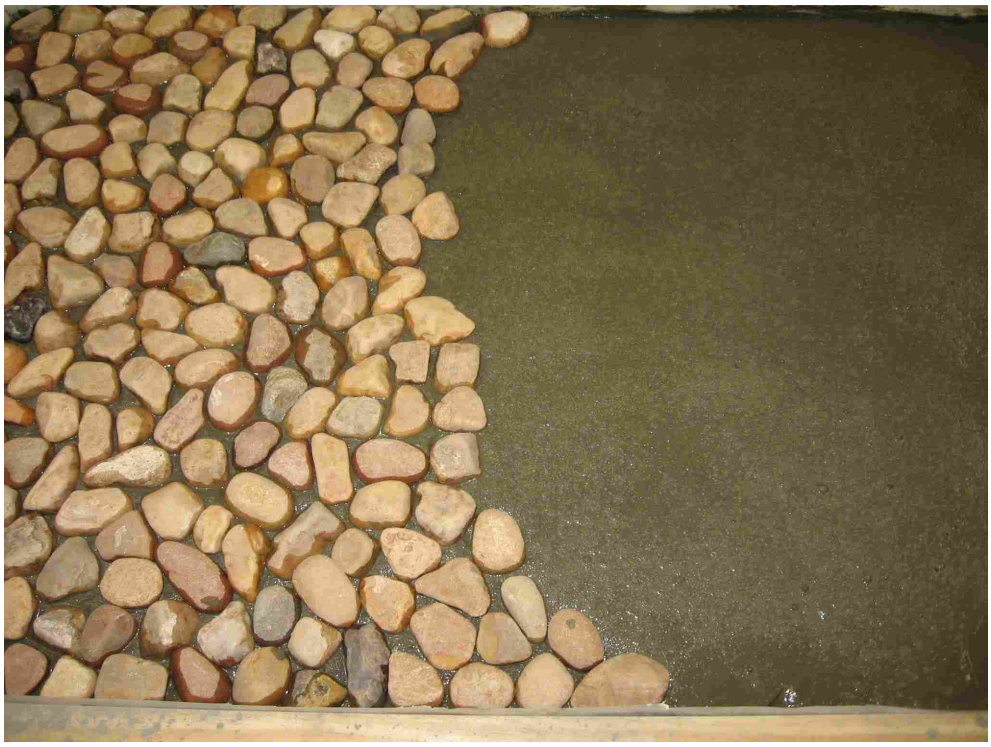

Figure B.5: Placing gravel in the frame

had been placed on top of the concrete mixture, the tops were lightly tamped. This encouraged the tops of the gravel to be at the same datum.

The hardened concrete panels were hand placed into the flume bed side by side leaving a small gap between the panels. Concrete and gravel were then placed in these gaps to form a continuous fixed gravel bed. The remaining bed of the flume was covered with a loose gravel ($3/4 - 3/8$ inch) and tamped to the the same level as the fixed bed. This was done so that: the bed level did not abruptly change in the testing section, encouraged uniform flow, and helped in developing the flow become fully turbulent in the testing section.

B.2.3 Ensuring Fully-Developed Flow

As outlined by White [84] flow transitioning from Laminar to turbulent can be classified in seven steps moving downstream:

Figure B.6: Tamping the gravel

Figure B.7: Finished surface of angular and rounded gravel panels

Figure B.8: Placing the panels into the flume

- Stable laminar flow
- Unstable two-dimensional Tollmien-Schlichting waves
- Development of three-dimensional unstable waves and hairpin eddies
- Vortex breakdown at regions of high localized shear
- Cascading vortex breakdown into fully three-dimensional fluctuation
- Formation of turbulent spots at locally intense fluctuations
- Coalescence of spots into fully turbulent flow

A "natural transition" is the gradual process that develops the flow through the above seven steps. This occurs with a quiet flow that is in a smooth uniform channel. Since the gravel bed channel in this set of experiments is rough, a "bypass transition"

occurs. Assuming that the flow leaves the inlet box as laminar flow, the flow would skip the initial transition steps and goes to the vortex breakdown and formation of turbulent spots.

There is no fundamental theory of transition. There are a number of experiments that have been done that correlate several factors into the transition length. Some of these correlation parameters are pressure gradient, freestream turbulence and wall roughness.

It is know that as the distributed roughness of the bed increases, the transition length will decrease. Unfortunately the effect of distributed roughness on transition length has not been studied extensively. To ensure that there was fully developed flow in the testing section, the empirical equation expressed in *Boundary-Layer Theory* [58] was used.

$$\mathbb{R}_{xcrit} = \left(\frac{U_\infty x}{\nu}\right)_{crit} = 3.2.\,10^5 \tag{B.81}$$

Equation B.81 is based on empirical data from a flat plate. Using an velocity of 55 cm/sec the required length for transition would be 5.8 m. Having a rough plate (such as gravel panels) would have a considerably shorter transition length.

The development of the fully developed turbulent flow was additionally checked by taking velocity profiles at different streamwise locations of the flume with the gravel panels in place. 10 vertical profiles were taken at every 1 m. The bed in the first five meters consisted of loose gravel (3/4 - 3/8 inch). The concrete gravel panels started at about 5 m from the entrance and ended at 10 m from the entrance. They collapsed into one profile starting at about 8 m from the inlet. The closest measurements taken were 9.1 m from the entrance. The furthest downstream that measurements were taken were 9.4 m from the entrance. The profiles are shown in Figure B.2.3.

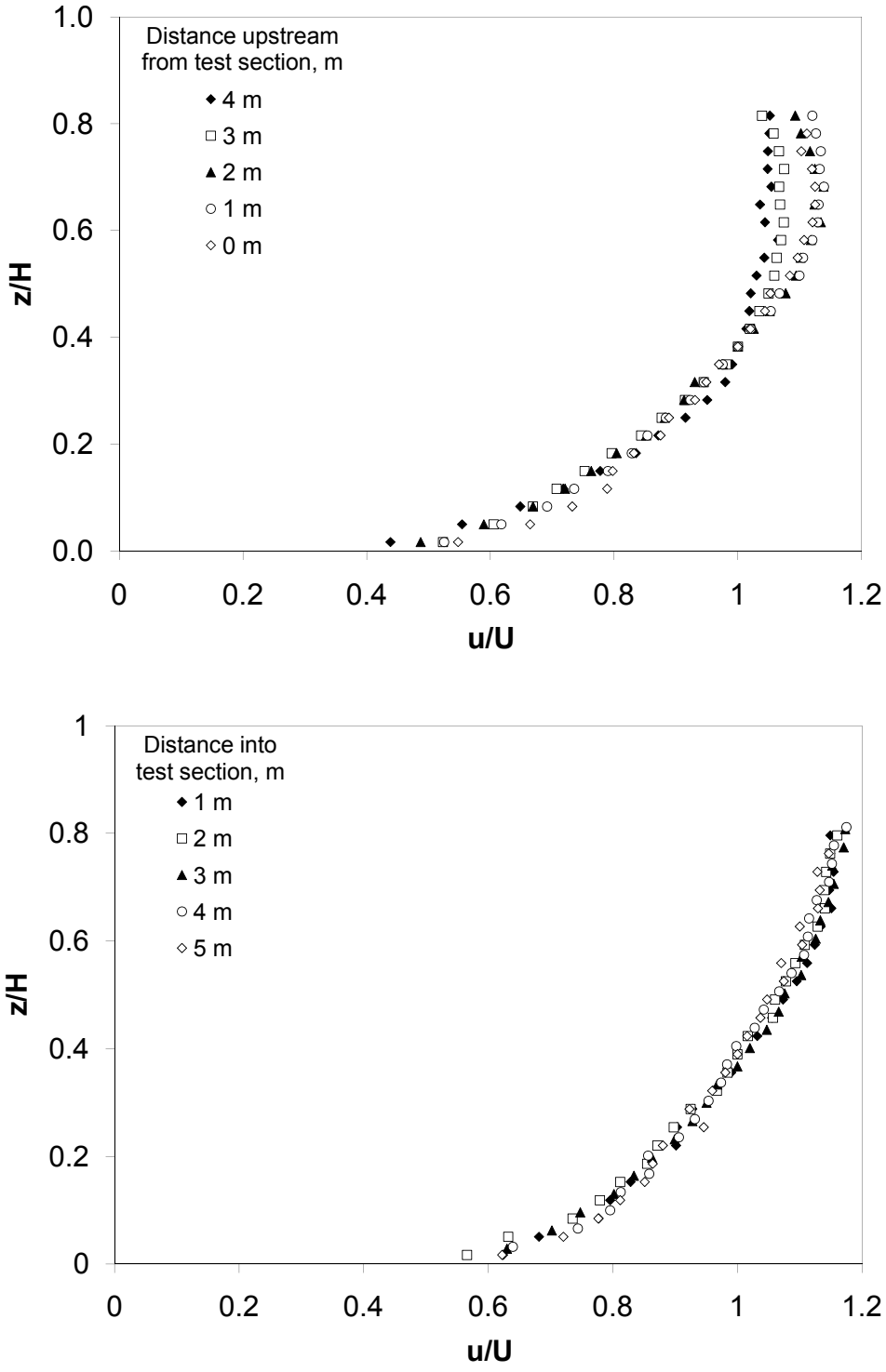

Figure B.9: Velocity profiles to ensure fully developed flow

B.2.4 Sampling Locations

Sampling locations were chosen at random in the fully developed velocity region. An imaginary 30 cm by 30 cm grid was set up with its center located 9.25 cm from the entrance. The square grid contained 100 possible choices for sampling locations. The flow was characterized by taking ADV measurements from 10 random cells. Figure B.2.4 shows the sampling grid locations.

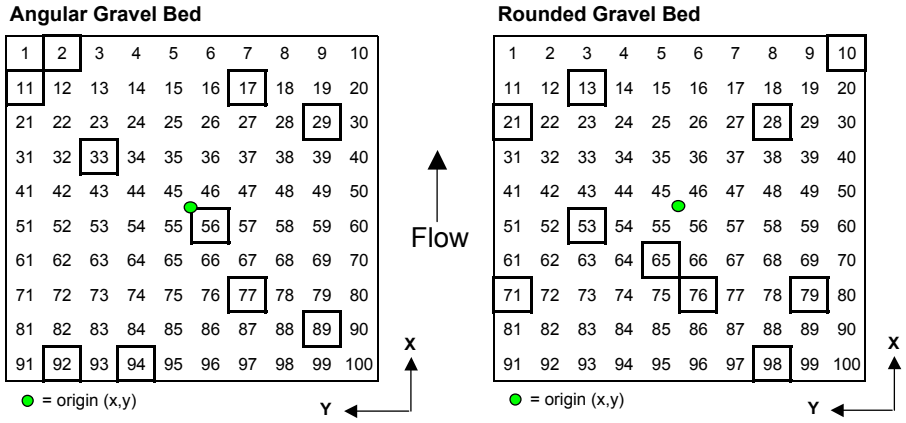

Figure B.10: Sampling locations

B.3 ADV Setup and Operating Principles

A Sontek 16-MHz field Micro Acoustic Doppler Velocimeter (ADV) was deployed for velocity measurements. The ADV hardware consists of an acoustic sensor consisting of three receivers and one transmitter. The sensor is connected to a flexible stem which is then connected to a signal conditioning module. The conditioning module is the cylindrical canister shown in Figure B.3. A 10m long flexible cable is connected from the conditioning module to the processor. The processor can then be connected to a computer to record and see "instantaneous" velocity measurements.

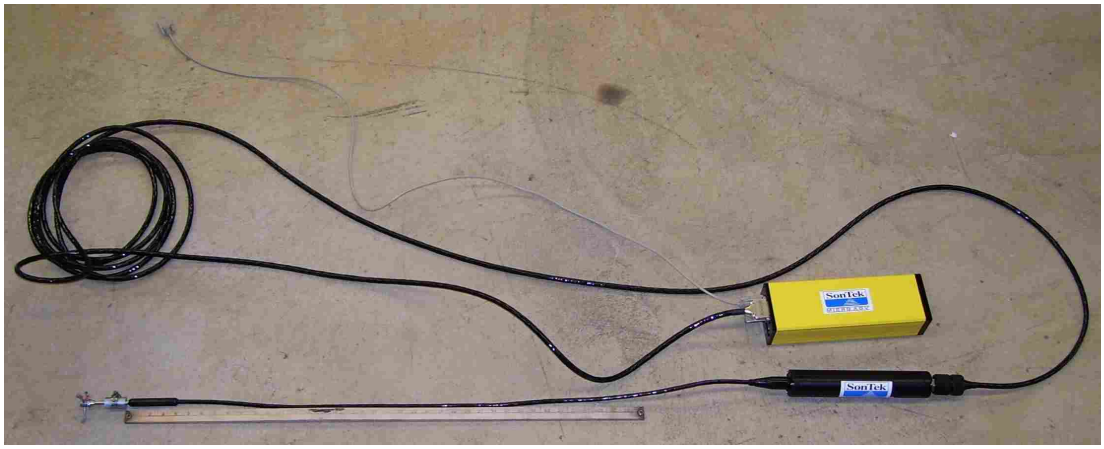

Figure B.11: Sontek 16-MHz Micro ADV

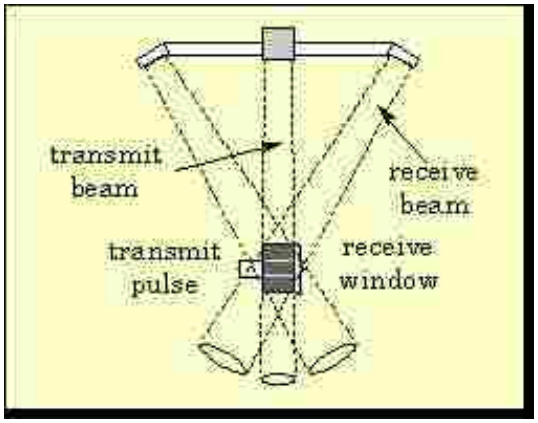

Figure B.12: ADV sampling volume (from [64])

The ADV has been selected as the instrument of choice for many turbulence measurements since it has relatively high sampling frequency, and has a relatively small remote sampling volume [27].

B.3.1 Sampling Volume

The sampling volume roughly resembles a cylinder. The diameter is set by the transmitter which is 4.5 mm ±0.3mm [68][64]. The height of the sampling volume is a little less exact. The height is defined by the "convolution of the transmitted acoustic pulse with the receive window over which the return signal is sampled" [64]. In the standard configuration it can be estimated that the sample volume height is

4.5mm [64], or 5.6mm [66] for the 16-MHz MicroADV. Assuming that the sample volume is a cylinder, the sampling volume could be estimated to be between 62mm^2 and 1.01cm^2.

B.3.2 Operating Principles

A description of ADV pulse coherent technology is described by Sontek's technical note on principles of operation [65] and also by McLelland and Nicholas [44]. The ADV calculates three-dimensional velocities by using the Doppler shift principle. A pair of pulses are emitted by the transmitter. The acoustic signal travels into the sampling volume and is reflected from particles in the water back to the three receivers. The pulse-to-pulse coherent Doppler technique [40] is used to determine the velocity of the particles (assumed equal to the velocity of the water).

A single estimate of velocity is referred to as a *ping*. Depending on the velocity setting of the instrument, the ADV pings at a rate of 150-250 times per second [65]. Pings are averaged together for each sample specified by the user frequency, f_R, setting. The highest setting for the 16-MHz microADV is 50Hz.

The signal strength is measured by the intensity of the acoustic reflections in the sampling volume. In other words, the more scattering particles in the water, the higher the signal strength will be. This signal to noise ratio (SNR) value is output with every sample. It has been recommended that SNR be at least 15 dB for turbulence measurements [65][80].

Correlation (COR) is another output for each sample. The correlation parameter indicates the relative consistency of the behavior of the scattering particles in the sampling volume during the sampling period [80]. A description of the COR calculation has been written by Martin et al. [42]. Sontek recommends using only samples that have COR values greater than 70% [65]. It has been argued that lower values of COR may still be valid in turbulent flow [80][42][70][13].

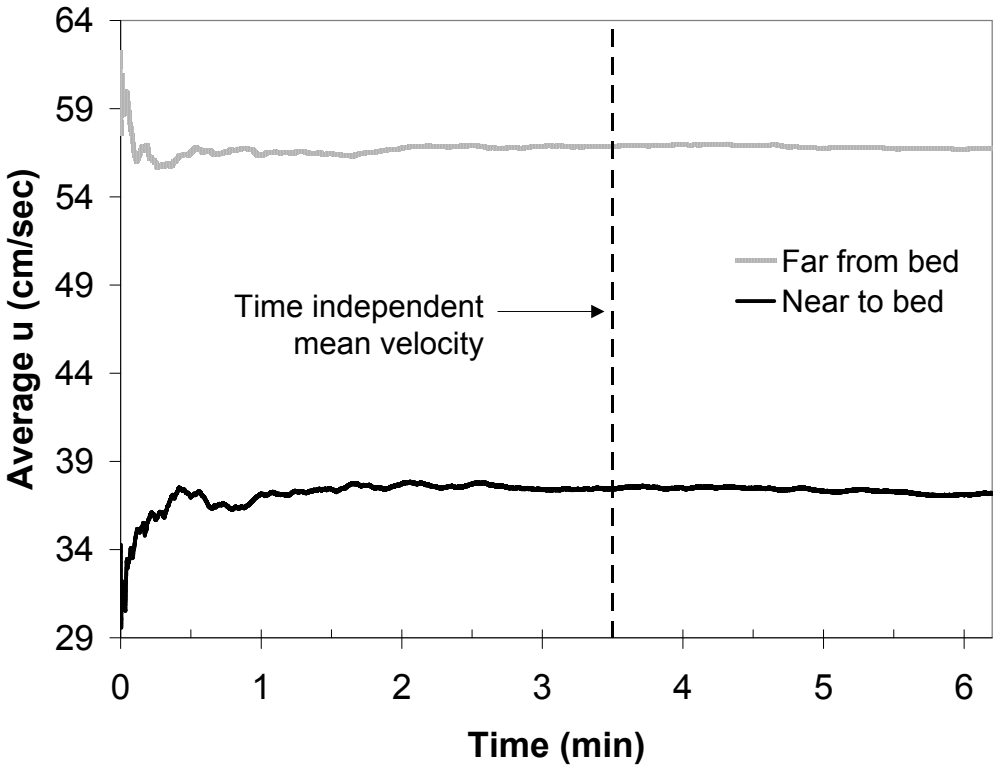

Figure B.13: ADV sampling time

B.3.3 Sampling Frequency and Duration

The ADV allowes user defined frequency settings for sample reporting. A sample is an average of pings as explained earlier. Higher frequency sampling allowed for smaller resolution of turbulence parameters. The frequency was set at 50Hz for all measurements since this was the highest setting of the ADV and allowed for the smallest turbulence resolution.

Sampling time was determined so that mean velocity measurements in the streamwise direction were independent of time (longer time periods would not change the average velocity). This was visually determined by plotting sampling time versus mean velocity. Figure B.3.3 shows the plot for two vertical location, one near and the other far from the bed. A sampling time of 3.5 minutes was used for all measurements.

Figure B.14: Trolley system

B.4 Traverse Setup and Finding a Datum

A traversing system with two *Velmex* step motors was set up to control the ADV location in the y and z direction. The traversing system is shown in Figure B.4. The motors could be moved with a remote control or with a software program named Cosmos. The location is controlled on the concept of steps in Cosmos. Once step in either the y or z direction represented 0.000635 cm. Cosmos commands are entered via a command line. As an example the command "C,I2M-400,R" would clear the system then move motor 2 (z-direction) up 400 steps (0.254 cm). The Velmex motors had a slightly different coordinate system than the ADV. Positive y-direction in Cosmos was downward toward the bed, and corresponded to the negative z-direction for the ADV. A positive x-direction for Cosmos was the positive y-direction for the ADV coordinate system (toward the left wall of the flume).

A digital point gauge with 0.01 mm resolution is attached to the instrument carriage and was used to measure water surface. The following process was used

in order to ensure the ADV and point gauge were on the same datum, and also to determine the location of the tops of the rocks:

- Flow was introduced at a low flowrate (pumps set at 25 Hz).
- A flat plate was rested on the top of the rocks in the testing section.
- The ADV probe was adjusted vertically to just touch the water surface.
- The y-location on the traversing system (Cosmo software) was changed to zero.
- The ADV was moved to a location where the sampling volume was at least 2.5 cm away from the boundary. (2.5 cm is recommended by Sontek [65])
- The distance between the sampling volume and the plate (read by the ADV) was recorded, along with the y-location of the traversing system (Cosmo software).
- The instrument carriage was moved so that the point gauge was above the same location that the ADV probe was.
- The point guage was set to zero when just touching the water surface.

Appendix C

Calculations and Results

C.1 Statistical Significance Between Population Means

One of the main objectives of this thesis was to determine if there were differences between the angular and rounded gravel for various flow parameters. When possible, the difference in the variable mean of interest was statistically determined significant or not. In order to compare the two population means, the "F-test" was performed to see if the population variances could be assumed equal or not. The "student t-test" was then followed to see if there was a statistical significance between the means.

C.1.1 F-test

The F-test was used to statistically determine if the variances between two populations were significantly different. The null hypothesis being that the two population variances are equal:

$$H_o : \sigma_1^2 = \sigma_2^2 \tag{C.82}$$

The F-test statistic uses the sample standard deviation (S):

$$F = \frac{S_1^2}{S_2^2} \tag{C.83}$$

If the two-tailed probability ($P(F \leq f)$) was less than 0.05, then the null hypothesis was rejected and the variances were assumed to be unequal.

C.1.2 T-test

The student T-test was used to determine if population means were significantly different. The calculation is based on the sample mean ($\overline{x}$), sample standard deviation (S), and the number of samples (n). The null hypothesis being that there was no difference in mean (μ) between the two populations:

$$H_o : (\mu_1 - \mu_2) = 0 \tag{C.84}$$

where the variances between the populations were equal the test statistic was:

$$t = \frac{(\overline{x_1} - \overline{x_2}) - (\mu_1 - \mu_2)}{\sqrt{Sp^2(\frac{1}{n_1} + \frac{1}{n_2})}} \qquad Sp^2 = \frac{(n_1 - 1)S_1^2 + (n_2 - 1)S_2^2}{n_1 + n_2 - 2} \tag{C.85}$$

where the variances between the populations were unequal the test statistic becomes:

$$t = \frac{(\overline{x_1} - \overline{x_2}) - (\mu_1 - \mu_2)}{\sqrt{\frac{S_1^2}{n_1} + \frac{S_2^2}{n_2}}} \tag{C.86}$$

If the two-tailed probablility ($P(T \leq t)$) was less than 0.05, then the null hypothesis was rejected and the population means were assumed different.

C.2 Particle Shape Analysis

There are several ways to quantify the shape of a particle, none of which are universally accepted [5]. The attempt here was to analyze the shape in some of the most common methods. Table C.1 lists length scales from 50 random samples for the rounded and angular gravel.

Table C.1: Length scales of gravel

Length Scale	Rounded mm	Angular mm
Average a-axis	37.0	39.9
Average b-axis	27.3	27.6
Average c-axis	14.9	15.1
Mean sieve opening	24.6	24.6
Nominal diameter	24.4	25.1

The mean sieve opening was determined by taking the average between the passing sieve size (25.4 mm) and the retaining sieve size (23.8 mm). The nominal diameter was calculated from Equation A.12. Statistical significance between the average length scales was computed from the student t-test as outlined in Section C.1. The only statistically significant different length was the a-axis. This means that the averages from all the length scales (except for the a-axis) most likely came from the same population mean.

Sphericity and shape were classified as well with Zingg's classification (See Figure C.2). The average of both the angular and rounded rock lie fairly close together in quadrant I, corresponding to the disc-shaped region. When compared to Figure A.5 it appears that averages of both the angular and rounded samples have a sphericity of about 0.65.

Form and Sphericity were also classified using the Sneed and Folk [62] classification. The average form factor, F, (see Equation A.14) for the rounded and angular rock were respectively 0.43 and 0.48. The values of compactness, S, (see Equation A.15) were 0.41 and 0.39 for the rounded and angular gravel respectively. The F and S values for both sets of gravel classified them both into the same category. Both were classified in the Bladed (B) category as seen in Figure A.9.

Quantifying the shape of particles by image analysis has recently received some attention with regards to hot-mix asphalt design [43] [83] [4]. Quantifying shape from an image of a particle is referred to as image analysis. A color image is transformed into a two tone image (each pixel having only one of two possible values). From this

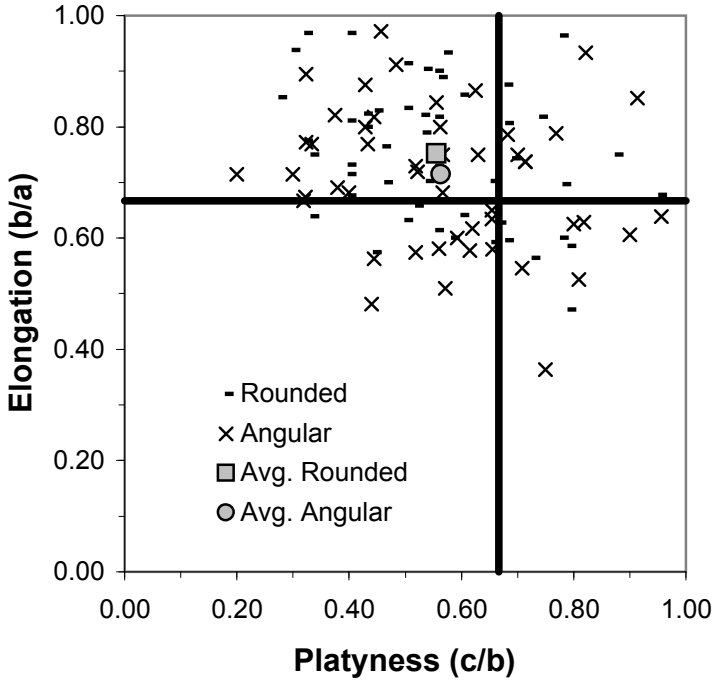

Figure C.2: Zingg's classification for 50 bed particle samples

two-tone image, the edge of the particle can be distinguished. By using a computer algorithm, the area, perimeter, and corresponding calculations can be performed to quantify the shape.

The software *ImageJ* was used to carry out the image analysis of the gravel. "Form factor" (FF) is generally accepted as a way to describe the irregularities of a particle. Not to be confused with the "form factor" (F) computed from axis lengths, form factor (FF) using image analysis is defined as:

$$FF = \frac{4\pi A}{p^2} \tag{C.87}$$

where A and p are the particle's area and perimeter respectively. The form factor (FF) is usually presented as a value less than 1. A smooth round particle will have a FF of 1. As the irregularities of the particle increase the FF value will decrease. Digital image analysis has automated the FF calculation method and provides a way

to quantitatively describe rock angularity [43]. Image analysis is inherently a two-dimensional analysis. Wang et al. found that the orientation of the particle does not introduce significant bias in the analysis [83]. So, a two-dimensional image analysis can in effect be used to represent the three-dimensional object.

The Shape Descriptor class written by Gary Chinga was used in conjunction with ImageJ to calculate Form Factor (FF) along with Roundness (Ro), Compactness (Co), and Aspect Ratio (AR) which are computed as follows:

$$Ro = \frac{4A}{\pi\sqrt{a}} \tag{C.88}$$

$$Co = \frac{\sqrt{(4/\pi)A}}{a} \tag{C.89}$$

$$AR = a/b \tag{C.90}$$

where A is the area, p is the perimeter, a and b are the major and minor axes (of 2-dimensional image) respectively.

350 random samples were taken from the angular and rounded gravel (700 total) to characterize differences in shape using image analysis. The gravel was painted black and rested on a white backdrop to improve the contrast between the gravel and the background. A makeshift studio was built to keep the camera distance consistent and to provide additional lighting. To capture the angularity characteristics of the particle it has been recommended that the pixel size be at most 1% of the particle diameter [4]. The gravel diameters in this experiment range from 2.38 cm to 2.54 cm, so the image resolution needed was 0.23 mm per pixel or smaller. In this experiment the pixel resolution used was 0.18 mm per pixel. A "Kodak Easy Share C433" digital camera was used to take the pictures. Built-in features of ImageJ allowed the images to be transformed from a color image to a grayscale image and finally to a two-tone image. With each pixel representing one of two possible values, the necessary parameters for Equations C.87 - C.90 could be calculated.

Figure C.3: Makeshift photo studio for image analysis

The image analysis showed a differences between the two gravel sets as shown in Table C.2. The angular and rounded rock shown in Figure C.4 both have the average FF values of their respective sets. The t-test probability shows that the two groups come from different populations.

Table C.2: Image analysis results

	Angular	Rounded	P*
Form Factor, FF	0.75	0.82	9.64E-71
Roundness, Ro	0.71	0.76	3.44E-07
Compactness, Co	0.84	0.87	2.80E-07
Aspec Ratio, AR	1.46	1.35	2.11E-07

* T-test P-value that the means are equal

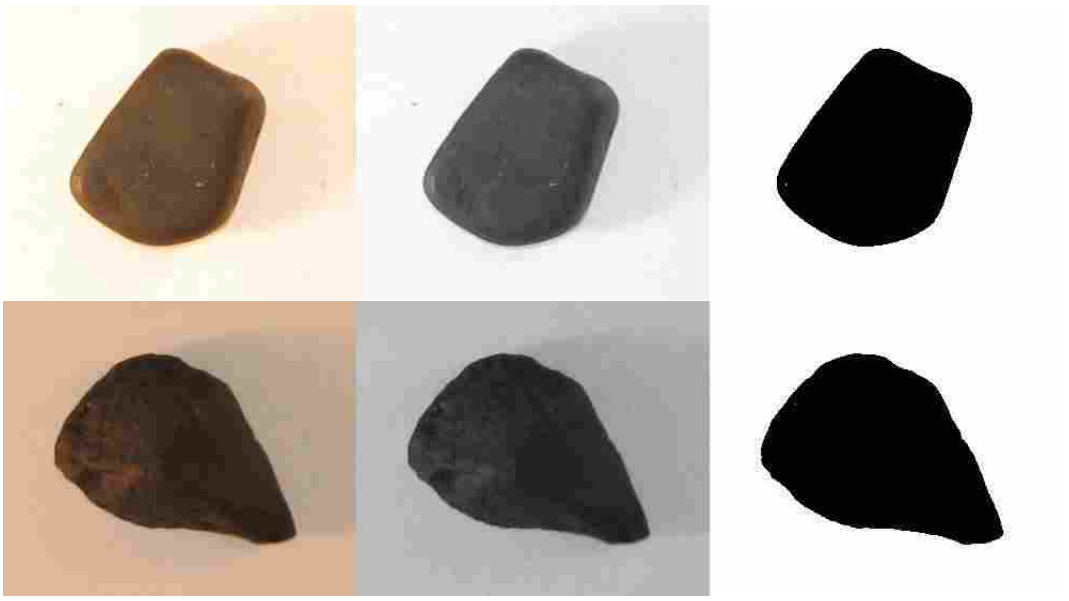

Figure C.4: Photograph transformation for image analysis

C.3 Filtering the ADV Data

Processing the raw ADV data was accomplished primarily by the software program *WinADV*, developed by Tony Wahl of the Bureau of Reclamation. Features of the program can be found in the article, "Analyzing ADV Data Using WinADV" by Tony Wahl [80] and also on the Bureau of Reclamation web site (www.usbr.gov).

Filtering the raw ADV data usually involves choosing a cut-off value for the signal-to-noise ratio (SNR_{CR}) and the Correlation (COR_{CR}) value. Once the SNR_{CR} and COR_{CR} value were determined, the mean velocity and turbulence intensity profiles were visually examined to filter out unusual points.

Sontek recommends using $\mathrm{SNR}_{CR} = 15$ and $\mathrm{COR}_{CR} = 70$, but these values (especially COR_{CR}) have come under scrutiny recently since they filter out much of the data in turbulent flows near the bed [80][42][70][13]. The average SNR values recorded in this set of experiments were higher than the recommended value (see Figure C.5, so SNR_{CR} was set at 15. Leaving the COR_{CR} at 70, however, filtered out much of the individual points in the data files. Low correlation scores can be

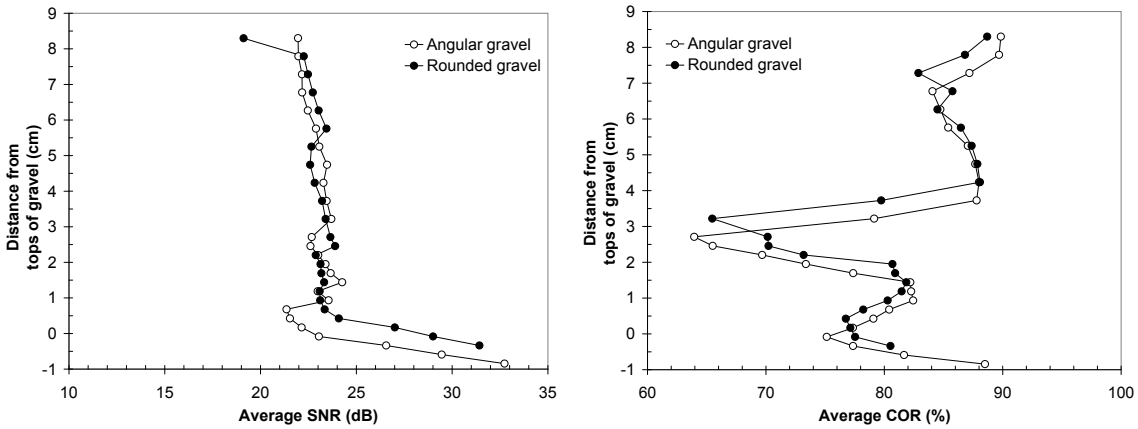

Figure C.5: Average SNR and COR for unfiltered data

caused by turbulent flows, air bubbles, low SNR values, large velocity gradients in the sampling volume, large individual particles near the sampling volume, and/or interference from the boundary [42]. A process was developed to find a value for COR_{CR} that would allow the most data to be filtered out but still leave sufficient data to gain insight into the flow characteristics.

The process used for finding COR_{CR} was similar to that used by Strom and Papanicolaou [70]. The velocity data distribution at each measuring point appears to follow a normal distribution. As points are filtered out, the distribution strays from its gaussianity. A normal probability plot was insufficient to visualize any drop in normality, so the coefficient of determination (R^2) between the data z-score and a normal distribution was used.

By systematically varying the COR_{CR} and recording the R^2-value, a cut-off value of 50 was visually selected. The R^2 value appeared to drop down after COR_{CR} of 50 (see Figure C.6). Meaning that using $\mathrm{COR}_{CR} > 50$ caused undersampling of the data. This COR_{CR} value is in agreement with Strom and Papanicolaou's value of 50 [70] and Martin et al.'s value of 40 [42].

Along with the SNR_{CR} and COR_{CR} filters, the phase space threshold despiking algorithm developed by Goring and Nikora [29] and modified by Wahl [81] was used.

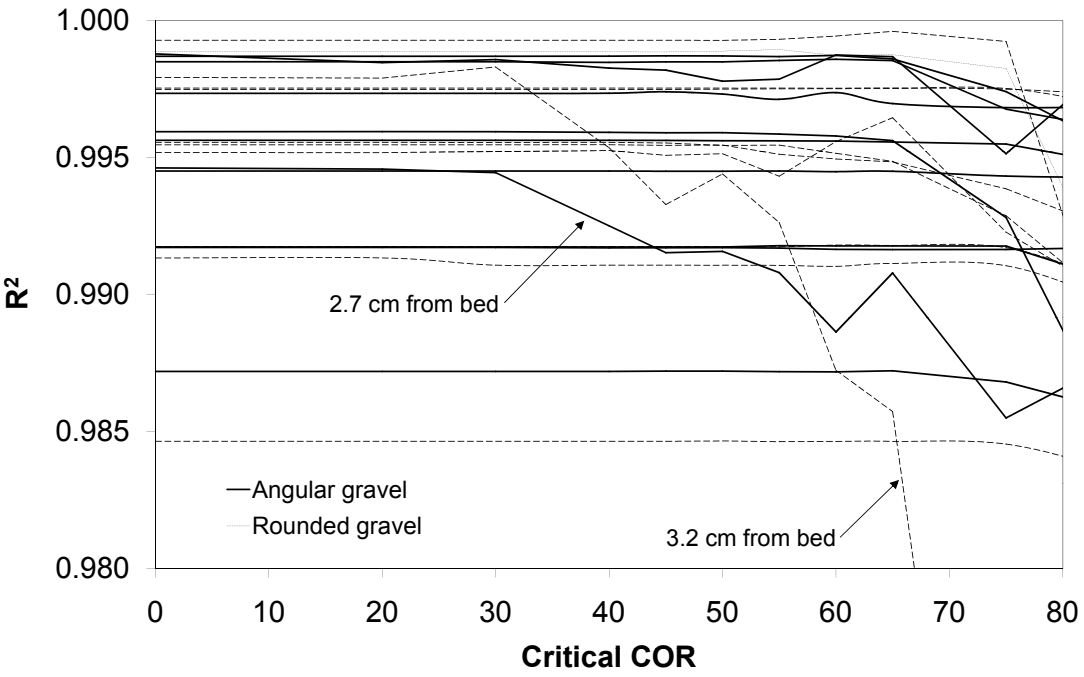

Figure C.6: Determining COR_{CR} at various depths

In order to retain as much "good" data as possible, two possible filters were applied. The data was first filtered using the despiking algorithm, along with a SNR_{CR} of 15 and COR_{CR} of 70. If more than 70% of the data was retained, then no more filtering was done. If the data set had more than 30% of the data removed, then a second filter was used on the original data. The second filter was the same as the first, but COR_{CR} was set at 50 instead of 70. If the data set still had more than 30% of the data removed, then the entire point was thrown out.

The first filter resulted in 15% of the data (13% of the angular and 16% of the rounded) needing the second filter applied. Of those 15% needing the second filter, 21% (27% of the angular and 15% of the rounded) were thrown out.

The mean velocity and turbulence intensity profiles were examined after the first filtering process to remove any non conforming data. Points removed by visual filtering are shown as open symbols in Figures C.7 and C.8.

There appeared to be a "velocity hole" located at about 3 cm from the bed. This can be seen by the spike in low COR values in Figure C.5. These two low COR spikes are most likely due to interference with the boundary [67]. Interference occurs when the return signal from the boundary reaches the receivers at the same time as the return signal from the sample volume. The signal from the sample volume is in effect hidden by the noise from this boundary reflection [42] [39] [29]. This interference caused most of the data in this region to be filtered out.

C.4 Virtual Bed Level

Where exactly the origin of a bed for smooth walls is a trivial matter. For rough beds, however, the origin becomes a little fuzzy. The origin could be argued to be located anywhere between the highest peak to the lowest point between roughness elements. Experimentally the origin can be found by extending the logarithmic portion of the velocity profile down to the bed. The origin being where this extended velocity profile is zero [18]. Many have suggested where this virtual origin should be located below the tops of the roughness elements: $0.25k_s$ [23] [74]; $0.5D_{50}$ [73];$0.2k_s$ [37]; and $0.033k_s$ [22]. Other have suggested a more complex method of defining the bed origin. It have been argued that the origin should be located where a smooth bed origin would be having the same volume (as the rough bed) and constant thickness [25] [12].

The origin was found for each experimental data set by extending a least-squares polynomial curve fit of the logarithmic layer down to where $u = 0$. The results for the angular and rounded gravel beds are shown in Figures C.9 and C.11. Run 9 for the rounded gravel bed resulted in an unrealistic origin (higher than the tops of the gravel), most likely due to a lack of good data closer to the bed. For further calculations the origin for run 9 was assumed equal to the average of the origin found for the other 9 rounded gravel runs. The statistical student t-test found a 52%

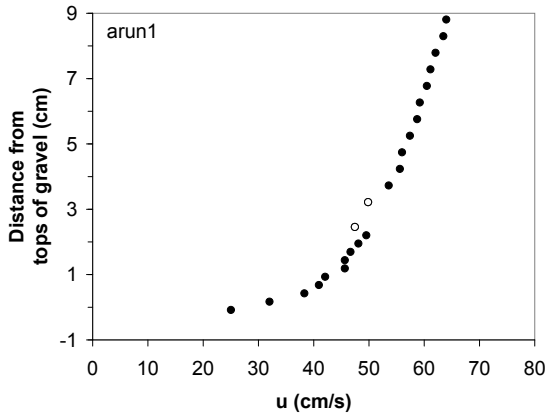
arun1
Distance from tops of gravel (cm)
u (cm/s)

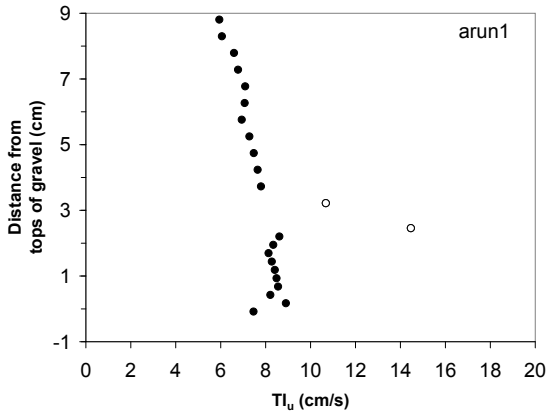
arun1
Distance from tops of gravel (cm)
TI_u (cm/s)

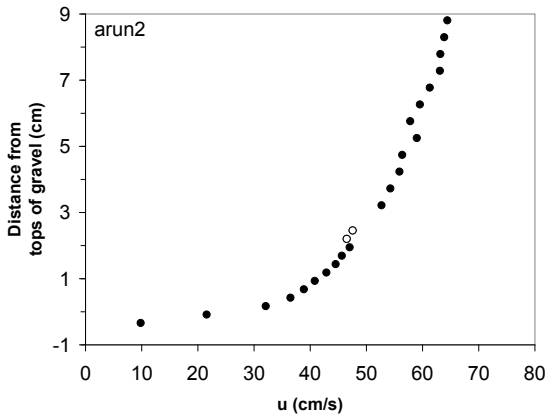
arun2
Distance from tops of gravel (cm)
u (cm/s)

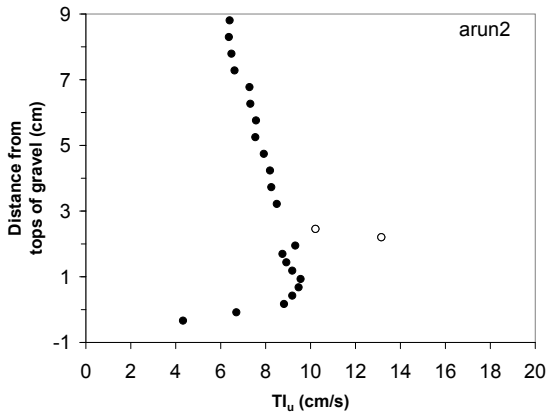
arun2
Distance from tops of gravel (cm)
TI_u (cm/s)

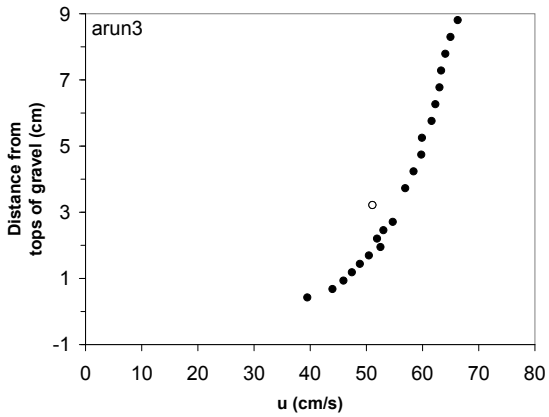
arun3
Distance from tops of gravel (cm)
u (cm/s)

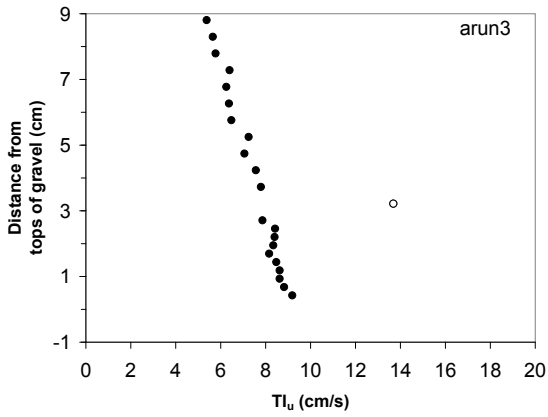
arun3
Distance from tops of gravel (cm)
TI_u (cm/s)

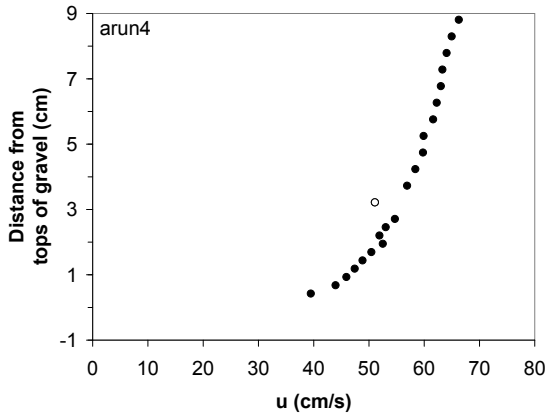
arun4
Distance from tops of gravel (cm)
u (cm/s)

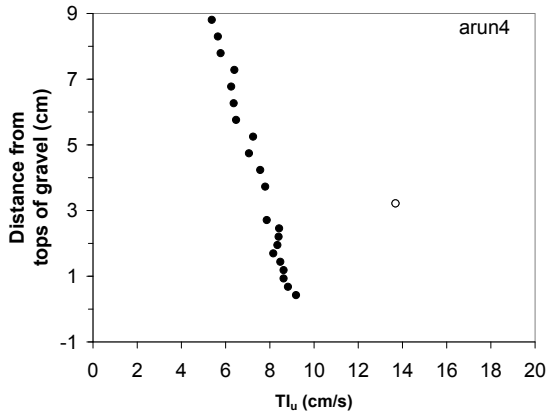
arun4
Distance from tops of gravel (cm)
TI_u (cm/s)

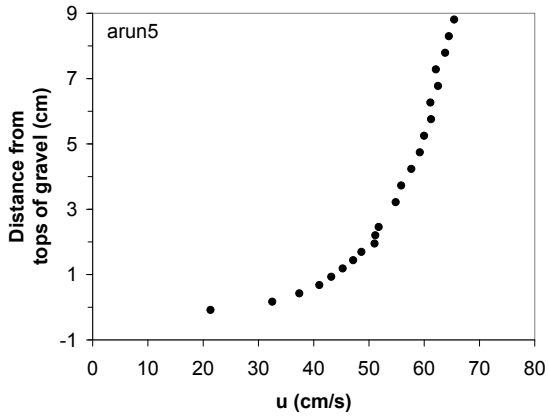
arun5
Distance from tops of gravel (cm)
u (cm/s)

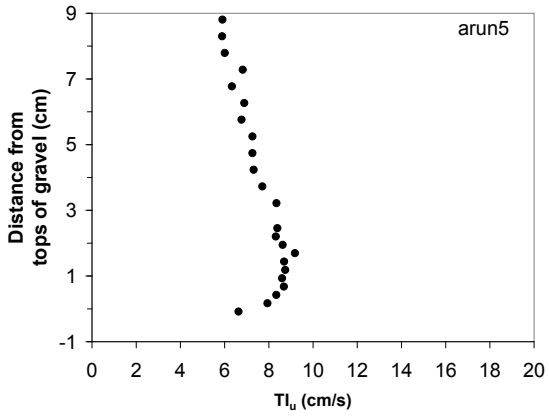
arun5
Distance from tops of gravel (cm)
Tl$_u$ (cm/s)

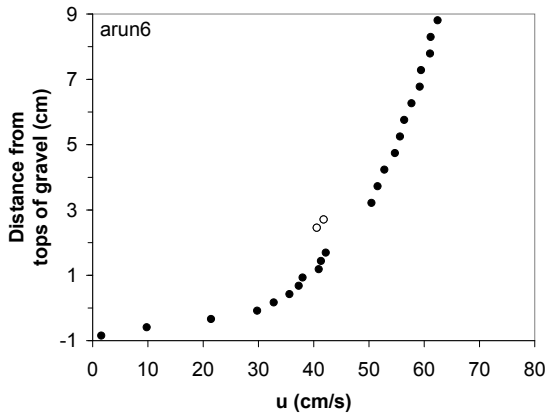
arun6
Distance from tops of gravel (cm)
u (cm/s)

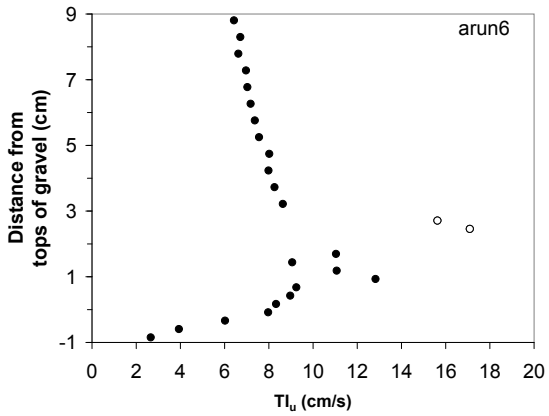
arun6
Distance from tops of gravel (cm)
Tl$_u$ (cm/s)

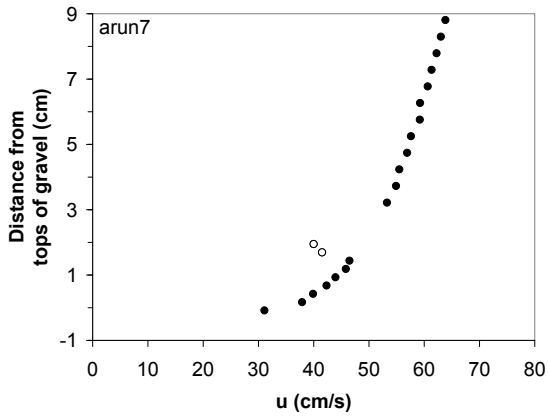
arun7
Distance from tops of gravel (cm)
u (cm/s)

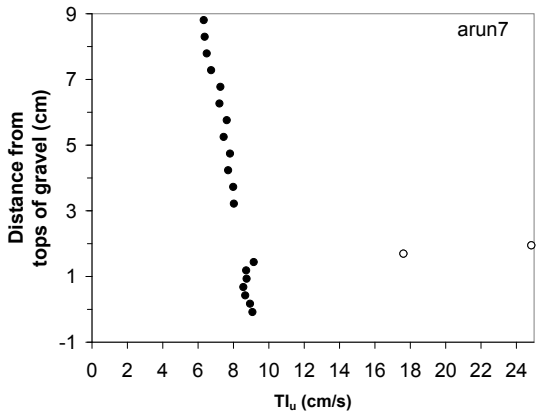
arun7
Distance from tops of gravel (cm)
Tl$_u$ (cm/s)

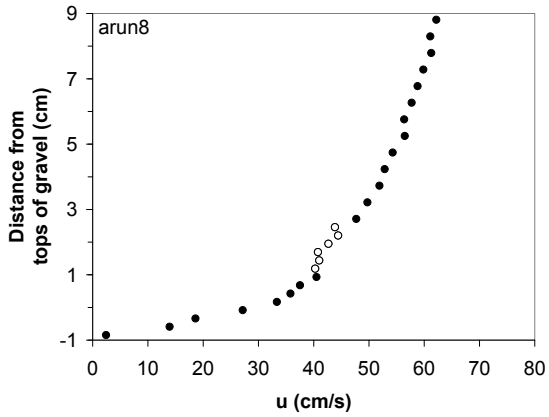
arun8
Distance from tops of gravel (cm)
u (cm/s)

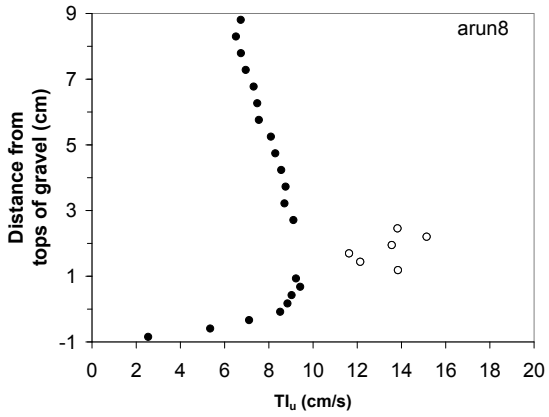
arun8
Distance from tops of gravel (cm)
Tl$_u$ (cm/s)

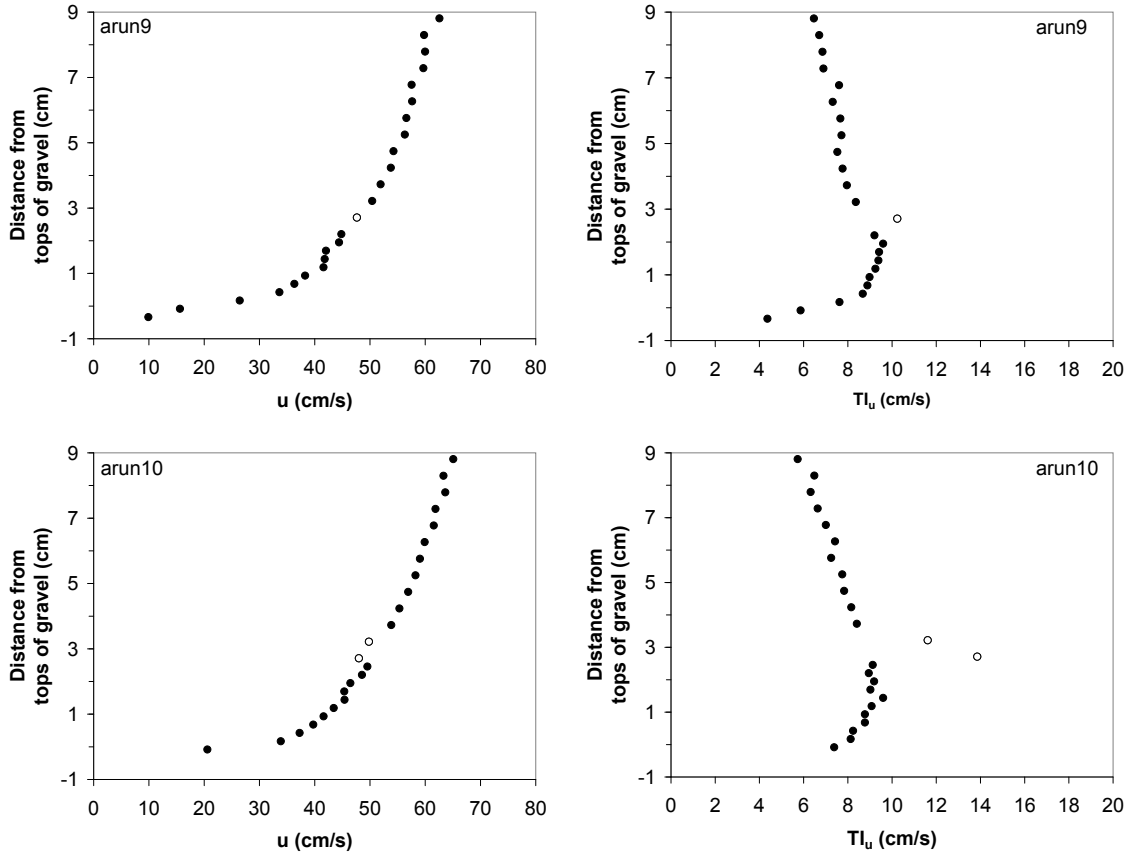

Figure C.7: Visual filter for angular gravel runs, open symbols represent filtered data points

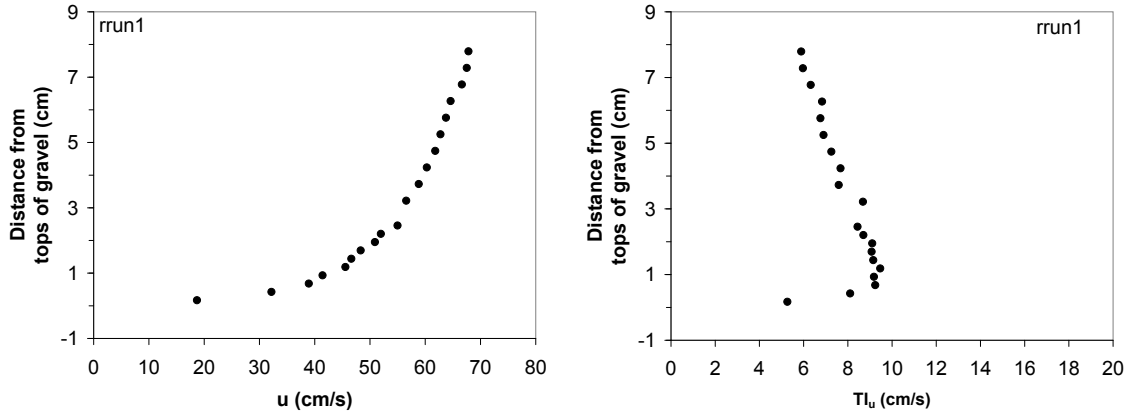

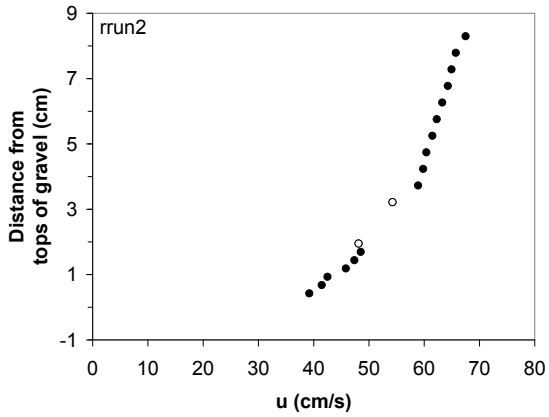
rrun2
Distance from tops of gravel (cm)
u (cm/s)

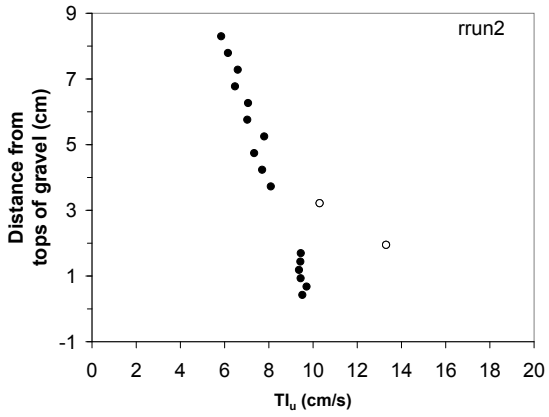
rrun2
Distance from tops of gravel (cm)
Tlu (cm/s)

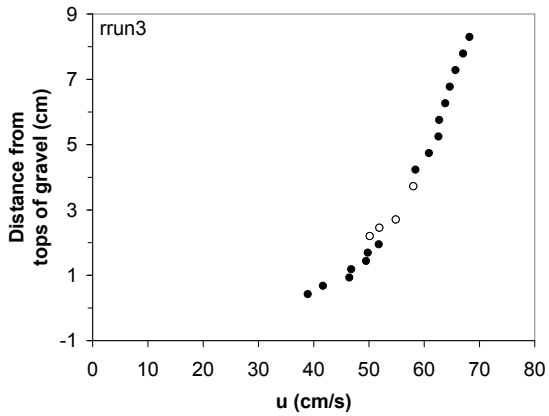
rrun3
Distance from tops of gravel (cm)
u (cm/s)

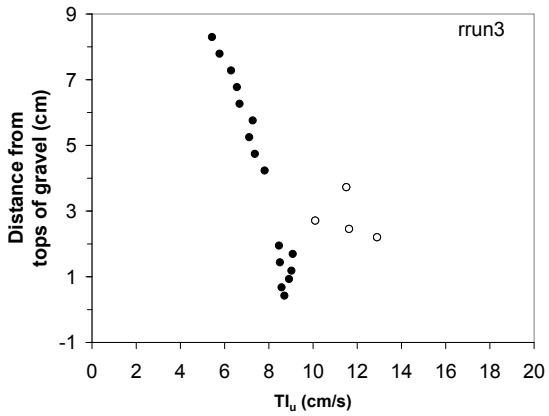
rrun3
Distance from tops of gravel (cm)
Tlu (cm/s)

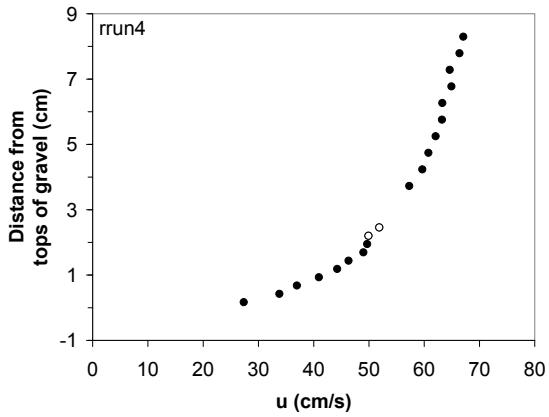
rrun4
Distance from tops of gravel (cm)
u (cm/s)

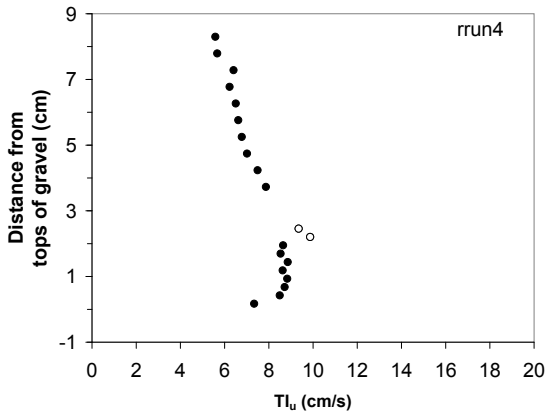
rrun4
Distance from tops of gravel (cm)
Tlu (cm/s)

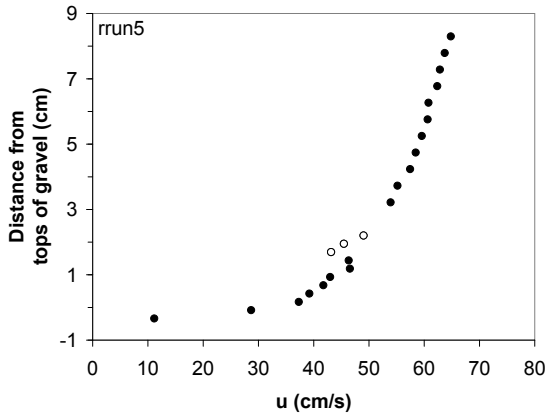
rrun5
Distance from tops of gravel (cm)
u (cm/s)

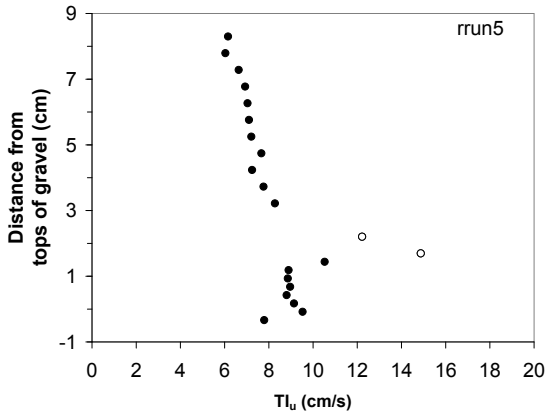
rrun5
Distance from tops of gravel (cm)
Tlu (cm/s)

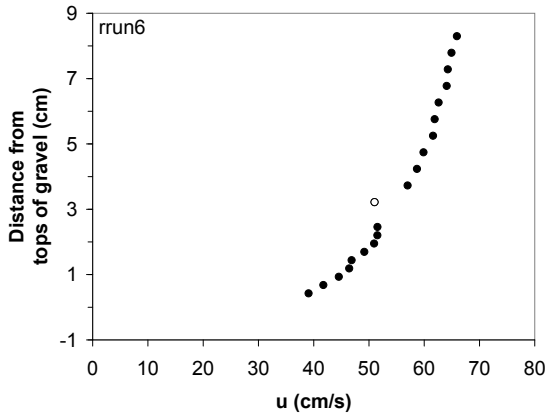
rrun6
Distance from tops of gravel (cm)
u (cm/s)

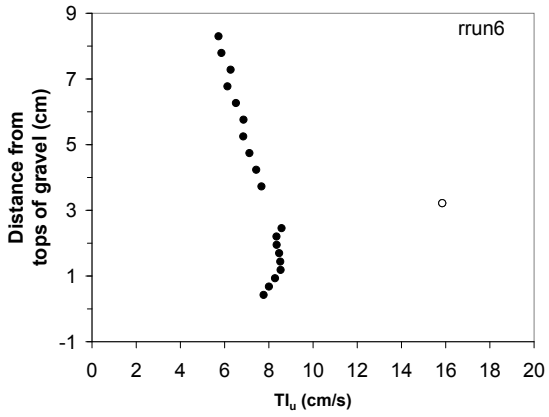
rrun6
Distance from tops of gravel (cm)
Tl$_u$ (cm/s)

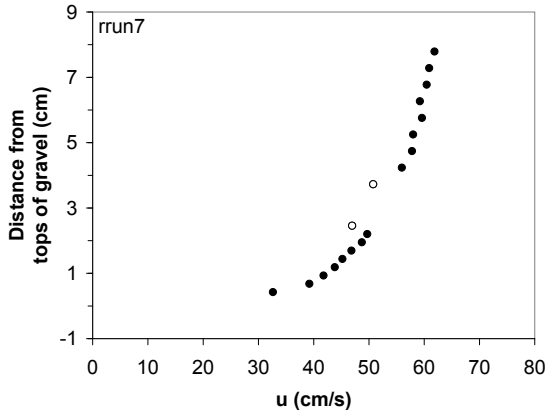
rrun7
Distance from tops of gravel (cm)
u (cm/s)

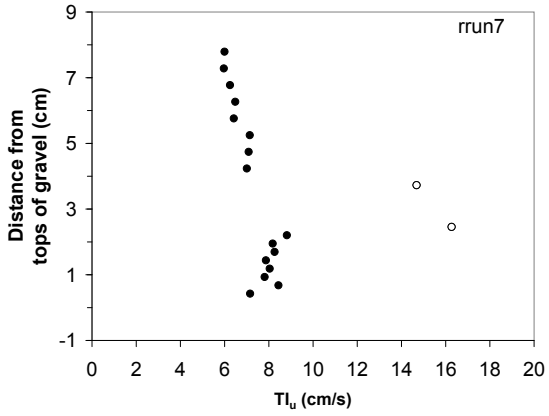
rrun7
Distance from tops of gravel (cm)
Tl$_u$ (cm/s)

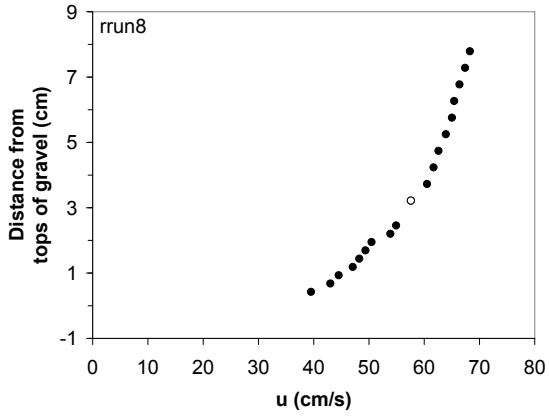
rrun8
Distance from tops of gravel (cm)
u (cm/s)

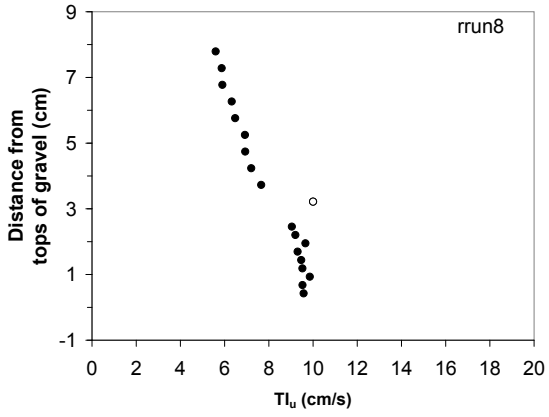
rrun8
Distance from tops of gravel (cm)
Tl$_u$ (cm/s)

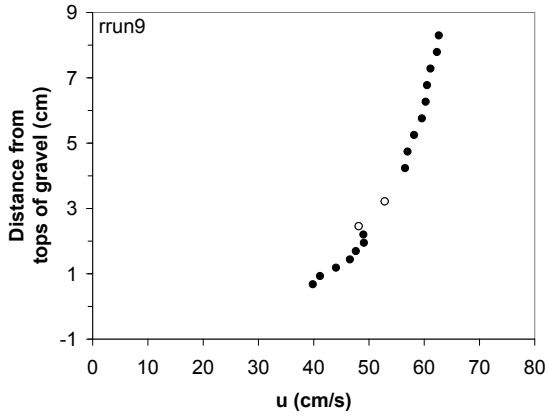
rrun9
Distance from tops of gravel (cm)
u (cm/s)

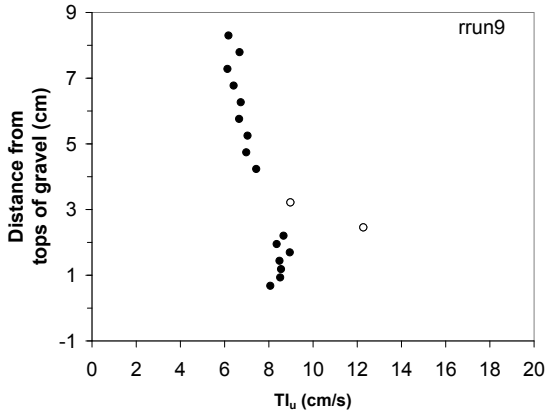
rrun9
Distance from tops of gravel (cm)
Tl$_u$ (cm/s)

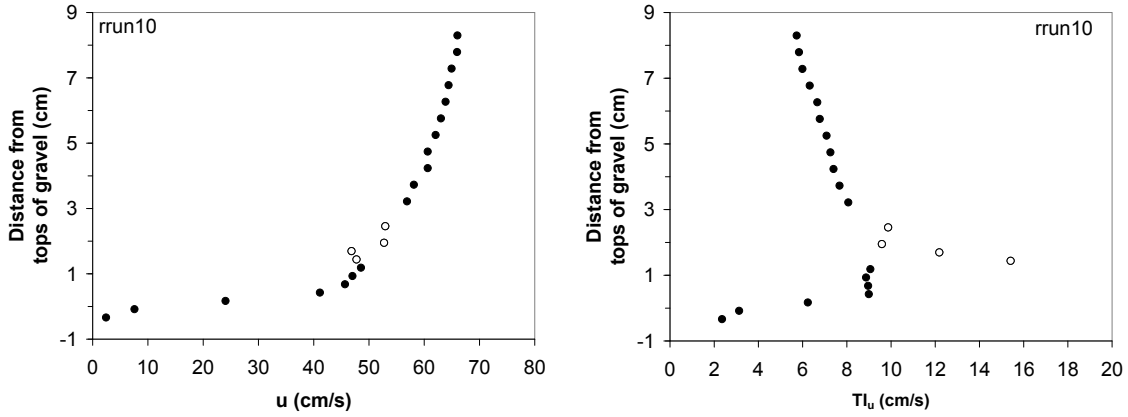

Figure C.8: Visual filter for rounded gravel runs, open symbols represent filtered data points

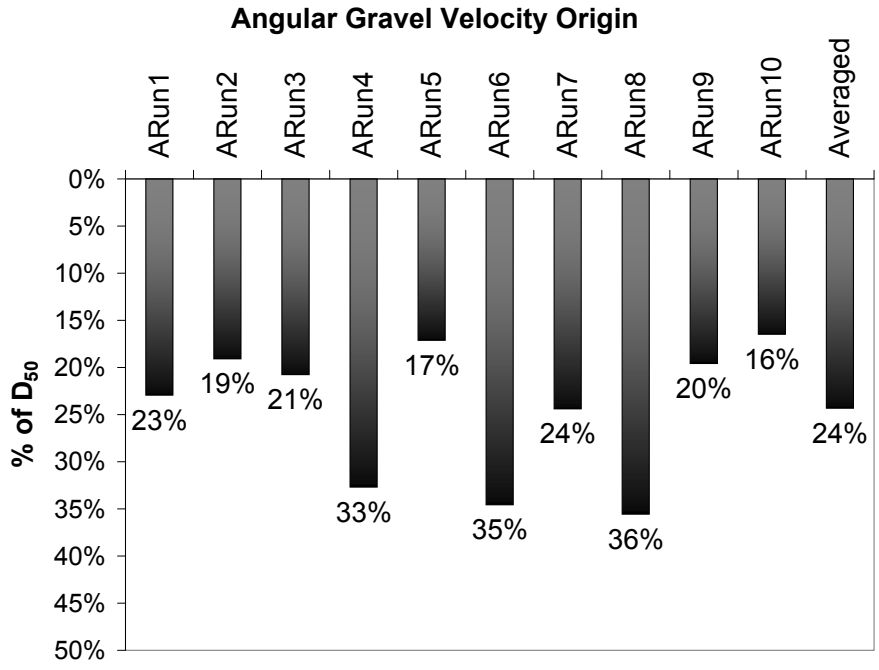

Figure C.9: Virtual origin for angular gravel bed

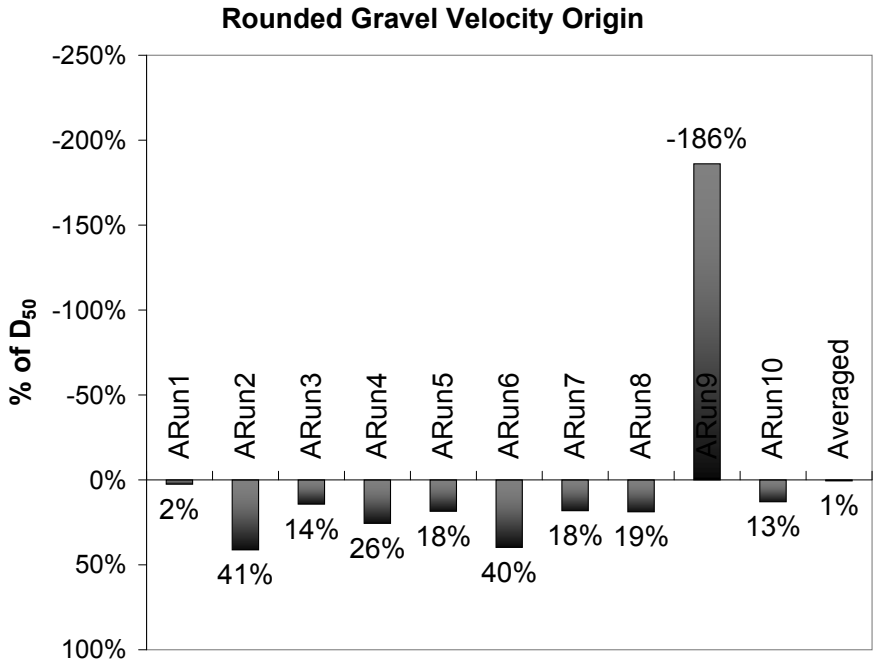

Figure C.10: Virtual origin for rounded gravel bed

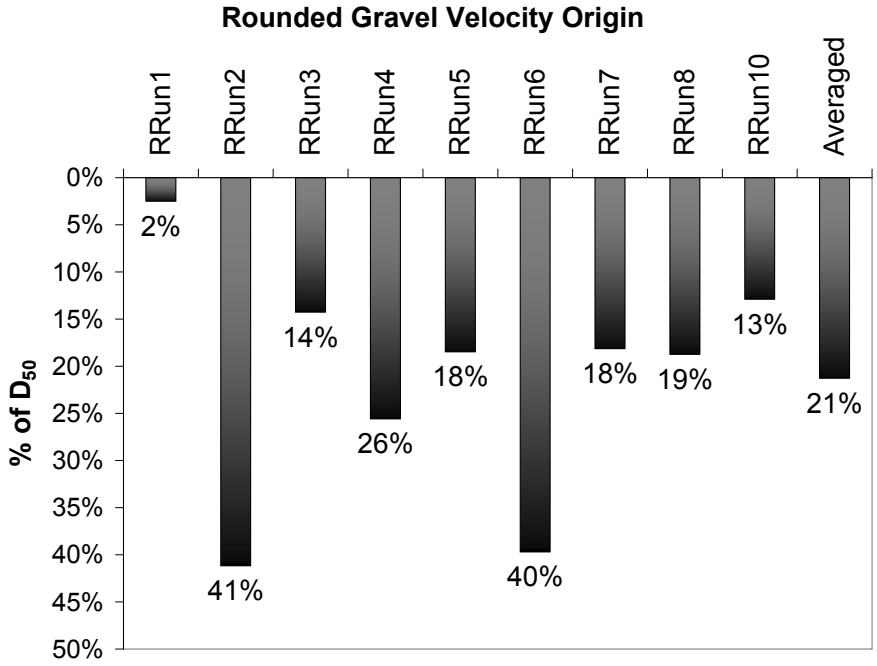

Figure C.11: Virtual origin for rounded gravel excluding run 9

probability that the average origin level between the angular and gravel beds are the same. Therefore, there is not enough evidence to support the idea that angularity changes the origin level.

Figure C.12 show and example of the velocity profile extrapolated to the origin. For the sake of not taking the natural log of a negative number, the z-elevation was initially offset 2 cm above the tops of the gravel.

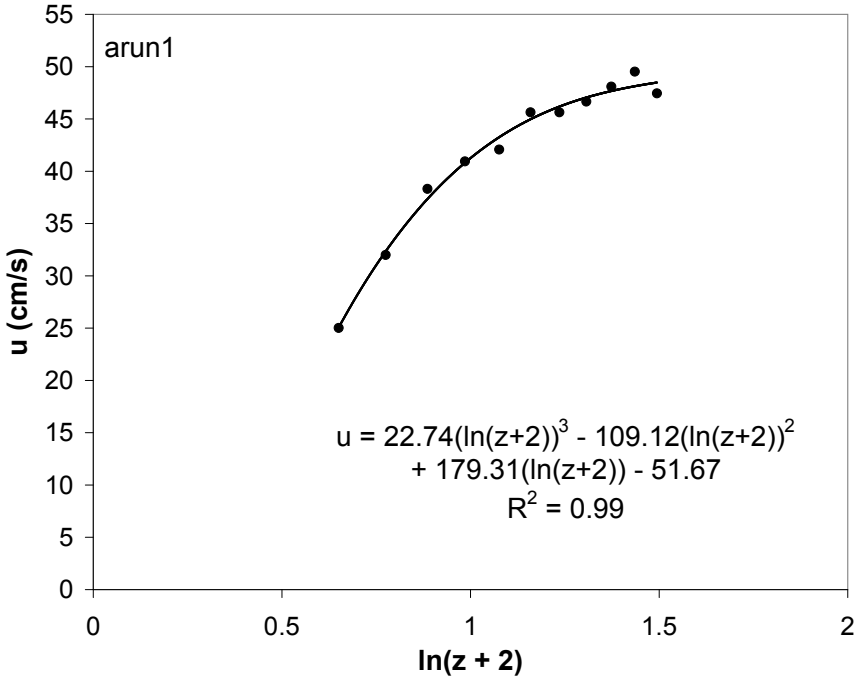

Figure C.12: Extrapolation of velocity data to find origin

C.5 Shear Velocity

A scaling factor that is often used in describing flow parameters is shear velocity (u_τ) sometimes refered to as *friction velocity* [9] or *wall-friction velocity* [84]. The definition of shear velocity is as follows:

$$u_\tau \equiv \left(\frac{\tau_w}{\rho}\right)^{1/2} \tag{C.91}$$

There are several ways to calculate u_τ. Some of them are the St Venant method, the Reynolds stress method, and the Clauser method. Each of these will be discussed in turn.

C.5.1 St Venant Method

The shear stress on the bed, τ_w, can be estimated from a global perspective using:

$$\tau_w = \gamma RS \tag{C.92}$$

R is the hydraulic radius, and S is the friction slope (equal to the bed slope in uniform flow). Combining Equations C.91 and C.92 gives the following equation for shear velocity [2] [17].

$$u_\tau = \sqrt{gRS} \tag{C.93}$$

The gravitational acceleration constant, g, is assumed equal to 9.81 m/sec. The depth used to find the hydraulic radius was based on the virtual origin as explained in section C.4. Since the side-walls of the flume had a different roughness than the bed, a side-wall correction was used to find the hydraulic radius. The side-wall correction procedure of Vanoni and Brooks was used [75]. The shear velocities for each experimental run are shown in Table C.3.

C.5.2 Reynolds Stress Method

Shear stress for two-dimensional turbulent flow can be divided into viscous and Reynolds stresses.

$$\tau = \mu \frac{d\overline{u}}{dz} - \rho \overline{u'w'} \tag{C.94}$$

Table C.3: Shear velocity found by St Venant method

Angular	u_τ cm/sec	Rounded	u_τ cm/sec
arun1	5.25	rrun1	4.94
arun2	5.23	rrun2	5.13
arun3	5.24	rrun3	5.00
arun4	5.30	rrun4	5.05
arun5	5.23	rrun5	5.02
arun6	5.31	rrun6	5.12
arun7	5.26	rrun7	5.02
arun8	5.31	rrun8	5.02
arun9	5.24	rrun9	5.03
arun10	5.22	rrun10	4.99
Avg.	5.26	Avg.	5.03

where μ is the dynamic viscosity, $d\overline{u}/dz$ is the velocity gradient in the vertical direction, and $\overline{u'w'}$ (often called Reynolds stress tensor) is the time averaged cross correlation coefficient between the streamwise (u) and vertical (w) velocities. For open-channel turbulent flows away from the wall, the Reynolds stress term dominates as seen in Figure C.13. For two dimensional flow, the shear velocity can be found by integrating the Navier-Stokes equations for the water depth [49]. This new equation for shear velocity based on Reynolds stress distribution can be expressed as:

$$u_\tau = \sqrt{\frac{-\overline{u'w'}}{1-\frac{z}{H}}} \tag{C.95}$$

Extrapolating the Reynolds stress term to the wall ($z = 0$), allows the determination of u_τ. The Reynolds stress term ($\overline{u'w'}$) was found by *WinADV's* covariance function (COV-XZ). Figure C.14 is an example of how the shear stress was found for all experimental runs. Near-bed measurements were not used for the extrapolation line, since viscous stresses dominate near the bed. The shear velocities for each experimental run are shown in Table C.4.

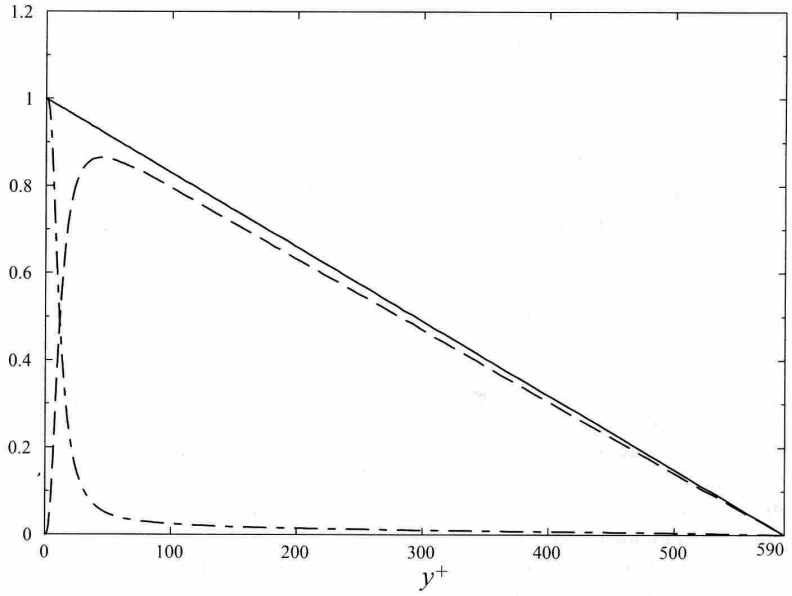

Figure C.13: Decomposition of total shear stress (— — = $\overline{u'w'}$, — - — = $d\bar{u}/dz$) (from [9])

C.5.3 Clauser Method

The Clauser method of finding shear velocity is well documented by Kironoto and Graf [37]. This method used the assumption that the *log-law* equation can be fit to the inner (viscous) region. The log-law equation is written as:

$$\frac{\bar{u}}{u_\tau} = \frac{1}{\kappa} \ln\left(\frac{z}{k_s}\right) + B \tag{C.96}$$

Since the log-law equation has several unknowns, it is necessary to make a few assumptions. The first assumption that was made is that the Von Karman value (κ) is 0.41. Another assumption can be made for the equivalent Nikuradse sand roughness, k_s. Here k_s was assumed equal to the median diameter (sieve size) of gravel (2.46 cm). By plotting $\ln(z/k_s)$ versus velocity, u, the shear velocity, u_τ, and integration constant, B, can be found. This was done for all experimental runs for angular and rounded gravel beds. Figure C.15 is an example of shear velocity found for one run. A linear equation based on the least squared fit line in the log region allows unknown

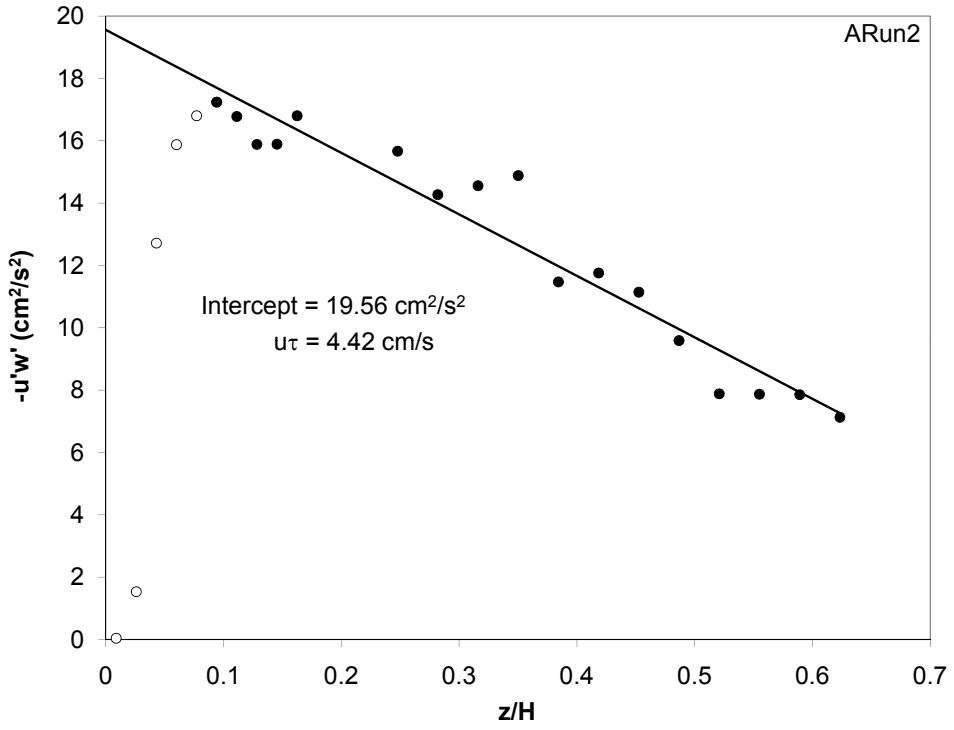

Figure C.14: u_τ **found by Reynolds stress method**

variables to be found. The shear velocity is found be multiplying the von Karman constant, κ, with the slope of the line. The integration constant, B, can then be found by taking the y-inercept of the line and dividing by the shear velocity. The shear velocities, and integration constants for each experimental run are shown in Table C.5.

C.5.4 Conclusion

The three methods used to find shear velocity gave similar values. The question posed is if any of the methods show a difference in shear velocity between the angular and rounded gravel beds. This analysis was done using the statistical t-test. Table C.6 shows the probability that the population mean values for shear velocity between the angular and rounded gravel beds are equal. We are left to conclude that the only statistically significant difference between shear velocities comes from the St Venant

Table C.4: Shear velocity from Reynolds stress method

Angular	u_τ cm/sec	Rounded	u_τ cm/sec
arun1	4.44	rrun1	4.46
arun2	4.42	rrun2	4.90
arun3	4.36	rrun3	4.64
arun4	4.37	rrun4	4.56
arun5	4.17	rrun5	4.48
arun6	4.49	rrun6	4.58
arun7	4.45	rrun7	4.38
arun8	5.06	rrun8	4.84
arun9	4.57	rrun9	4.14
arun10	4.79	rrun10	4.14
Avg.	4.51	Avg.	4.51

Table C.5: u_τ and B from Clauser method

Angular	u_τ cm/sec	B	Rounded	u_τ cm/sec	B
arun1	5.53	6.54	rrun1	5.85	9.26
arun2	5.33	9.00	rrun2	6.26	7.52
arun3	4.67	11.04	rrun3	4.82	10.92
arun4	4.55	11.37	rrun4	7.96	6.23
arun5	5.67	9.00	rrun5	5.18	9.94
arun6	5.73	7.59	rrun6	6.36	7.54
arun7	4.46	11.02	rrun7	5.89	8.35
arun8	6.23	7.21	rrun8	4.84	10.66
arun9	5.39	8.32	rrun9	5.15	9.44
arun10	4.86	9.94	rrun10	9.58	6.67
Avg.	5.24	9.10	Avg.	6.19	8.66

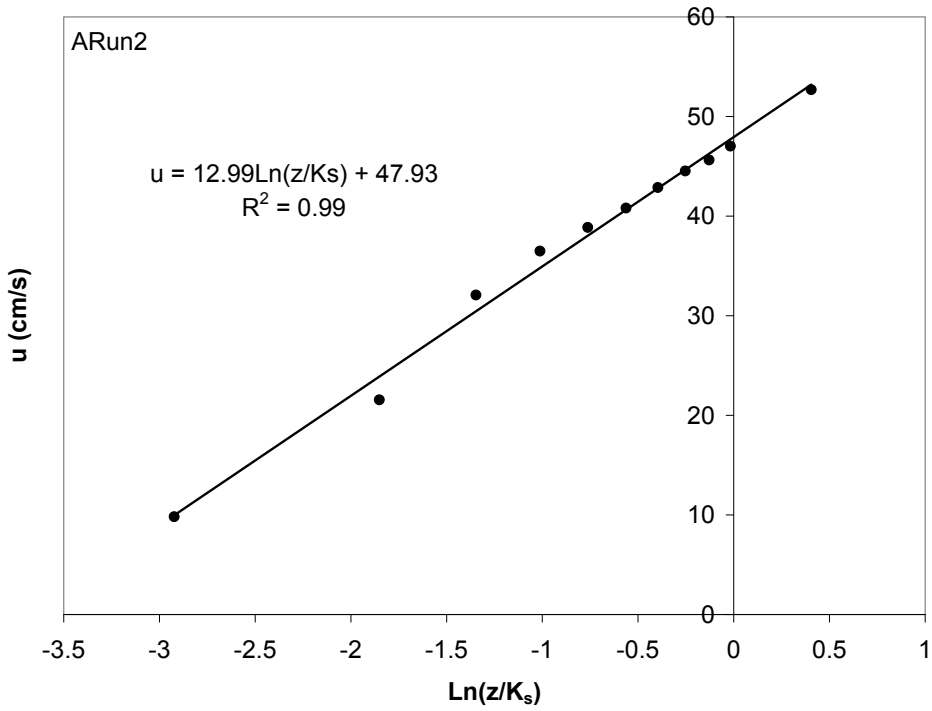

Figure C.15: u_τ **found by Clauser method**

method. The difference is due to the St Venant method being directly effected by the depth of the water. As expected, the angular gravel bed caused the depth of water to increase when compared to the rounded gravel bed.

Table C.6: Probability u_τ **being equal for both sets of gravel**

St Venant	2.89e-9
Reynolds Stress	0.99
Clauser	0.09

C.6 Nikuradse Sand Roughness and Coles Wake Parameter

As with the shear velocity calculations there are a few different ways to calculate k_s and Π. As with the shear velocity calculations, a few assumptions need to be made to carry out the calculation, since there are more unknowns than equa-

tions. Continuing with the shear velocity calculations, k_s and Π can be found with the Reynolds stress method and the Clauser method.

C.6.1 Reynolds Stress Method

One way is to guess values of k_s and Π until the calculated velocity values match the experimental values. The law of the wake (Equation A.46) was used to calculate velocity based on shear velocities found using the Reynolds stress method (see Section C.5.2). Changing the value for Nikurase's equivalent sand roughness, k_s, changes the location of the curve. Changing Coles' wake parameter, Π, effects the slope of the curve. A best fit curve was visually applied for each experimental data set. An example of this is shown in Figure C.16. The resulting values for k_s and Π are shown in Table C.7.

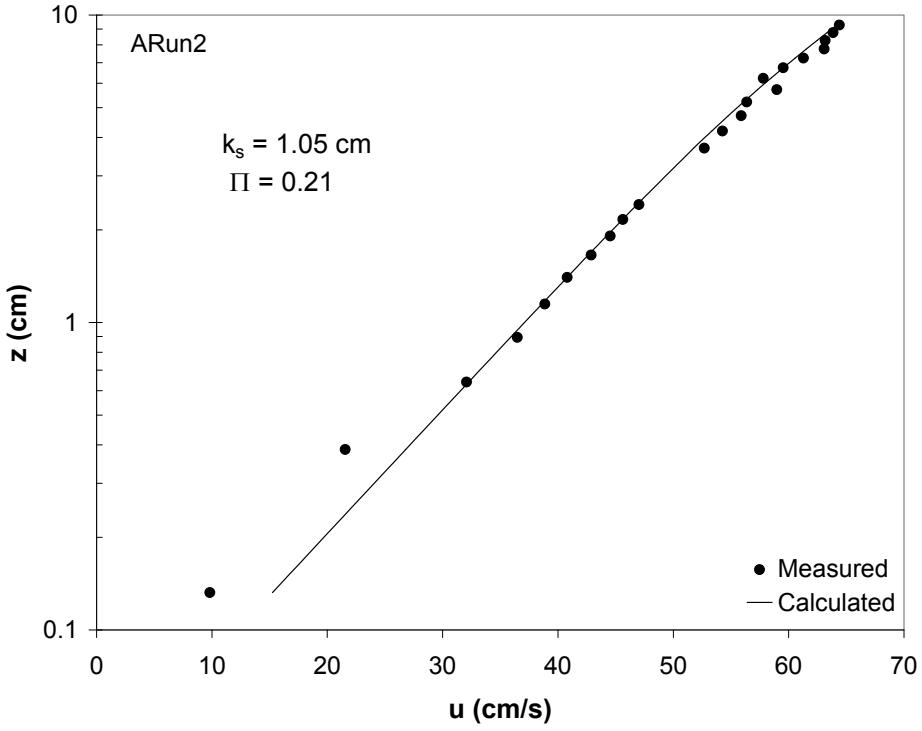

Figure C.16: k_s and Π found by Reynolds stress method

Table C.7: k_s and Π from Reynolds stress method

Angular	k_s cm	Π	Rounded	k_s cm	Π
arun1	0.97	0.07	rrun1	0.63	0.15
arun2	1.05	0.22	rrun2	1.26	0.05
arun3	0.64	0.00	rrun3	0.80	0.05
arun4	0.65	0.00	rrun4	0.85	0.13
arun5	0.60	0.12	rrun5	0.85	0.05
arun6	1.60	0.25	rrun6	1.05	0.15
arun7	0.90	0.00	rrun7	0.91	0.07
arun8	2.40	0.09	rrun8	1.00	0.10
arun9	1.50	0.12	rrun9	0.66	0.08
arun10	1.30	0.05	rrun10	0.40	0.00
Avg.	1.16	0.09	Avg.	0.84	0.08

C.6.2 Clauser Method

Another way to find k_s and Π is to extend the Clauser method approach. Unknown parameters are k_s, Π, κ, and B. κ was assumed to equal 0.41. Either k_s or B can be assumed to find the other unknowns. To find k_s the same method used in Section C.5.3 was employed. Changing the value of k_s changes the y-intercept of the trend line, but does affect the slope. This means that shear velocity stays the same as found previously. Instead of assuming a k_s, the B constant was assumed equal to 8.5. The value of k_s was manipulated until the least-squares fit line produced a value of $B = 8.5$. A value of 8.5 has often been sited in literature as the appropriate integration constant for rough gravel beds [63] [56].

To find Π, Coles law of the wake expressed in terms of velocity defect (Equation A.47) is used. The calculated term $(u_m - u)/u_\tau$ is plotted on the y-axis. u_m is the maximum streamwise velocity found in the vertical. Since the ADV did not allow measurements close to the water surface, the velocity data was extrapolated to the surface and assumed to equal u_m. z/H is plotted on the x-axis. A least squares line was fit to inner region ($z/\delta \leq 0.2$), and extrapolated to where $z/\delta = 1$. When

$z/\delta = 1$, Equation A.47 reduces to:

$$\frac{\overline{u_m} - u}{u_\tau} = \frac{2\Pi}{\kappa} \tag{C.97}$$

Figure C.17 shows an example of how the wake parameter was found.

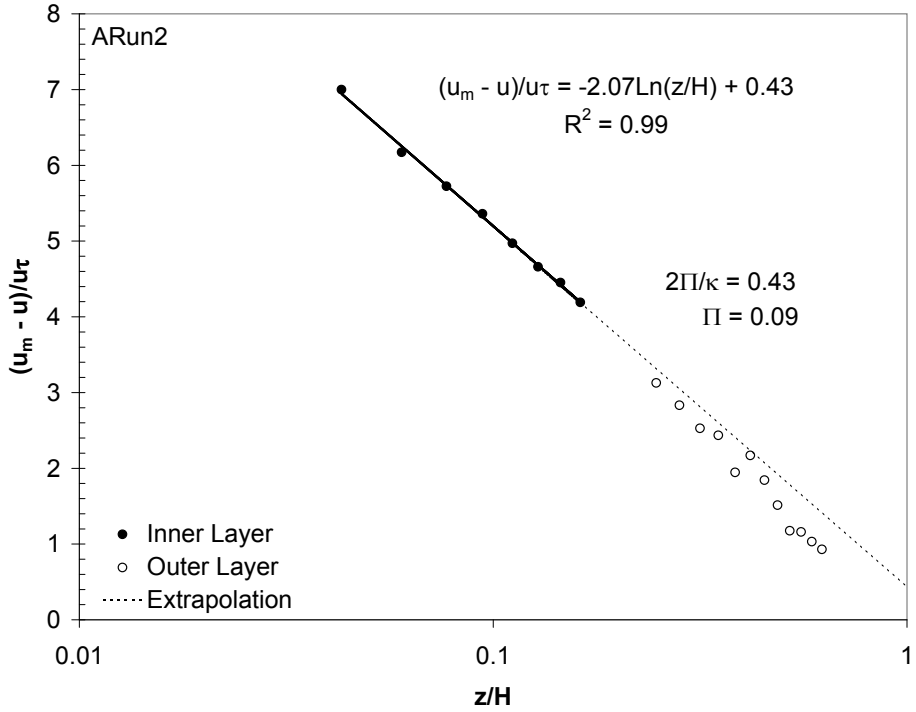

Figure C.17: Π found by Clauser method

The resulting equivalent sand roughness, k_s, and Coles wake parameter, Π are shown in Table C.8.

C.6.3 Conclusion

It is interesting to note that the Nikuradse equivalent sand roughness found by shear velocities from the Reynolds stress method were closer to the c-axis rather than the conventional b-axis length. For the angular gravel, the average $k_s = 1.16$ cm with the average c-axis = 1.51 cm. For the rounded gravel, the average $k_s = 0.84$ cm

Table C.8: k_s and Π from Clauser method

Angular	k_s cm	Π	Rounded	k_s cm	Π
arun1	2.17	0.08	rrun1	1.80	-0.12
arun2	2.00	0.09	rrun2	3.67	-0.09
arun3	0.87	-0.03	rrun3	0.91	-0.06
arun4	0.76	-0.01	rrun4	6.23	-0.31
arun5	2.01	-0.10	rrun5	1.36	-0.11
arun6	3.58	0.15	rrun6	3.64	-0.10
arun7	0.87	0.19	rrun7	2.62	-0.09
arun8	4.18	0.08	rrun8	1.02	-0.02
arun9	2.65	0.10	rrun9	1.67	0.05
arun10	1.36	0.20	rrun10	5.21	0.00
Avg.	2.05	0.08	Avg.	2.81	-0.08

with the average c-axis = 1.49 cm. The gravel c-axis was placed vertically up and down in the fixed bed since this was its most natural way to lie.

Finding the Nikuradse equivalent sand roughness using the Clauser method (shown in Table C.8) appears to be a closer match to the traditional b-axis length. For the angular gravel, the average $k_s = 2.05$ cm with the average c-axis = 2.76 cm. For the rounded gravel, the average $k_s = 2.81$ cm with the average c-axis = 2.73 cm.

Coles Wake Parameter, Π, shows similar values using shear velocities from the Reynolds stress method and from the Clauser method, with one exception. The Π value for the rounded gravel bed using the Clauser method averaged -0.08 instead of the 0.09 and 0.08 seen in the others. This difference was statistically significant as tested with the student t-test as seen in Table C.9 which show the probability that the population means (between the angular and rounded gravel beds) for k_s and Π are the same.

Table C.9: Probability of k_s and Π being equal for both sets of gravel beds

	k_s	Π
Reynolds stress method	0.12	0.78
Clauser method	0.28	1.70e-3

C.7 Velocity Distribution

Once the shear velocity has been determined it is possible to plot the velocity profile in terms of wall units (u^+, z^+). Validity of the log law and coles law of the wake were assumed in the Reynolds stress and Clauser methods for finding shear velocity. Since shear velocity was calculated using three different methods, this is reflected in three different velocity distribution representations shown in Figures C.18 - C.20.

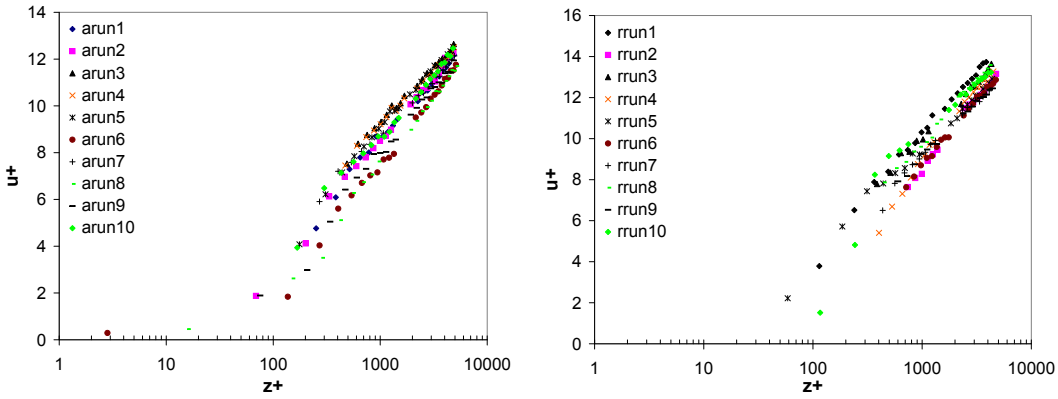

Figure C.18: Velocity distribution in wall units (St Venant method)

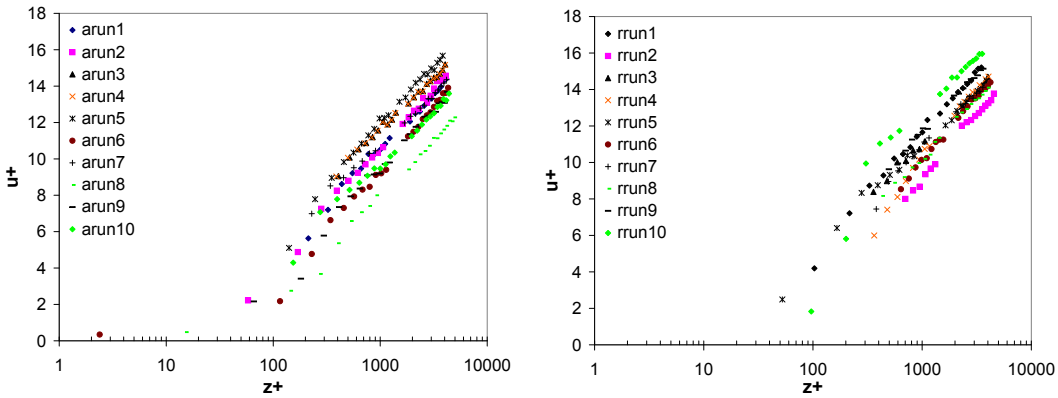

Figure C.19: Velocity distribution in wall units (Reynolds stress method)

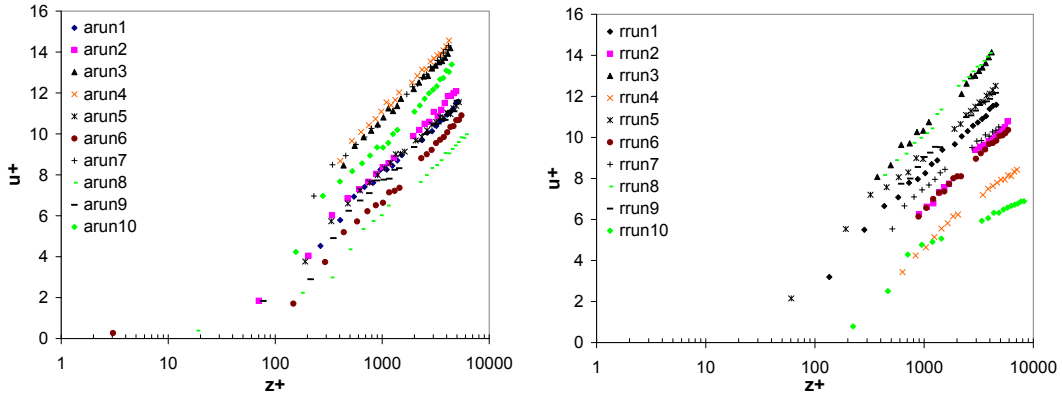

Figure C.20: Velocity distribution in wall units (Clauser method)

C.8 Roughness

C.8.1 Relative Roughness

Relative roughness relates the depth of water to the size of the roughness element. Bathurst et al. [7] divides roughness into three scales: large, intermediate and small. They used the following criteria to distinguish roughness scale. Large-scale roughness elements affect the free surface. This requires the ratio of H/D_{50} to be less than four. Where H is the depth, and D_{50} is the mean element height. The roughness is intermediate-scale if H/D_{50} is between 4 and 15. Anything above 15 is considered small-scale roughness.

Relative roughness can also be expressed as the ratio of the roughness height to flow depth (k_s/H).

Using the definition of Bathurst, the experiments carried out here fell in the range of intermediate roughness ($H/S_{50} \approx 9 - 10$).

C.8.2 Roughness Reynolds Number

The roughness Reynolds number, $\mathbb{R}_\tau$, is calculated using Equation A.17. $\mathbb{R}_\tau$ greater than 67 represents a rough wall condition. Assuming k_s is equal to D_{50}, the roughness Reynolds number for this set of experiments ranged from about 1026 to

1533 for the angular gravel bed, and from about 1018 to 2356 for the rounded gravel (variation comes from the calculation of u_τ). The average roughness Reynolds number was 1203 for the angular bed and 1267 for the rounded bed. Since both of these were well above 67, they both represented a "rough" bed.

C.8.3 Darcy-Weisbach Friction Factor

The Darcy-Weisbach friction factor (f) is calculated as:

$$f = \frac{8gR_bS}{U^2} \tag{C.98}$$

The hydraulic radius of the bed was found using the side-wall correction procedure in Section C.9. The resulting values for the angular and rounded beds are shown in Table C.10.

Table C.10: Flume setup and roughness values

Gravel Bed	Pump Speed Hz	Flume Width m	Flume Slope %	Water Depth m	Manning n	Darcy f	Chezy c $m^{1/2}/sec$
Angular	33.5	1.20	0.2	0.138	0.020	0.059	36.35
Rounded	33.5	1.20	0.2	0.150	0.022	0.073	32.75

C.8.4 Manning n

Resistance to flow and the corresponding change in average velocity for uniform flow is often calculated in engineering situations using the Manning equation.

$$n = \frac{1}{U}R_b^{(2/3)}S^{(1/2)} \tag{C.99}$$

Where U is the depth averaged velocity, n is the manning roughness coefficient, R_b is the hydraulic radius of the bed (see Section C.9), and S is the energy line slope. The

flowrate (Q) obtained from the flume Venturi meter, was used to find the average velocity (U). The resulting values for the angular and rounded gravel beds are shown in Table C.10.

C.8.5 Chezy Coefficient

The Chezy coefficient can be found by:

$$C = \frac{V}{R_b^{1/2} S^{1/2}} \tag{C.100}$$

The resulting values for the angular and rounded gravel beds are shown in Table C.10.

C.9 Side-Wall Correction

The side-wall correction procedure proposed by Johnson [35] and modified by Vanoni and Brooks [76] [75] was used in this set of experiments. These steps are outlined below.

1. Reynolds number ($\mathbb{R}$) and Darcy friction factor (f) were found from the experimental data.

$$\mathbb{R} = 4UR/\nu \tag{C.101}$$

where U is the average channel velocity, R is the hydraulic radius, and ν is the kinematic viscosity. The flowrate (Q) obtained from the flume Venturi meter, was used to find the average velocity (U).

$$\frac{U^2}{S} = \frac{8gA}{fp} = \frac{8gA_b}{f_b p_b} = \frac{8gA_w}{f_w p_w} \tag{C.102}$$

where S is the energy slope, g is the gravitational acceleration constant, A is the cross-sectional area of flow, and p is the wetted perimeter. Subscripts b and

w represent the bed and wall respectively.

$$\frac{\mathbb{R}_b}{f_b} = \frac{\mathbb{R}_w}{f_w} = \frac{\mathbb{R}}{f} \tag{C.103}$$

2. The Darcy friction factor for the wall (f_w) was determined from the relationship developed by Chien and Wan [16] for smooth walls.

$$\frac{\mathbb{R}}{f} = \frac{10^{\left(\frac{1}{2\sqrt{f_w}}+0.40\right)}}{f_w^{1.5}} \tag{C.104}$$

3. The Darcy friction factor for the bed (f_b) was calculated using the following:

$$f_b = f + \frac{2H}{b}(f - f_w) \tag{C.105}$$

where H is the water depth.

4. The hydraulic radius of the bed ($R_b = (A_b/p_b)$) was then calculated from Equation C.102.

The resulting average hydraulic radius of the bed was 14.13 cm for the angular bed, and 12.92 cm for the rounded gravel bed.

C.10 Turbulence Characteristics

C.10.1 Turbulence Intensity Distribution

Turbulence intensity is the "root mean square" (standard deviation) of the fluctuating velocity component (see Equation A.72). WinADV was used to calculate the turbulence intensity in each component direction (u, v, and w). The distributions of turbulence intensities for a rough bed have been proposed to have an exponential relationship away from the bed (see Equations A.73 and A.74). This same exponential

format was followed for the transverse (v) direction.

$$\frac{TI_v}{u_t au} = D_v e^{-\lambda_v (z/H)} \tag{C.106}$$

The goal of investigating the turbulence intensity distribution was to validate the proposed exponential relationships and also to see how angularity plays a role in changing the proposed coefficients. The Turbulence Intensity, TI, distributions for the angular and rounded gravel beds are shown in Figures C.21 - C.23 (u_τ calculated using the St Venant method).

The distribution for each experimental run was fit with a least-squares line for only the data $z/\delta > 0.2$. Figure C.24 is an example for one data set. Since u_τ was calculated using three different methods, each of these gave different values for: the exponential constants (D_u, D_w, and D_v, λ_u, λ_w, and λ_v), the maximum value for turbulence intensity (TI_{max}), and the location of the maximum turbulence intensity (z_t). Dashes (-) indicate the peak could not be located.

The average value of z_t/δ increased from 0.11 for angular to 0.12 for the rounded gravel. Since the relative roughness (k_s/H) also increased for the rounded bed this supports the conclusion of Carollo et al [12], that z_t increases as relative roughness increases. Carollo et al [12] also observed that TI_{max} decreased as relative roughness increased. With the exception of the St Venant method, this was also confirmed for the streamwise direction.

In investigate whether the difference in turbulence intensities between the angular and rounded gravel is statistically significant, the student t-test was performed as outlined in Section C.1. The null hypothesis was that there was no difference in the means between the two sets of turbulence intensity variables. Table C.17 show the t-test probability, that the z_t/δ means are equal between the angular and rounded gravel beds. Tables C.18 - C.20 show the t-test probabilities for turbulence intensity

distribution coefficients for the u, v, and w components. If the probability is less than 5%, then the difference was considered statistically significant (these are **bold** in the tables).

The streamwise component (u) of turbulence intensity showed no statistical significance between angular and rounded gravel beds. The vertical component (w) showed a difference in D_w using both the Reynolds stress method and the Clauser method. The Reynolds stress method also shows a difference for TI_{max}. The traverse component (v) also showed a statistical difference for TI_{max} using the Clauser method.

This lack of statistical difference in the u direction supports the idea that beyond $0.2z/\delta$ (for large relative roughness) the roughness elements do not change the turbulence intensity distribution. The distribution for smooth and rough beds can be represented by a single curve.

In the region close to the bed ($z \leq z_t$), the gravel geometry (form, size, and position) are expected to influence the turbulence intensity [12]. Figure C.28 shows the measurable pairs of z/z_t, TI_u/TI_{max} for each bed roughness. TI values in the inner region are shown in Figure C.29. A difference in the angular and rounded gravel beds could not be distinguished. Measurements close to the bed were difficult to make, and results showed considerable scatter in TI values up to about 0.25 z/H.

Away from the bed ($z/H > 0.25$) the data was much more trustworthy. Interference with the boundary was not a problem, and the values of TI were less scattered than in the inner region. Wang et al. [82] performed a series of experiments using an LDV to determine the effects of relative roughness (H/K_s) on turbulence intensity distribution. They concluded that for $H/K_s \geq 4.0$, the TI_u values D_u and λ_u could be considered constant. Assuming that K_s is equal to D_{50} (2.46 cm), then H/K_s for the angular bed was 6.1 and 5.6 for the rounded bed. A best fit curve for $z/H > 0.25$ was fit to the TI distribution.

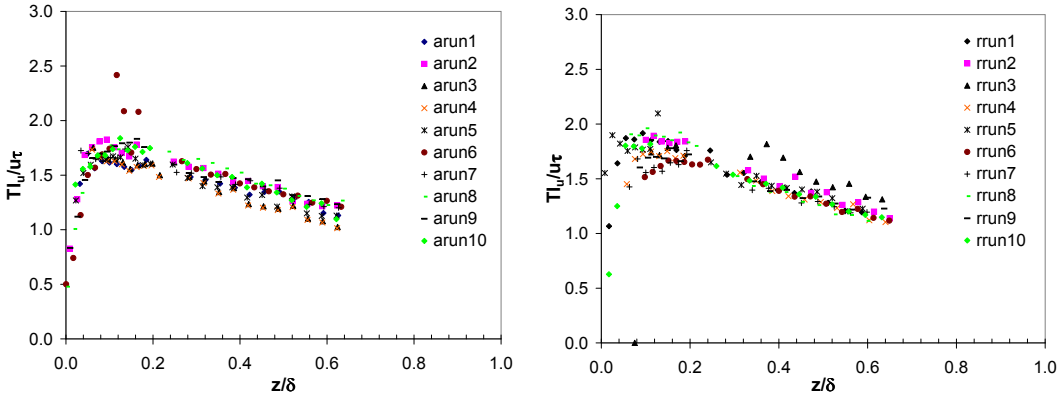

Figure C.21: TI_u **for angular and rounded gravel beds**

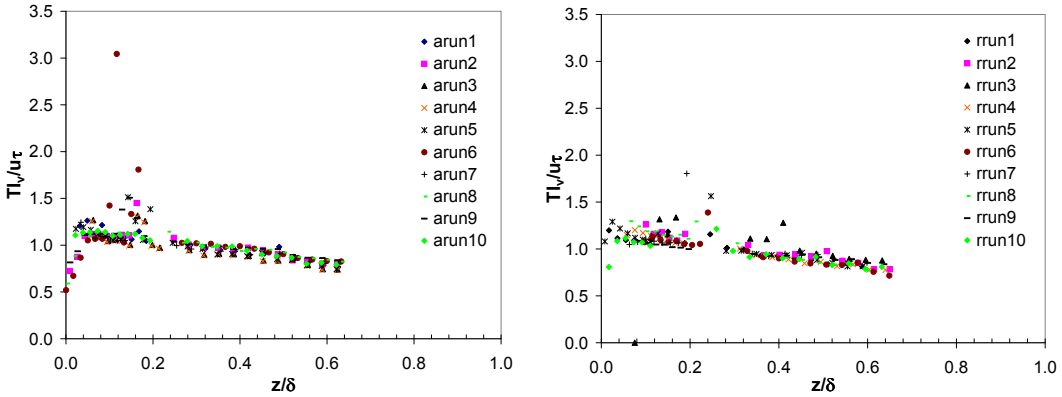

Figure C.22: TI_v **for angular and rounded gravel beds**

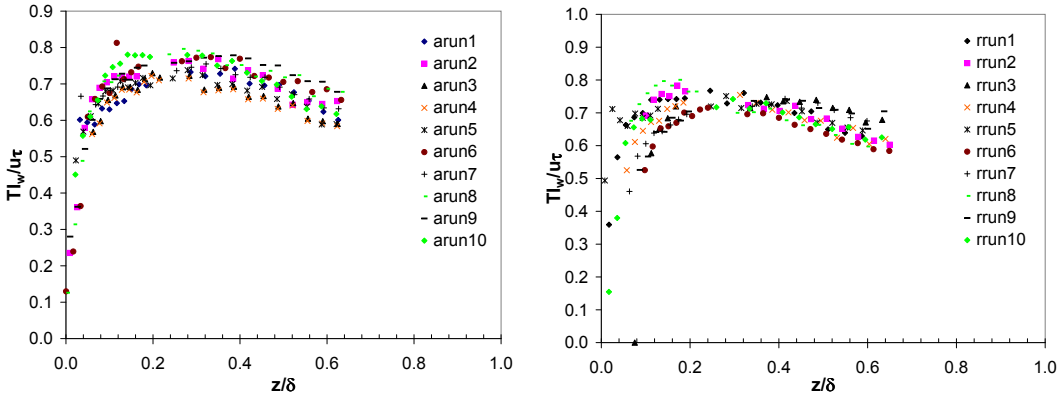

Figure C.23: TI_w **for angular and rounded gravel beds**

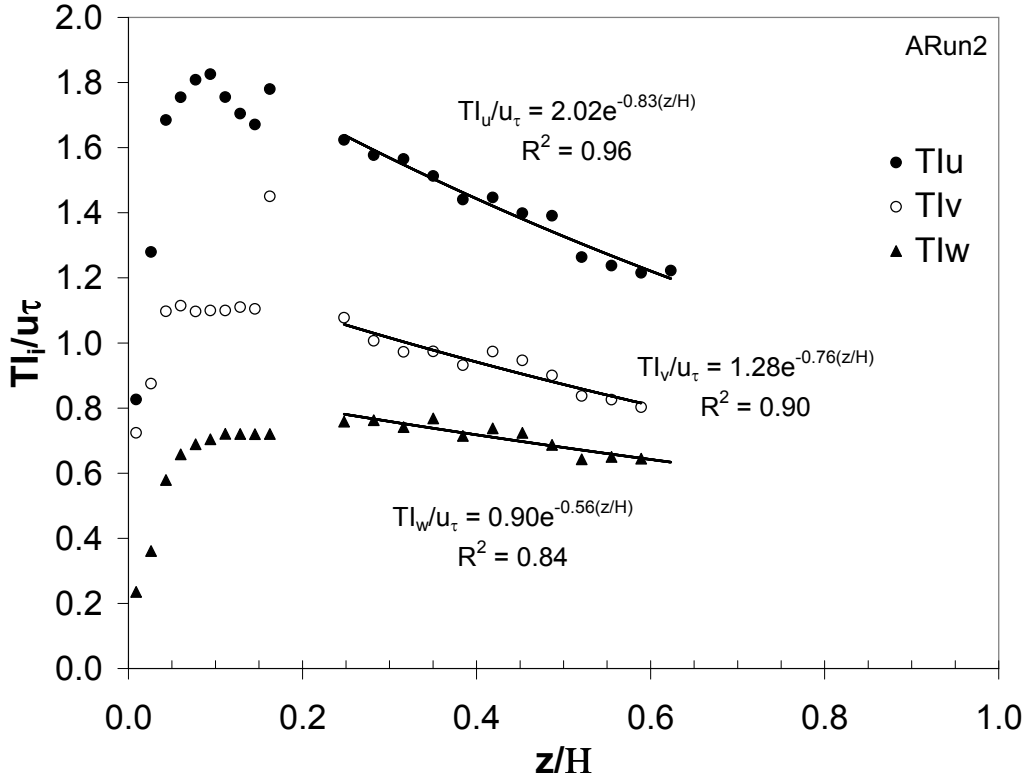

Figure C.24: Example curve fit for TI values

Table C.11: TI_u distribution values for angular gravel

	ARun	1	2	3	4	5	6	7	8	9	10	Avg.
	z_t/δ	0.08	0.09	-	-	0.11	0.10	-	0.10	0.16	0.12	0.11
	R^2	0.91	0.96	0.96	0.95	0.91	0.98	0.93	0.97	0.89	0.95	0.94
St Venant	D_u	1.86	2.02	1.92	1.90	1.89	1.97	1.86	2.12	1.82	2.16	1.95
	λ_u	0.75	0.83	0.97	0.97	0.85	0.78	0.69	0.87	0.59	1.01	0.83
	TI_{max}	1.63	1.83	-	-	1.67	1.74	-	1.77	1.83	1.84	1.76
Reynolds	D_u	2.20	2.39	2.31	2.30	2.37	2.33	2.2	2.22	2.09	2.35	2.28
	λ_u	0.75	0.83	0.97	0.97	0.85	0.78	0.69	0.87	0.59	1.01	0.83
	TI_{max}	1.93	2.16	-	-	2.09	2.06	-	1.86	2.10	2.00	2.03
Clauser	D_u	1.77	1.98	2.16	2.21	1.74	1.82	2.2	1.81	1.77	2.32	1.98
	λ_u	0.75	0.83	0.97	0.97	0.85	0.78	0.69	0.87	0.59	1.01	0.83
	TI_{max}	1.55	1.79	-	-	1.54	1.61	-	1.51	1.78	1.98	1.68

Table C.12: TI_u distribution values for rounded gravel

	RRun	1	2	3	4	5	6	7	8	9	10	Avg.
	z_t/δ	0.09	0.12	-	0.11	-	0.15	-	0.10	0.12	-	0.12
	R^2	0.94	0.92	0.95	0.94	0.90	0.98	0.87	0.97	0.75	0.99	0.92
St Venant	D_u	2.14	2.17	2.31	2.06	1.96	2.04	1.85	2.20	1.73	2.04	2.05
	λ_u	1.01	0.96	1.14	0.96	0.79	0.93	0.76	1.16	0.54	0.92	0.92
	TI_{max}	1.92	1.89	-	1.75	-	1.67	-	1.96	1.70	-	1.82
Reynolds	D_u	2.37	2.27	2.49	2.28	2.20	2.28	2.12	2.28	2.10	2.46	2.29
	λ_u	1.01	0.96	1.14	0.96	0.79	0.93	0.76	1.16	0.54	0.92	0.92
	TI_{max}	2.12	1.98	-	1.94	-	1.86	-	2.04	2.07	-	2.00
Clauser	D_u	1.81	1.78	2.40	1.31	1.90	1.64	1.58	2.29	1.69	1.06	1.75
	λ_u	1.01	0.96	1.14	0.96	0.79	0.93	0.76	1.16	0.54	0.92	0.92
	TI_{max}	1.62	1.55	-	1.11	-	1.34	-	2.04	1.66	-	1.55

Table C.13: TI_v distribution values for angular gravel

	ARun	1	2	3	4	5	6	7	8	9	10	Avg.
	z_t/δ	-	0.06	-	-	-	0.07	-	0.09	0.08	0.07	0.07
	R^2	0.77	0.92	0.92	0.90	0.94	0.96	0.91	0.92	0.92	0.96	0.91
St Venant	D_v	1.32	1.35	1.22	1.20	1.31	1.35	1.25	1.36	1.27	1.40	1.30
	λ_v	0.71	0.74	0.65	0.65	0.77	0.68	0.60	0.68	0.54	0.82	0.68
	TI_{max}	-	1.11	-	-	-	1.07	-	1.14	1.12	1.15	1.12
Reynolds	D_v	1.24	1.28	0.82	0.81	1.23	1.26	1.17	1.27	1.19	1.31	1.16
	λ_v	0.71	0.74	0.65	0.65	0.77	0.68	0.60	0.68	0.54	0.82	0.68
	TI_{max}	-	1.32	-	-	-	1.23	-	1.2	1.29	1.26	1.26
Clauser	D_v	1.18	1.25	1.28	1.31	1.13	1.17	1.38	1.08	1.16	1.41	1.24
	λ_v	0.71	0.74	0.65	0.65	0.77	0.68	0.60	0.68	0.54	0.82	0.68
	TI_{max}	-	1.10	-	-	-	0.99	-	0.97	1.09	1.24	1.08

Table C.14: TI_v distribution values for rounded gravel

	RRun	1	2	3	4	5	6	7	8	9	10	Avg.
	z_t/δ	-	-	-	0.08	-	0.12	0.10	-	-	0.05	0.09
	R^2	0.89	0.78	0.91	0.93	0.59	0.77	0.75	0.89	0.86	0.74	0.81
St Venant	D_v	1.32	1.31	1.27	1.21	1.58	1.45	1.10	1.50	1.10	1.31	1.32
St Venant	λ_v	0.86	0.76	0.76	0.71	1.21	1.08	0.40	1.15	0.40	0.82	0.82
St Venant	TI_{max}	-	-	-	1.20	-	1.13	1.11	-	-	1.12	1.14
Reynolds	D_v	1.47	1.37	1.37	1.34	1.77	1.62	1.26	1.56	1.34	1.57	1.47
Reynolds	λ_v	0.86	0.76	0.76	0.71	1.21	1.08	0.40	1.15	0.40	0.82	0.82
Reynolds	TI_{max}	-	-	-	1.33	-	1.26	1.27	-	-	1.35	1.30
Clauser	D_v	1.12	1.07	1.32	0.77	1.53	1.17	0.94	1.56	1.07	0.68	1.12
Clauser	λ_v	0.86	0.76	0.76	0.71	1.21	1.08	0.40	1.15	0.40	0.82	0.82
Clauser	TI_{max}	-	-	-	0.76	-	0.91	0.94	-	-	0.58	0.80

Table C.15: TI_w distribution values for angular gravel

	ARun	1	2	3	4	5	6	7	8	9	10	Avg.
	z_t/δ	0.39	0.35	-	0.20	0.28	0.30	0.32	0.27	0.35	-	0.31
	R^2	0.85	0.85	0.92	0.92	0.85	0.89	0.89	0.89	0.71	0.96	0.87
St Venant	D_w	0.89	0.90	1.14	1.13	0.85	0.88	0.87	0.89	0.85	0.98	0.94
St Venant	λ_w	0.56	0.52	0.52	0.52	0.55	0.44	0.49	0.43	0.31	0.74	0.51
St Venant	TI_{max}	0.74	0.77	-	0.72	0.74	0.77	0.75	0.80	0.78	-	0.76
Reynolds	D_w	1.05	1.05	0.99	0.99	1.07	1.04	1.03	0.93	0.97	1.07	1.02
Reynolds	λ_w	0.56	0.52	0.52	0.52	0.55	0.44	0.49	0.43	0.31	0.74	0.51
Reynolds	TI_{max}	0.88	0.91	-	0.88	0.92	0.91	0.89	0.84	0.89	-	0.89
Clauser	D_w	0.84	0.87	0.93	0.95	0.79	0.82	1.03	0.76	0.83	1.06	0.89
Clauser	λ_w	0.56	0.52	0.52	0.52	0.55	0.44	0.49	0.43	0.31	0.74	0.51
Clauser	TI_{max}	0.70	0.75	-	0.84	0.68	0.72	0.89	0.68	0.76	-	0.75

Table C.16: TI_w distribution values for rounded gravel

	RRun	1	2	3	4	5	6	7	8	9	10	Avg.
	z_t/δ	-	0.17	0.37	-	0.28	-	0.41	0.17	0.42	0.30	0.30
	R^2	0.89	0.92	0.94	0.92	0.75	0.95	0.60	0.94	0.57	0.90	0.84
St Venant	D_w	0.89	0.90	0.95	0.91	0.83	0.82	0.81	0.87	0.82	0.84	0.86
	λ_w	0.58	0.61	0.69	0.64	0.39	0.51	0.27	0.61	0.30	0.47	0.51
	TI_{max}	-	0.78	0.74	-	0.75	-	0.74	0.80	0.74	0.74	0.76
Reynolds	D_w	0.99	0.95	1.02	1.01	0.92	0.92	0.93	0.90	1	1.01	0.97
	λ_w	0.58	0.61	0.69	0.64	0.39	0.51	0.27	0.61	0.30	0.47	0.51
	TI_{max}	-	0.82	0.80	-	0.84	-	0.85	0.83	0.90	0.90	0.85
Clauser	D_w	0.75	0.74	0.98	0.58	0.80	0.66	0.69	0.90	0.81	0.44	0.74
	λ_w	0.58	0.61	0.69	0.64	0.39	0.51	0.27	0.61	0.30	0.47	0.51
	TI_{max}	-	0.64	0.77	-	0.73	-	0.63	0.83	0.72	0.39	0.67

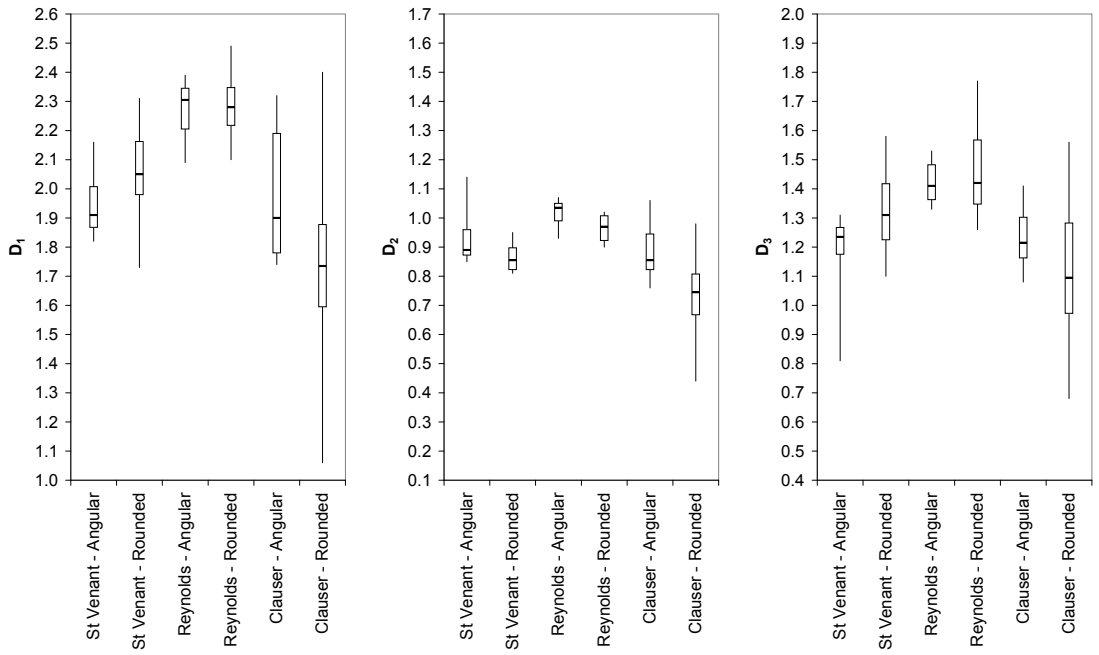

Figure C.25: Box plot of D_u, D_w and D_v values

Table C.17: t-test probability for z_t/δ

Component	z_t/δ
u	0.64
v	0.38
w	0.92

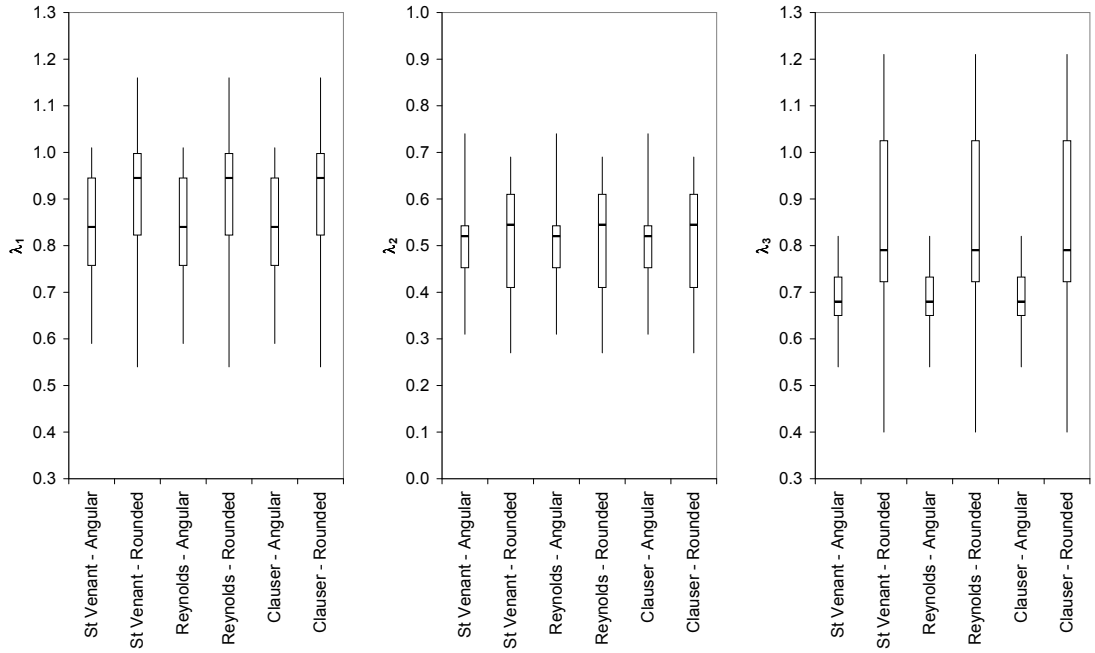

Figure C.26: Box plot of λ_u, λ_w and λ_v values

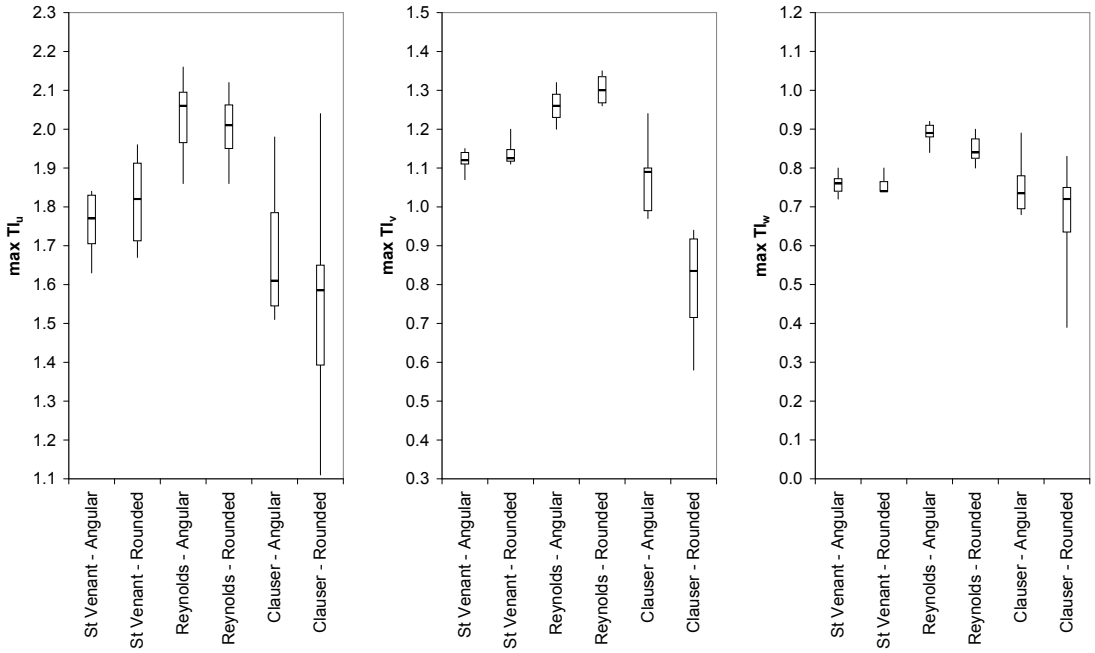

Figure C.27: Box plot of Maximum TI values

Table C.18: t-test probability for TI_u parameters

Method	D_u	λ_u	TI_{max}
St Venant	0.25	0.21	0.49
Reynolds	0.86	0.25	0.64
Clauser	0.13	0.25	0.38

Table C.19: t-test probability for TI_v parameters

Method	D_v	λ_v	TI_{max}
St Venant	0.16	0.18	0.75
Reynolds	0.43	0.18	0.21
Clauser	0.28	0.18	**0.02**

Table C.20: t-test probability for TI_w parameters

Method	D_w	λ_w	TI_{max}
St Venant	0.41	0.99	0.39
Reynolds	**0.02**	0.99	**0.03**
Clauser	**0.02**	0.99	0.19

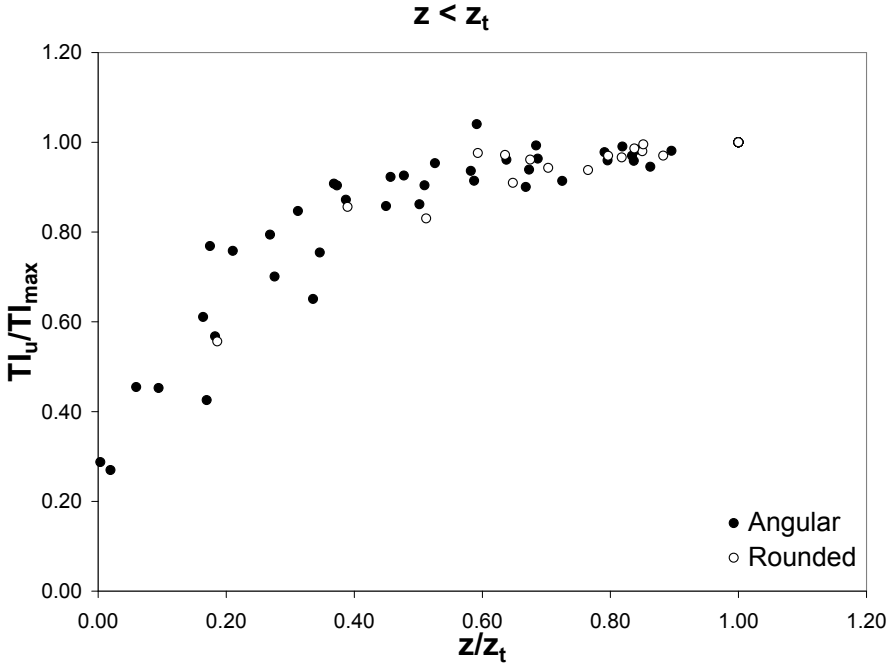

Figure C.28: TI_u distribution for $z \leq z_t$

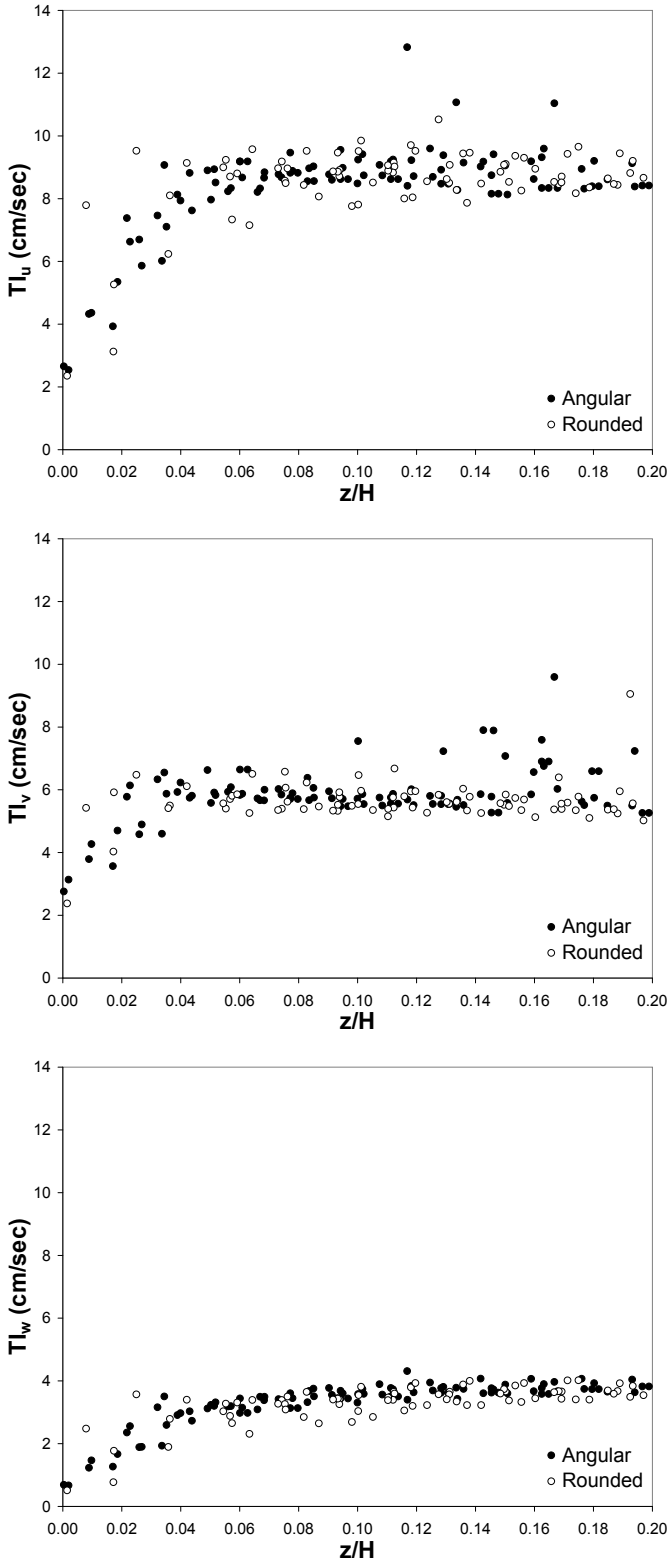

Figure C.29: TI_i **distribution for** $z \leq z_t$

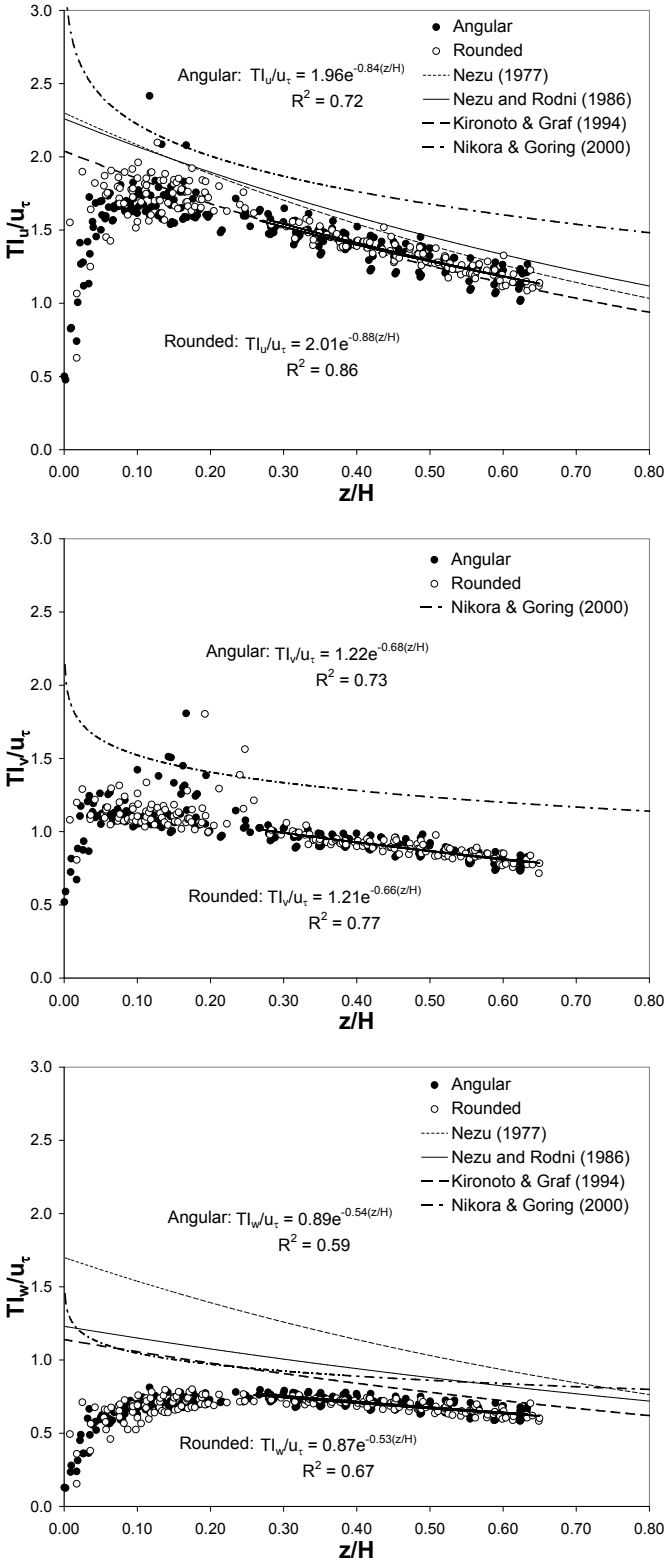

Figure C.30: TI_i/u_τ **distribution for** $z > 0.25H$ **(St Venant method)**

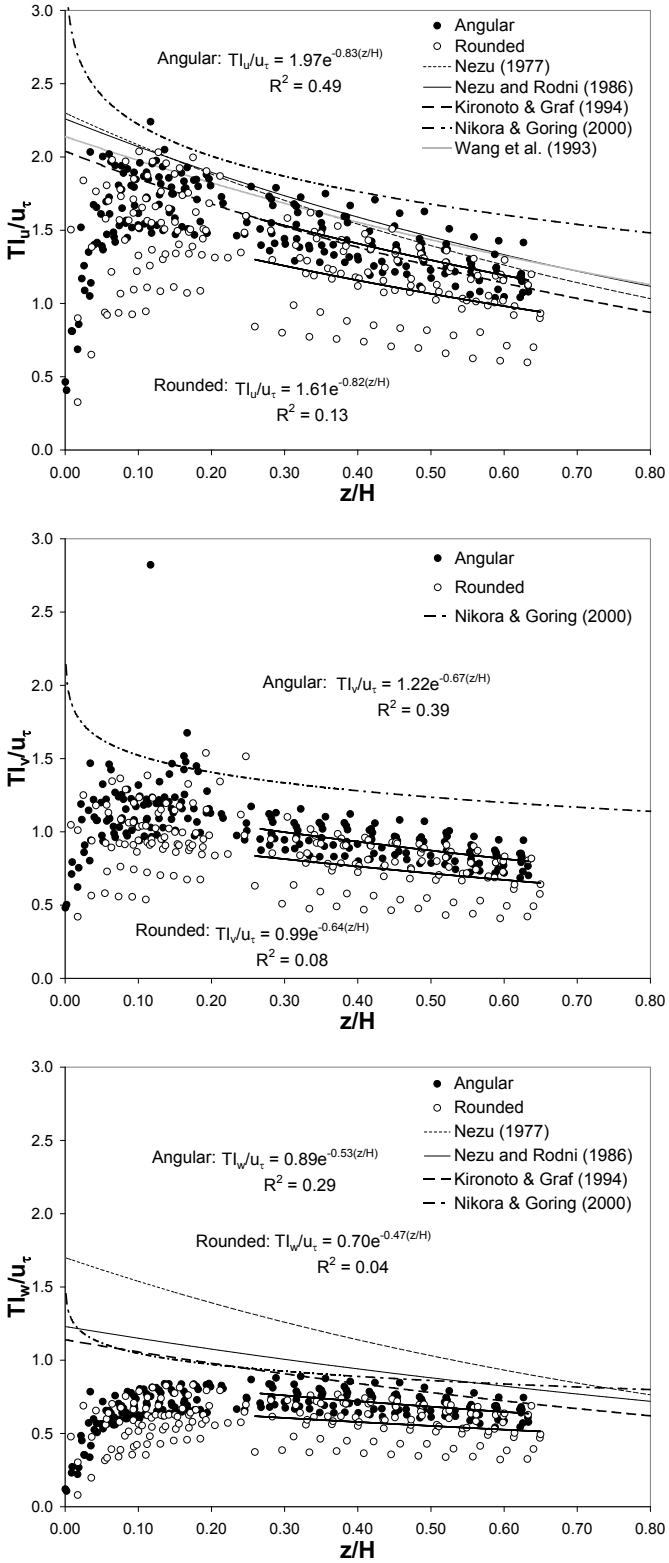

Figure C.31: TI_i/u_τ **distribution for** $z > 0.25H$ **(Clauser method)**

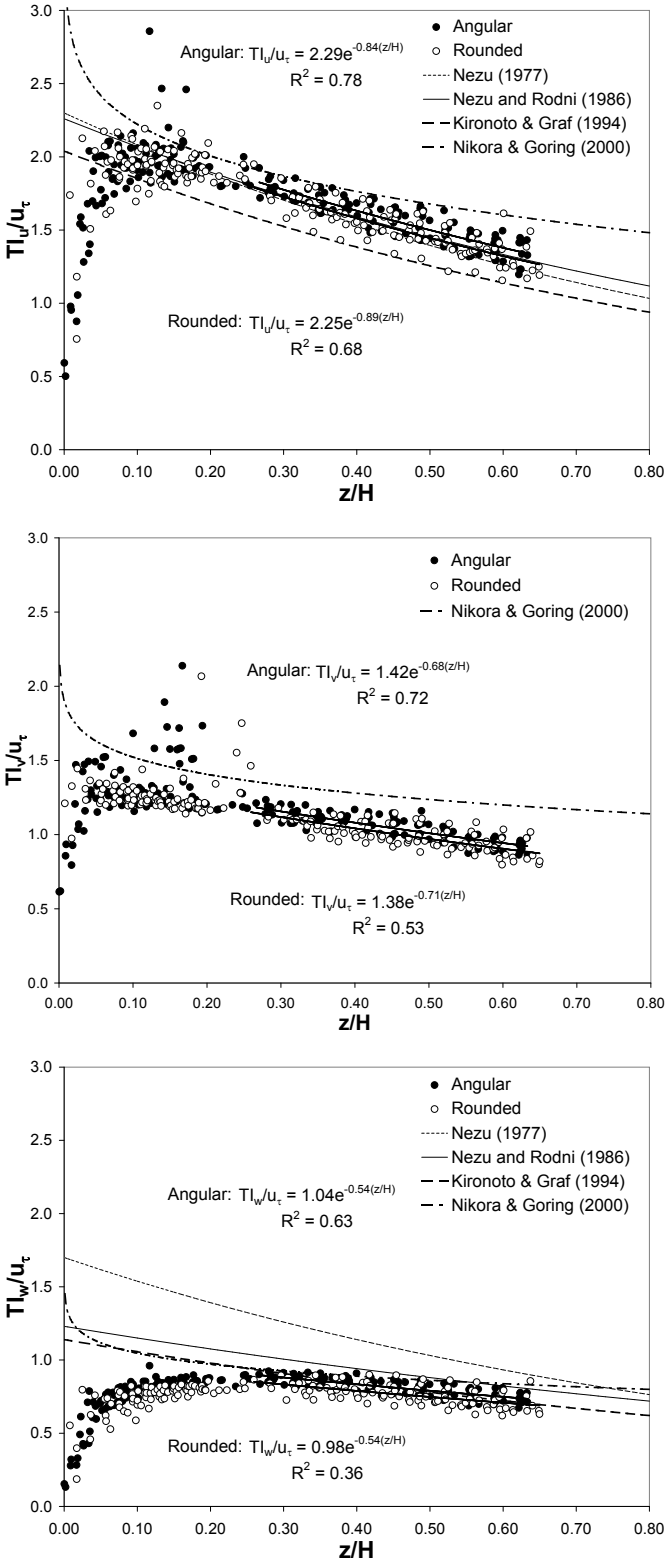

Figure C.32: TI_i/u_τ **distribution for** $z > 0.25H$ **(Reynolds method)**

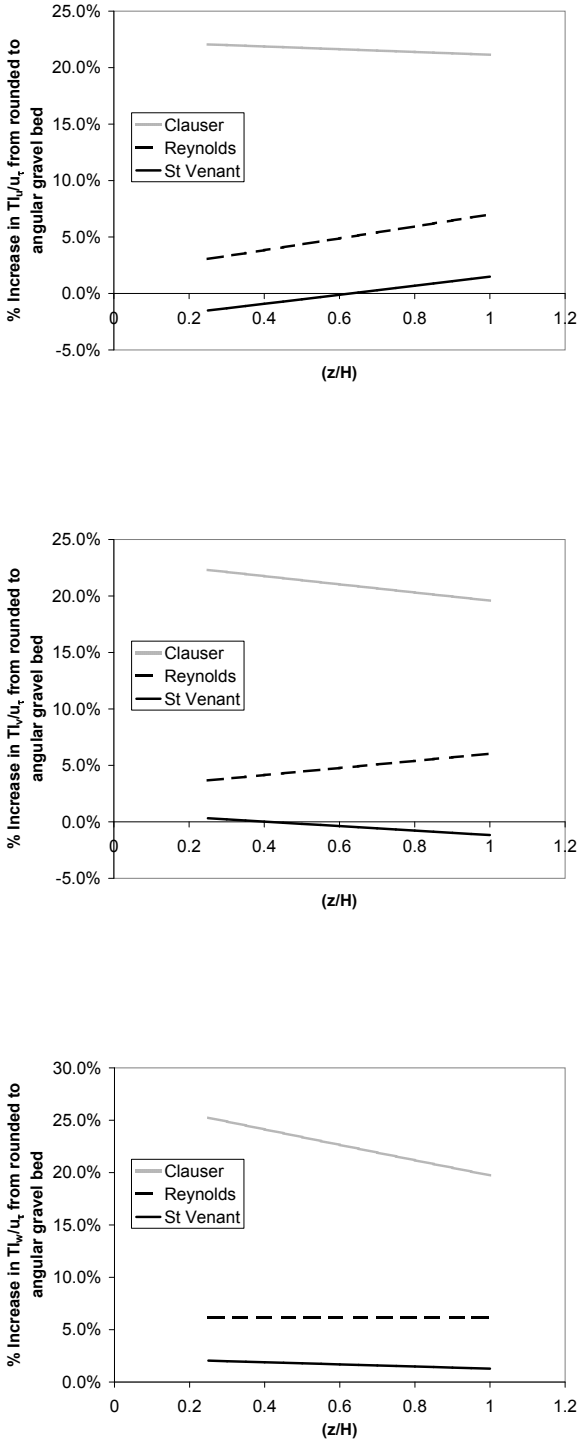

Figure C.33: Percent increase in TI_w/u_τ distribution for $z > 0.25H$

C.10.2 Turbulent Kinetic Energy Distribution

Turbulent kinetic energy, K, is found using Equation A.77. Often K is scaled with shear velocity (u_τ). The distribution found between angular and rounded gravel is shown in Figures C.34-C.36 , using the three different methods to of finding u_τ. No difference could be distinguished between the two roughness gravel beds. The plots also contain the universal expressions for K as expressed by Nezu and Nakagawa, Equation A.78, and Nikora and Goring, Equation A.79.

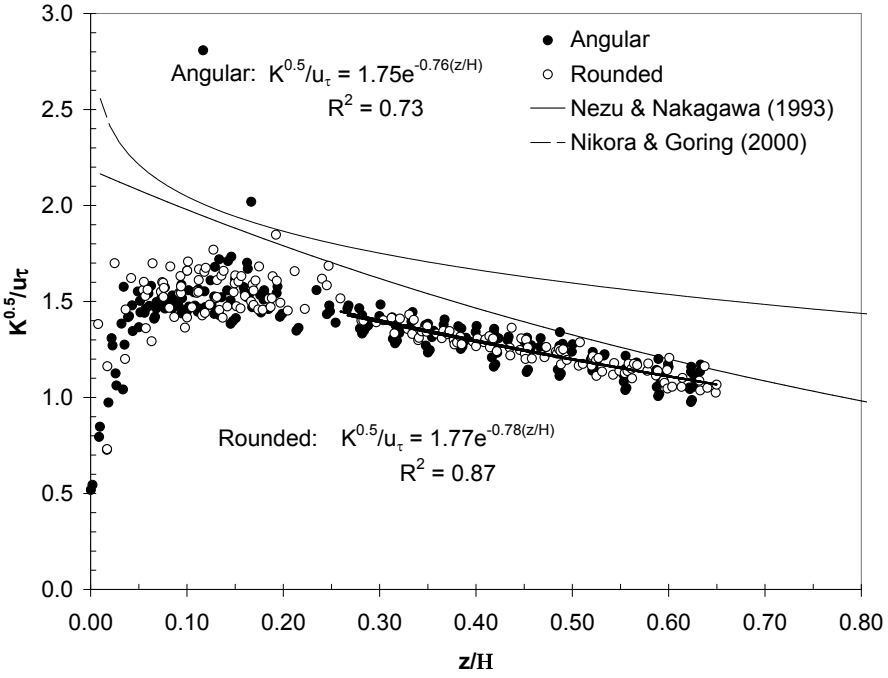

Figure C.34: K distribution (u_τ from St Venant method)

C.10.3 Length and Time Scales

There are three standard scales used to give insight into the structure of turbulence. The integral scale is the largest and is representative of the energy-containing eddies. The Taylor microscale is representative of the eddy size where the turbulent kinetic energy is in equilibrium (dissipation and generation are at the same rate).

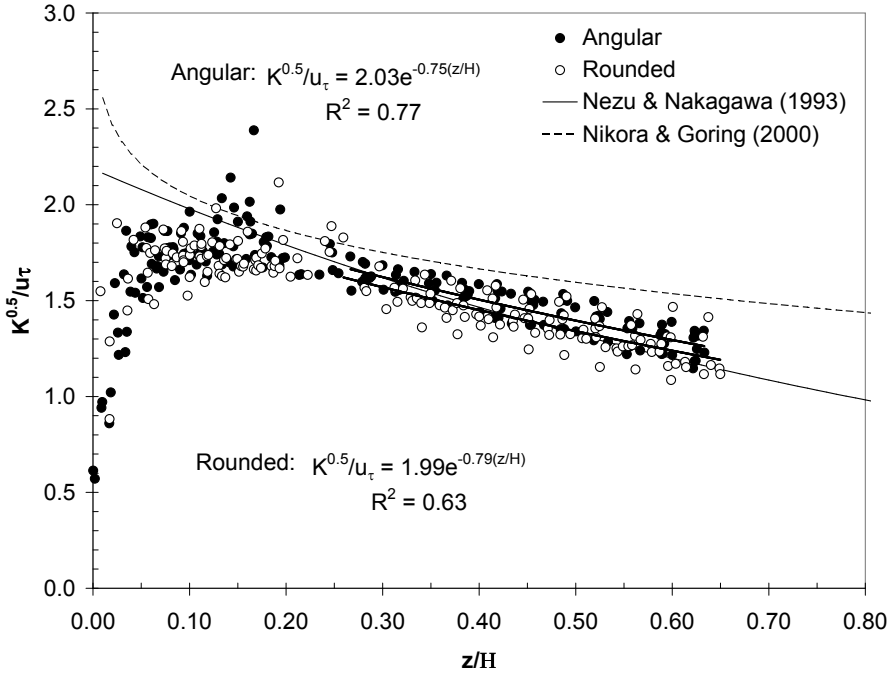

Figure C.35: K **distribution (**u_τ **from Reynolds stress method)**

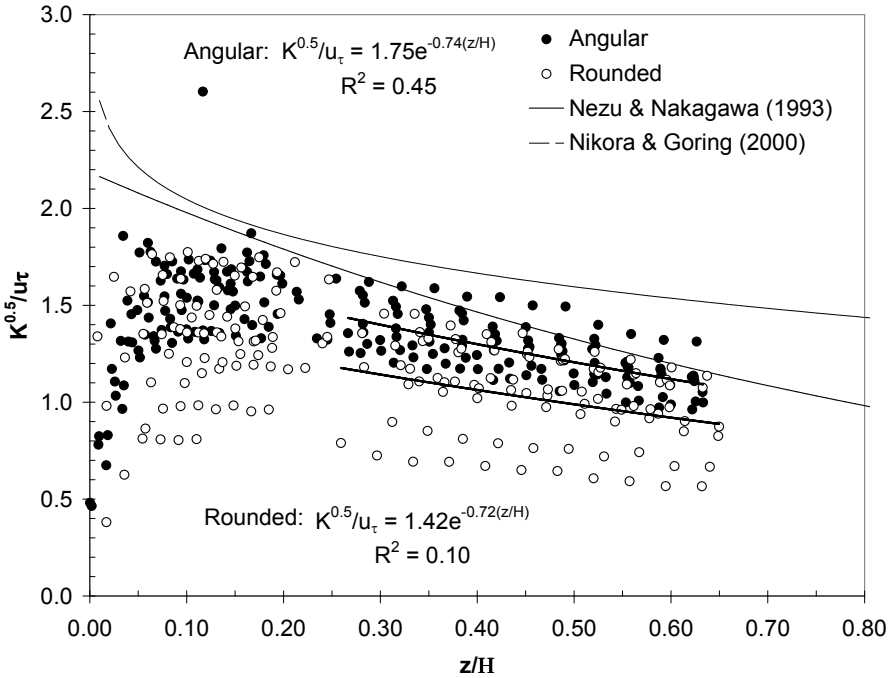

Figure C.36: K **distribution (**u_τ **from Clauser method)**

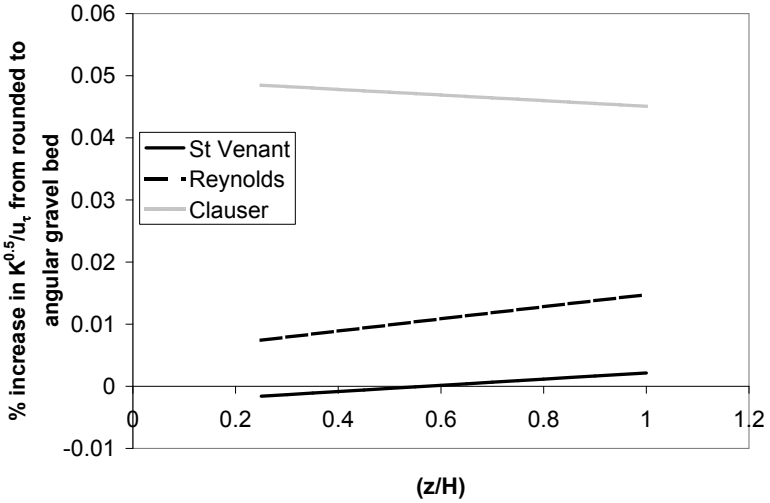

Figure C.37: % increase in $K^{0.5}/u_\tau$ from rounded to angular gravel bed

The smallest scale is the Kolmogorov miscroscale which corresponds to the energy dissipation size. The integral scale (Λ) and Taylor microscale (λ) can be estimated using the autocorrelation function.

The autocorrelation (R_h) is calculated as:

$$R_h = C_h/C_o \tag{C.107}$$

where C_h is the autocovariance function, and C_o is the variance function, which are calculated as follows:

$$C_h = \frac{1}{N}\sum_{t=1}^{N-h}(u'_t)(u'_{t+h}) \tag{C.108}$$

$$C_o = \frac{1}{N}\sum_{t=1}^{N}(u'_t)^2 \tag{C.109}$$

where N is the number of samples of velocity for a single spatial location, h is the time step.

The autocorrelation gives insight into how closely related the velocity fluctuations are in time and hence the eddy size. The integral of the autocorrelation function gives what is known as the integral time scale (Λ_T). Multiplying the integral time scale by the average velocity at that spatial location establishes the integral length scale (Λ_L). As Schlichting [58] puts it, the integral length scale, "establishes a measure of the extent of the mass which moves as a unit and gives an idea of the average size of the turbulent eddies".

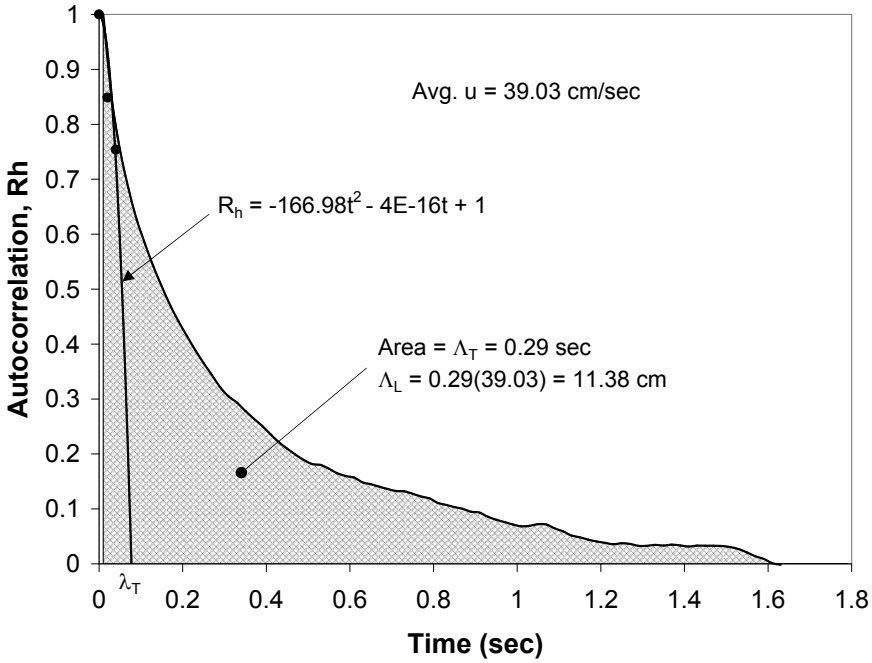

Figure C.38: Example calculation of integral scale and Taylor microscale

The autocorrelation calculation was performed for each run at two points in the vertical. The two points were 0.679cm and 6.267cm from the tops of the gravel. The calculation was performed using MATLAB code provided later in this section. Numerical integration was used to find the area below the curve up to the first zero crossing. This area corresponds to the integral time scale. Multiplying the average

velocity by the integral time scale gives the integral length scale. A graphical example of this is shown in Figure C.38.

The Taylor time microscale (λ_T) is found by fitting a parabolic curve to the first three points in the autocorrelation function, and extrapolating to where the autocorrelation is zero ($R_h = 0$). An example of this is shown in Figure C.38.

The integral scale and Taylor microscale are shown for each run at 0.679cm and 6.267cm above the top of the gravel bed in Tables C.21 - C.24. A t-test statistic was performed on the scales to see if there was a significant difference between angular and rounded gravel. The probability that the means are the same are shown in Table C.25. Since the probabilities are all larger than 0.05, there is not enough evidence to support a difference of turbulence scales based on angularity of the bed.

C.10.4 Autocorrelation MATLAB Code

```
% Written by Benjamin Haws.  You are welcome to use it.
% Calculates the Autocorrelation coefficient from velocity data in
% excel file 'Velocity_u'

clear all; clc;

u= xlsread('Velocity_u', 'Sheet1', 'D10:D10510');
time= xlsread('Velocity_u', 'Sheet1', 'A10:A10510');
M= length(u);
sumu = 0;

%finds the sum of all velocity values
for n=1:M
    sumu=u(n)+sumu;
end

%finds the average of the velocity values
ubar=sumu/M;

%Adds M more values to array with value of zero
%calculates fluctuating component u'
u_prime=u-ubar;
```

```
for n=M:(M+M)
    u_prime(n)=0;
end

%calculates the variance function Co
    Var = 0;
    for i = 1:M
        Var = (u_prime(i))^2 + Var;
    end
        Co = Var;

%Rh is the autocorrelation coefficient
for k=1:M
    Ch=0;
    for i=1:M
        Ch = u_prime(i)*u_prime(i+k-1) + Ch;
    end
    Rh(k)=Ch/Co;
end

xlswrite('Rh_Velocity_u', time, 'A2:A10502')
xlswrite('Rh_Velocity_u', Rh', 'B2:B10502')
```

Table C.21: Turbulent scales for angular gravel close to bed (0.679 cm)

	Λ_T sec	Λ_L cm	λ_T sec	λ_L cm
arun1	0.28	11.44	0.06	2.60
arun2	0.29	11.38	0.08	3.02
arun3	0.28	12.52	0.07	3.01
arun4	0.29	12.38	0.08	3.17
arun5	0.23	9.52	0.07	2.73
arun6	0.23	8.61	0.06	2.25
arun7	0.24	10.06	0.07	3.10
arun8	0.32	11.88	0.08	3.03
arun9	0.30	10.98	0.07	2.72
arun10	0.28	11.33	0.07	2.93
Avg.	0.27	11.01	0.07	2.86

Table C.22: Turbulent scales for rounded gravel close to bed (0.679 cm)

	Λ_T sec	Λ_L cm	λ_T sec	λ_L cm
rrun1	0.30	11.64	0.07	2.77
rrun2	0.49	20.18	0.07	2.99
rrun3	0.23	9.58	0.06	2.61
rrun4	0.25	9.35	0.07	2.51
rrun5	0.35	14.64	0.07	3.11
rrun6	0.19	7.85	0.06	2.70
rrun7	0.26	10.14	0.06	2.49
rrun8	0.23	9.89	0.07	2.93
rrun9	0.23	9.33	0.07	2.79
rrun10	0.26	11.81	0.07	3.21
Avg.	0.28	11.44	0.07	2.81

Table C.23: Turbulent scales for angular gravel far from bed (6.267 cm)

	Λ_T sec	Λ_L cm	λ_T sec	λ_L cm
arun1	0.33	19.72	0.07	4.43
arun2	0.25	14.75	0.07	4.39
arun3	0.31	19.33	0.07	4.63
arun4	0.28	16.61	0.07	4.43
arun5	0.29	17.96	0.08	4.67
arun6	0.29	16.79	0.08	4.49
arun7	0.33	19.40	0.08	4.63
arun8	0.42	24.19	0.08	4.44
arun9	0.30	17.35	0.07	4.28
arun10	0.32	19.30	0.08	4.67
Avg.	0.31	18.54	0.08	4.51

Table C.24: Turbulent scales for rounded gravel far from bed (6.267 cm)

	Λ_T sec	Λ_L cm	λ_T sec	λ_L cm
rrun1	0.35	22.60	0.08	4.96
rrun2	0.30	18.82	0.07	4.31
rrun3	0.35	22.21	0.08	4.80
rrun4	0.26	16.19	0.07	4.64
rrun5	0.40	24.51	0.07	4.52
rrun6	0.48	29.88	0.07	4.68
rrun7	0.24	14.31	0.07	4.16
rrun8	0.40	25.89	0.07	4.68
rrun9	0.29	17.72	0.08	4.63
rrun10	0.27	17.33	0.08	4.84
Avg.	0.33	20.95	0.07	4.62

Table C.25: Probability that turbulent scales are the same between gravel sets

Position*	0.679	6.267
Λ_T	0.91	0.45
Λ_L	0.73	0.18
λ_T	0.24	0.07
λ_L	0.71	0.20

* from tops of gravel (cm)

C.11 ADV Performance Curves

With the ADV being used extensively for field and laboratory measurements there was an article written by García et al. [27] to address some of the instruments known issues. The article gives a good summary of the operating principles of ADV's and some of the limitations of the digital averaging of the velocity signals. Some bias of turbulence measurements comes when certain conditions are not satisfied. These restrictions are related to the instruments' sampling frequency and noise energy level, and the flow conditions. Based on these restrictions, the authors developed a few figures that they named acoustic Doppler velocimeter performance curves (APC's) that are recommended sampling environments for turbulence measurements. They recommend using the following dimensionless frequency equation:

$$F = f_R \frac{L}{U_c} \tag{C.110}$$

where f_R is the acoustic Doppler velocimeter's user-set frequency, L is the energy containing eddy length scale, and U_c is the convective velocity ($U_c \approx \overline{u}$). It is recommend using 20 as the minimum F value to analyze turbulence.

The integral length scale (Λ_L) as found in Section C.10), and average velocity ($\overline{u}$) were used for L and U_c in Equation C.110 respectively. Tables C.26 and C.27 give calculated F values for two vertical location for the angular and rounded runs [27].

Because of the white noise averaging inherent in Doppler technology, Garcia et al. found that the autocorrelation function is bias toward higher values. This results

in increased integral scales [27]. Recomputing the F-values using water depth (H) for the eddy length scale (L) gives the following as seen in Table C.27. As can be seen by Tables C.26 and C.27, for the F-values were usually below 20, meaning that the ADV did not well resolve the turbulence.

Table C.26: APC F-values using computed integral scales

Position*	0.679cm	6.267cm	Position*	0.679cm	6.267cm
arun1	14.0	16.7	rrun1	14.9	17.5
arun2	12.8	12.4	rrun2	24.3	14.9
arun3	14.2	15.5	rrun3	11.5	17.4
arun4	14.7	13.8	rrun4	12.7	12.8
arun5	11.6	14.7	rrun5	17.5	20.2
arun6	11.3	14.6	rrun6	9.4	23.9
arun7	11.9	16.4	rrun7	12.9	12.1
arun8	15.8	21.0	rrun8	11.5	19.8
arun9	15.1	15.1	rrun9	11.7	14.7
arun10	14.3	16.1	rrun10	12.6	13.6
Avg.	13.6	15.6	Avg.	13.9	16.7

* From tops of gravel

Table C.27: APC F-values using water depth for length scale

Position*	0.679cm	6.267cm	Position*	0.679cm	6.267cm
arun1	18.3	12.6	rrun1	17.2	10.4
arun2	16.7	12.5	rrun2	17.3	11.3
arun3	17.0	12.0	rrun3	16.4	10.7
arun4	17.7	12.3	rrun4	18.9	11.0
arun5	18.1	12.1	rrun5	17.8	12.2
arun6	20.1	13.2	rrun6	17.1	11.4
arun7	17.7	12.7	rrun7	17.5	11.6
arun8	20.4	13.2	rrun8	16.0	10.5
arun9	20.5	12.9	rrun9	17.4	11.5
arun10	18.6	12.4	rrun10	14.6	10.7
Avg.	18.5	12.6	Avg.	17.0	11.1

* From tops of gravel